Aramco Journal of Technology

SUMMER 2022

The *Aramco Journal of Technology* is published quarterly by the Saudi Arabian Oil Company, Dhahran, Saudi Arabia, to provide the company's scientific and engineering communities a forum for the exchange of ideas through the presentation of technical information aimed at advancing knowledge in the hydrocarbon industry.

Editor

William E. Bradshaw
william.bradshaw.1@aramco.com.sa
tel: +966-013-876-0498

Production Coordination

Richard E. Doughty
Corporate Publications, Aramco Americas

Design

Graphic Engine Design Studio
Austin, Texas, U.S.A.

The *Aramco Journal of Technology* gratefully acknowledges the assistance, contribution and cooperation of numerous operating organizations throughout the company.

ISSN 1319-2388

Contents

Preparation of a Synthetic Geopolymer Cement Utilizing Saudi Arabian Volcanic Ash for a Sustainable Development: Method, Preparation and Applications

Khawlah A. Alanqari, Dr. Abdullah S. Al-Yami and Dr. Vikrant B. Wagle

Abstract /

The global production of cement is the third largest source of carbon dioxide (CO_2) emissions into the environment, which comes from the decomposition of carbonates. Geopolymer cements can reduce CO_2 emissions by 64% to 80% compared to conventional ordinary Portland cement (OPC). In other words, OPC produces around 900 kg of CO_2 for every 1,000 kg of cement production. Whereas, geopolymer cements emit zero CO_2 emissions while in production.

In addition, geopolymer cements can be prepared utilizing waste materials such as fly ash. In Saudi Arabia, there is enough volcanic ash to sustain the development of this eco-friendly cement. Geopolymer cements have demonstrated promising mechanical properties in comparison to OPCs. We successfully developed a novel geopolymer cement utilizing a Saudi Arabian volcanic ash for primary cementing applications for the oil and gas industry that can completely replace OPCs. This novel cement was prepared by activating the volcanic ash particles with an alkali solution to undergo a geopolymerization reaction.

The objective of this article is to prepare a geopolymer cement with excellent strength and to discuss the synthesis of this cement based on the chemical composition of the volcanic ash. Additionally, we will investigate the effect of the type and concentration of the activating solution on the final geopolymer mechanical properties as well as to detail lab testing.

The volcanic ash particles were activated by a mixture of sodium hydroxide, sodium silicate (Na_2SiO_3), and water, to develop a geopolymer cement. In this study, we prepared four different activating solutions by varying the alkali concentration based on the volcanic ash's chemical composition. The effect of these variations on the setting time and compressive strength of the final geopolymer volcanic ash-based cement were investigated. This was done to develop a cement with excellent strength and controlled setting to ensure a correct cement placement. In addition, the chemical conditions were evaluated to simulate a variety of downhole conditions to prove the effectiveness of this novel geopolymer composition as a cement for primary cementing applications.

The lab testing includes thickening time measurement, compressive strength, and a chemical analysis of the volcanic ash. Test results indicate that the resulting compressive strength and thickening time are strongly affected by the alkali concentration and the additional amounts of the activating solution. Based on this study, we were able to prepare a geopolymer cement with good rheology, setting time, and compressive strength for primary cementing application.

Introduction

Geopolymers are inorganic molecules that can be prepared from aluminosilicate materials to form binders through a geopolymerization reaction without any source of ordinary Portland cement (OPC). This reaction is fast and involves a dissolution of silicon and aluminum oxide species in the aluminosilicate source materials under alkaline conditions[1, 2]. As a result, oligomers as inorganic monomers are formed. These oligomer monomers undergo a polycondensation forming Si-O-Al covalent bonds as a 3D chain with tetrahedral structures; composed of AlO_4 and SiO_4 linked together through oxygen atoms[3, 4].

This geopolymer binder shows exceptional properties in terms of strength and durability; in addition, it shows high resistance to various acids and high temperatures, as well as low shrinkage and permeability values[5]. Geopolymer cements have demonstrated promising mechanical and chemical properties in comparison to OPCs. It shows higher compressive strength and lower fluid loss values[5, 6]. In addition, geopolymers have higher and better resistance to sulfuric acid and chloric acid compared to OPC. This is due to the polycondensation reaction in geopolymerization that produce a stronger chain and polymer structure. Consequently, in OPC, it

shows a clear surface deterioration and weight loss after an acid attack[7]. In addition, OPCs experience strength retrogression at temperatures higher than 230 °F[8, 9].

Besides mechanical property issues in OPC, it poses environmental concerns. As we know, the global production of cement is the third largest source of carbon dioxide (CO_2) emissions into the environment, which comes from the decomposition of carbonates, Eqn. 1. Geopolymer cements can reduce CO_2 emissions by 80% to 90% compared to conventional cement (OPC). In other words, OPC produces around 900 kg of CO_2 for every 1,000 kg of cement production. Whereas, geopolymer cement emits zero CO_2 emissions while in production[10, 11].

$$5\ CaCO_3 + 2\ SiO_2 \rightarrow (3\ CaO, SiO_2)(2CaO, SiO_2) + 5\ CO_2 \quad (1)$$

where $CaCO_3$ is calcium carbonate, SiO_2 is silicon dioxide, CaO is calcium oxide, and CO_2 is carbon dioxide.

Geopolymer cements can be prepared utilizing waste materials as an aluminosilicate source such as fly ash, slag, silica fume, etc.[12]. In addition, different clays can be used as metakaolin[13]. Fortunately, in Saudi Arabia, there is enough volcanic ash to sustain the development of this eco-friendly cement.

In this study, we successfully developed a novel geopolymer cement utilizing local volcanic ash for primary cementing applications for the oil and gas industry that can replace OPCs completely. This novel cement was prepared by activating the volcanic ash particles with an alkali solution to undergo a geopolymerization reaction.

The objective of this article is to prepare a geopolymer cement with excellent strength and to discuss the synthesis of this cement based on the chemical composition of the volcanic ash. Additionally, we will investigate the effect of the type and concentration of the activating solution on the final geopolymer mechanical properties as well as to detail lab testing.

Geopolymer Preparation

As previously mentioned, geopolymer binders can be prepared from geological and waste materials that contain sources of aluminosilicates such as fly ash, slag, silica fume, clays, and others. In general, geopolymerization can occur under an alkaline condition using sodium or potassium hydroxide solutions[14]. Under high pH values, the geological source particles could be activated to undergo a geopolymerization reaction. This chemical reaction is fast and involves a polycondensation of silicate and aluminate monomers under high pH value[1, 15]. In other words, the geopolymerization reaction involves three different steps, Fig. 1.

The first step happens during the initial mixing. In this step, the silicate and aluminate species (SiO_2 and aluminum oxide (Al_2O_3)) are being dissolved under high pH value to initiate the polymerization reaction. Then, a polycondensation reaction occurs between the mixed hydroxyl ion species to form oxygen bonds between Si and Al ions. In the last step, a N-A-S-H gel forms as a rigid material in the form of a 3D chain with a tetrahedral structure that is composed of silicate and aluminate linked to each other through oxygen atoms, Fig. 2[15, 16]. By looking at the chemical structure, you can see that the Al atom in these gels coordinates into four oxygen atoms; as a result, it produces a negative charge on AlO^{4-}. This charge can be balanced by metallic Na+ ions[16, 17].

Development of a Novel Geopolymer Cement

In this study, we utilized the volcanic ash as an aluminosilicate source. The volcanic ash sample is a fine sample

Fig. 1 *The geopolymerization process steps.*

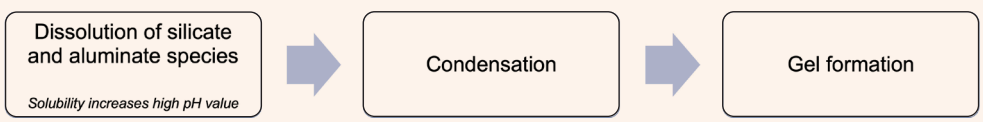

Fig. 2 *The chemical structure of a N-A-S-H gel.*

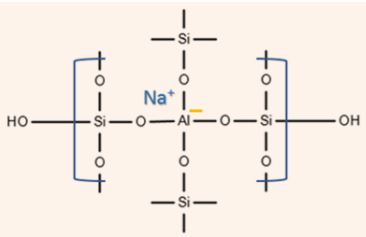

Nan [(-SiO_2) z –AlO_2] n . y H_2O

n: is the degree of polymerization.
Z: can be 2, 3, 4, or higher, it depends on the amount of soluble silicate present and involved in polymerization.

with a particle size distribution of 60% to 80% less than 45 microns. For the alkaline activator, we developed a liquid solution mixture of sodium hydroxide (NaOH) and sodium silicate (Na_2SiO_3). The NaOH solution is prepared overnight in 6 to 10 Molar. Therefore, a mixture of NaOH, Na_2SiO_3, and water developed a geopolymer cement, activated by the volcanic ash particles, Fig. 3[18].

For the development of a novel geopolymer cement, we prepared four different activating solutions by varying the alkali concentration and the addition amounts based on the volcanic ash chemical composition, Table 1. The effect of these variations on the setting time and compressive strength of the final geopolymer volcanic ash-based cement were investigated. This was done to develop a cement with an excellent strength and controlled setting to assure the right cement placement.

In addition, the chemical conditions were evaluated to simulate a variety of downhole conditions to prove the effectiveness of this novel geopolymer composition as a cement for primary cementing applications.

Experimental Study

The lab testing includes thickening time measurement, compressive strength measurement, and a chemical analysis of the volcanic ash.

X-ray Powder Diffraction (XRD)

The analytical X-ray powder diffractometer with a cobalt X-ray tube is used to measure the high-resolution X-ray powder diffraction (XRD) data of the volcanic ash sample. This technique is used to determine the crystallographic structure of a material.

Consistometer

A standard API high-pressure, high temperature consistometer was used to test and investigate the pump ability of the prepared geopolymer slurries. The consistometer is used to determine how long the geopolymer formulation will remain in a fluid state in downhole conditions. Thickening time is the time taken by the geopolymer slurries to reach a consistency of 70 BC to 100 BC. The geopolymer slurry is poured from the blender into an API slurry cup. The geopolymer slurry is then placed in the consistometer and is then subsequently subjected to the required temperature and pressure.

Ultrasonic Cement Analyzer (UCA)

The UCA is used to measure the compressive strength of different geopolymer slurries. It works by sending a continuous sound pulse into the cement slurry. Sound pulse travels faster through the cement matrix when the slurry gels and hardens. The transit time is correlated to the compressive strength of the hardened cement.

Table 1 The four geopolymer testing formulations.

	F1	F2	F3	F4
SiO_2/Al_2O_3 (in volcanic ash sample)	6.14	6.14	6.14	6.14
Na_2O, NaOH, Al_2O_3	0.43	0.65	0.9	1
NaOH Molarity	6 M	6 M	10 M	10 M

Results and Discussion

The XRD results of the volcanic ash in Table 2 shows that it contains 44.44% and 15.97% of SiO_2 and Al_2O_3 species, respectively. We prepared the four different testing formulations based on these quantities. So, the additional amounts of the activating solution are based on the molar ratios in Table 1.

Test results indicate that the resulting compressive

Table 2 The XRD composition of volcanic ash.

Compound	Wt%
Amorphous Material	70
Labradorite: $Ca_{0.65}Na_{0.32}(Al_{1.62}Si_{2.38}O_8)$	19
Augite: $Ca(Fe, Mg)Si_2O_6$	6
Forsterite: Mg_2SiO_4	5

Species	Percentage
CaO	8.53
SiO_2	44.44
Al_2O_3	15.97
Fe_2O_3	13.2
MgO	7.89
K_2O	1.37

Fig. 3 Development of geopolymer cement.

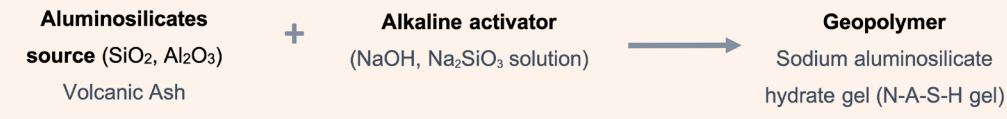

Table 3 *The thickening time and compressive strength results of the four geopolymer testing formulations in 24 hours.*

	F1	F2	F3	F4
Thickening Time (hr:min)	13:09	5:20	3:40	Gelled while mixing
Compressive Strength (psi)	340	2,565	1,009	—

Fig. 4 *The UCA results of formulation 2 with a strength of 2,250 psi within 12 hours.*

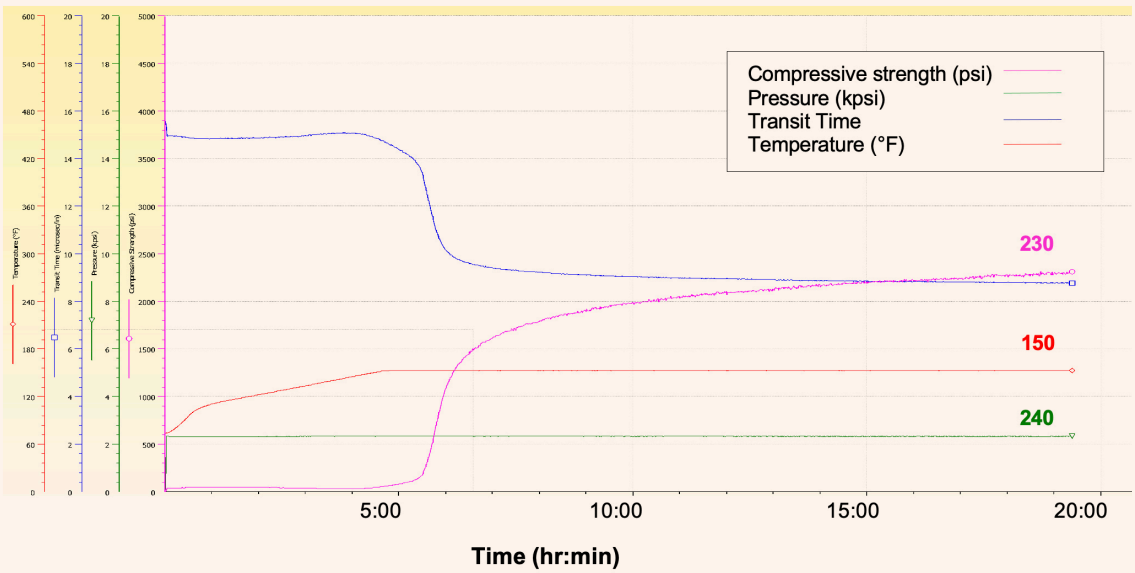

strength and thickening time are strongly affected by the alkali concentration and the addition amounts of the activating solution. The highest compressive strength is found in formulation 2, with a 6 Molar of NaOH solution, Table 3 and Fig. 4. The NaOH solution is prepared overnight to allow the solution to cool-down prior to use. This is important to avoid excess heat through the geopolymer cement formation that could accelerate gelling.

Using a high amount of the activating solution makes mix ability difficult due to the fast gelation of the geopolymer slurry as we faced in formulation 4. Based on this study, we were able to prepare a geopolymer cement with good rheology, setting time and compressive strength for primary cementing application.

Conclusions

In this article, we were able to prepare a geopolymer cement with good rheology, setting time and compressive strength for primary cementing application. This was done by activating the local volcanic ash particles under an alkaline solution that contains a mixture of NaOH, Na_2SiO_3, and water. Additional amounts were based on the volcanic ash chemical composition. Test results indicate that the resulting compressive strength and thickening time are strongly affected by the alkali concentration and the additional amounts of the activating solution. Where, the highest compressive strength is found in formulation 2 with a 6 Molar of NaOH solution being used.

Acknowledgments

This article was presented at the International Petroleum Technology Conference, Riyadh, Kingdom of Saudi Arabia, February 21-23, 2022.

References

1. Davidovits, J.: "Geopolymers Inorganic Polymeric New Materials," *Journal of Thermal Analysis and Calorimetry*, Vol. 37, Issue 8, August 1991, pp. 1633-1656.
2. Xu, H. and van Deventer, J.S.J.: "The Geopolymerization of Alumino-Silicate Minerals," *International Journal of Mineral Processing*, Vol. 59, Issue 3, June 2000, pp. 247-266.
3. Srinivasan, K. and Sivakumar, A.: "Geopolymer Binders: A Need for Future Concrete Construction," *ISRN Polymer Science*, Vol. 2013, Article ID 509185, January 2013.

4. Amritphale, S.S., Bhardwaj, P. and Gupta, R.: "Advanced Geopolymerization Technology," Chapter 2 in *Geopolymers and Other Geosynthetics*, (eds.) Alshaaer, M. and Jeon, H-Y., IntechOpen, 2019, 180 p.

5. Khalifeh, M., Todorovic, J., Vrålstad, T., Saasen, A., et al.: "Long-term Durability of Rock-Based Geopolymers Aged at Downhole Conditions for Oil Well Cementing Operations," *Journal of Sustainable Cement-Based Materials*, Vol. 6, Issue 4, 2017, pp. 217-230.

6. Salehi, S., Ali, N., Khattak, M.J. and Rizvi, H.: "Geopolymer Composites as Efficient and Economical Plugging Materials in Peanuts Price Oil Market," SPE paper 181426, presented at the SPE Annual Technical Conference and Exhibition, Dubai, UAE, September 26-28, 2016.

7. Davidovits, J.: "Properties of Geopolymer Cements," in *Proceedings of First International Conference on Alkaline Cements and Concretes*, Scientific Research Institute on Binders and Materials, Kiev, Ukraine, 1994, pp. 131-149.

8. Al-Bagoury, M., Revil, P. and Kåstad, A.: "Silica Dispersion for HT Oil Well Cement," paper AADE-16-FTCE-57, presented at the AADE Fluids Technical Conference and Exhibition, Houston, Texas, April 12-13, 2016.

9. Bu, Y., Du, J., Guo, S., Liu, H., et al.: "Properties of Oil Well Cement with High Dosage of Metakaolin," *Construction and Building Materials*, Vol. 112, June 2016, pp. 39-48.

10. Davidovits, J.: "Geopolymer Cement for Mitigation of Global Warming," Geopolymer Institute, *https://www.geopolymer.org/applications/global-warming/*, 2010.

11. Worrell, E., Price, L., Martin, N., Hendriks, C., et al.: "Carbon Dioxide Emissions from the Global Cement Industry," *Annual Review of Energy and the Environment*, Vol. 26, 2001, pp. 303-329.

12. Luukkonen, T., Abdollahnejad, Z., Yliniemi, J., Kinnunen, P., et al.: "One-Part Alkali-Activated Materials: A Review," *Cement and Concrete Research*, Vol. 103, January 2018, pp. 21-34.

13. Palomo, A., Blanco-Varela, M.T., Granizo, M.L., Puertas, F., et al.: "Chemical Stability of Cementitious Materials Based on Metakaolin," *Cement and Concrete Research*, Vol. 29, Issue 7, 1999, pp. 997-1004.

14. Davidovits, J.: "Geopolymers and Geopolymeric Materials," *Journal of Thermal Analysis*, Vol. 35, 1989, pp. 429-441.

15. Škvára, F., Doležal, J., Svoboda, P., Kopecký, L., et al.: "Concrete Based on Fly Ash Geopolymers," *Proceedings of 16th IBAUSIL*, Vol. 1, January 2006, pp. 1079-1097.

16. Davidovits, J.: "Chemistry of Geopolymeric Systems, Terminology," *Geopolymer*, Vol. 99, 1999, pp. 9-40.

17. Xie, Z. and Xi, Y.: "Hardening Mechanisms of an Alkaline-Activated Class F Fly Ash," *Cement and Concrete Research*, Vol. 31, Issue 9, September 2001, pp. 1245-1249.

18. Alanqari, K.A. and Al-Yami, A.S.: "Methods of Converting Drilling Fluids into Geopolymer Cements and Use Thereof," U.S. Patent 11,098,235, August 24, 2021.

About the Authors

Khawlah A. Alanqari

M.S. in Chemistry,
San Diego State University

Khawlah A. Alanqari is a Petroleum Scientist with the Drilling Technology Team of Saudi Aramco's Exploration and Petroleum Engineering Center – Advanced Research Center (EXPEC ARC). She received the Outstanding Young Professional Award at the EXPEC ARC 2021 Annual Awards. In addition, Khawlah was shortlisted for a number of global awards and received "highly commended" in the category of the Young Energy Professional at the Energy Institute 2020 Awards.

She has six granted patents, and 21 filed patent applications in the area of drilling fluids, cementing and loss circulation, as well as a number of published technical publications and journal papers. received her B.S. degree in Chemistry from the University of Dammam, Dammam, Saudi Arabia. She received her M.S. degree in Chemistry with a specialization in organic and organometallic chemistry from San Diego State University, San Diego, CA in 2017. She has a three years of research experience from a synthetic organic chemistry lab at San Diego State, focusing on the development of new reactions and methodologies in organic synthesis.

Khawlah also gained academic experience from working as a Chemistry Lecturer at Jubail University College before joining Saudi Aramco in 2018.

Dr. Abdullah S. Al-Yami

Ph.D. in Petroleum Engineering,
Texas A&M University

Dr. Abdullah S. Al-Yami is a Senior Petroleum Engineering Consultant with the Drilling Technology Team of Saudi Aramco's Exploration and Petroleum Engineering Center – Advanced Research Center (EXPEC ARC). He has 24 years of experience with Saudi Aramco and previously worked in different positions, including as a Lab Scientist and Drilling Engineer, conducting research related to drilling engineering.

Abdullah has received several awards during his career, including Saudi Aramco's Research and Development Center (R&DC) Innovation Award and its Successful Field Application Award for his research work. He also received Saudi Aramco's EXPEC ARC Effective Publications Award. A member of the Society of Petroleum of Engineers (SPE), Abdullah was awarded the 2009 SPE Outstanding Technical Editor Award for his work on the SPE *Drilling and Completion Journal*. He also received the 2014 SPE Regional (Middle East, North Africa and South Asia) Drilling Engineering Award, and both the 2015 and 2016 CEO Saudi Aramco Excellence Award. In 2016, Abdullah received Oil & Gas Middle East Award "highly commended" recognition in the category of internal control valve (ICV) Strategy of the Year for his efforts in developing drilling products utilizing a local resources strategy. In 2017, he was awarded the Saudi Arabian Board of Engineering Award.

Abdullah is a coauthor of the textbook *Underbalanced Drilling: Limits and Extremes*; he has 127 granted U.S. patents and 152 filed patents; and has more than 100 publications to his credit, all in the area of drilling and completions.

Abdullah received his B.S. degree in Chemistry from Florida Institute of Technology, Melbourne, FL; his M.S. degree in Petroleum Engineering from King Fahd University of Petroleum and Minerals (KFUPM), Dhahran, Saudi Arabia; and his Ph.D. degree in Petroleum Engineering from Texas A&M University, College Station, TX. Abdullah is currently a Chemistry Ph.D. candidate at KFUPM majoring in Organic Chemistry and Polymer Synthesis.

Dr. Vikrant B. Wagle

Ph.D. in Surfactant and Colloidal Science,
Mumbai University Institute of Chemical Technology

Dr. Vikrant B. Wagle is a Science Specialist with the Drilling Technology Team of Saudi Aramco's Exploration and Petroleum Engineering Center – Advanced Research Center (EXPEC ARC). His experience revolves around the design of novel, environmentally friendly drilling fluid additives and the development of high-pressure, high temperature tolerant drilling fluid systems.

Vikrant has 50 technical publications and 120 granted U.S. patents, and he has filed several other U.S. patent applications, all in the area of drilling fluids, cementing, and loss circulation.

He received his M.S. degree in Chemistry from the University of Mumbai, Mumbai, India, and his Ph.D. degree in Surfactant and Colloidal Science from the Mumbai University Institute of Chemical Technology, Mumbai, India.

Drilling Automation: The Step Forward for Improving Safety, Consistency, and Performance in Onshore Gas Drilling

Ernesto S. Gomez, Ebikebena M. Ombe, Rafael Carvalho and Brennan Goodkey

Abstract /

In the current oil and gas drilling industry, the modernization of rig fleets has been shifting toward high mobility, artificial intelligence, and computerized systems. Part of this shift includes a move toward automation. This article summarizes the successful application of a fully automated workflow to drill a stand, from slips out to slips back in, in a complex drilling environment in onshore gas.

Repeatable processes with adherence to plans and operating practices are a key requirement in the implementation of drilling procedures and vital for optimizing operations in a systematic way. A drilling automation solution has been deployed in two rigs enabling the automation of both pre-connection and post-connection activities as well as rotary drilling of an interval equivalent to a typical drillpipe stand (approximately 90 ft) while optimizing the rate of penetration (ROP) and managing drilling dysfunctionalities, such as stick-slip and drillstring vibrations in a consistent manner. So far, a total of nine wells have been drilled using this solution.

The automation system is configured with the outputs of the drilling program, including the drilling parameters roadmap, bottom-hole assembly tools, and subsurface constraints. Before drilling every stand, the driller is presented with the planned configuration and can adjust settings whenever necessary. Once a goal is specified, the system directs the rig control system to command the surface equipment — draw works, auto-driller, top drive, and pumps. Everything is undertaken in the context of a workflow that reflects standard operating procedures. This solution runs with minimal intervention from the driller and each workflow contextual information is continuously displayed to the driller, thereby giving him the best capacity to monitor and supervise the operational sequence. If drilling conditions change, the system will respond by automatically changing the sequence of activities to execute mitigation procedures and achieve the desired goal. At all times, the driller has the option to override the automation system and assume control by a simple touch on the rig controls.

Prior to deployment, key performance indicators (KPI), including automated rig state-based measures, were selected. These KPIs are then monitored while drilling each well with the automation system to compare performance with a pre-deployment baseline. The solution was used to drill approximately 60,000 ft of hole section with the system in control, and the results showed a 20% improvement in ROP with increased adherence to pre-connection and post-connection operations. Additionally, many lessons were learned from the use and observation of the automation workflow that was used to drive continuous improvement in efficiency and performance over the course of the project.

This deployment was the first in the region and the system is part of a comprehensive digital well construction solution that is continuously enriched with new capabilities. This adaptive automated drilling solution delivered a step change in performance, safety, and consistency in the drilling operations.

Introduction

Although the midstream and downstream sectors of the global oil and gas industry have seen a modest adoption of digital technology, upstream operations remain largely lacking of digital innovation. Despite appearances, however, this slow progress is much more a result of sector specific complexities than willful resistance. The complex network of experts and third-party organizations required to take a well from conception to production makes it very difficult to align stakeholders around a cross-domain digital project.

In well planning, for example, the use of traditional workflows generally results in a lengthy, disconnected, and iterative process, which introduces a lack of coherency between teams, and increases the planning risks. Once the plan has been painstakingly validated and is sent for execution, risks continue with operational deviations,

commonly due to misinterpretations, overlooked recommendations, and other human-related variabilities.

A modern approach to well construction centers on a cohesive, cloud-based ecosystem in which all well stakeholders gather to collaborate throughout the well planning, design, and execution. Rather than working independently in discipline specific silos, experts ranging from corporate planners to drilling engineers will collaborate, sharing new data and designs in real time.

With the cloud-based architecture, a wealth of relevant data will immediately be accessible to all involved parties, along with advanced computational resources to make faster, better informed decisions while eliminating time-consuming administrative tasks, which can easily be automated. Next, by communicating the plan directly to a cloud-enabled, automated drilling system, well owners can be certain that the well is drilled exactly to plan with precise adherence to all standard practices and recommendations. Finally, a rich reservoir of contextualized data will be collected throughout the drilling process and synced back to the cloud for use in improving future wells.

In this article, the successful deployment of the well planning and automated drilling components of the previously described solution will be detailed. Insight will be provided on the concept, the deployment process, and detailed descriptions of the results achieved to date. Given the close collaboration and alignment required to synchronize a digital project of this scale, details will be shared on steps taken by the operator, the oil field service company, and the rig contractor to ensure its success. Finally, a detailed description of the way forward will be discussed to highlight the future potential of fully digitalizing the well construction process.

Project Scope

The project's scope would result in the construction of multiple complex gas wells over a four-year period in an oil and gas field in the Middle East. The extended timeline provided the required span to safely transition to the digital solution without compromising operations while allowing adequate time for evaluation of the resulting gains in efficiency. To minimize disruption, the deployment of the proposed digital solution was scheduled in three phases:

1. Benchmarking: To accurately quantify the value added by the digital solution, it was imperative that a standard for comparison was established. To avoid the bias associated with project startups, a one and a half-year period was chosen to ensure that gains associated with the learning curve could be isolated. This would be combined with nearly a decade of benchmarks collected from previous partnerships between the two organizations with many of the same rigs and personnel in identical well types.

2. Learning: As with any technology deployment, navigating the learning curve is nonnegotiable. As such, a sixth-month period was defined to ensure personnel had adequate time to become familiarized with the new digital operating model as well as to stress test the software to identify and resolve any bugs.

3. Optimization: Before exiting the learning phase, a series of acceptance tests was scheduled to ensure the proficiency of users, and the software reliability were at an adequate level to reduce risks in the transition. Only when all gaps have been addressed, would the solution proceed to full implementation and into the operational optimization stage.

Defining Autonomy

Ever since the late 1960s, automation in drilling has regularly been discussed in industry literature citing a variety of initiatives such as auto-drillers, smart advisors, and rig floor mechanization[1]. With an inability to identify and adjust to the ever-changing drilling environments, its application has remained limited to a specific range of predetermined activities with extensive human intervention required whenever conditions change.

The next step change in value generation will come from systems that possess the intelligence to comprehend and react to the dynamic drilling environments. They will autonomously prioritize and execute competing activities while responding to unexpected events without human intervention. Industry literature recognizes this transition as a shift that crosses the boundary between simple "automation" and "system autonomy"[2]. These modern systems are characterized by intelligence, complexity, and decision making ability capable of interpreting complex alternatives and independently deciding on a course of action. This significantly lessens the cognitive burden on the driller by directly assuming responsibility for a portion of the driller's workload.

Figure 1[3] shows the progressive degrees of automation that are now possible in drilling operations from fully human operated systems to fully autonomous systems with minimal human intervention.

Technology Description

As described earlier, a full well construction solution was created to allow real-time collaboration in a cloud-based environment. Within this environment, a suite of modules was available for each phase of the well construction evolution from exploration to production optimization.

In this deployment, the well design and drilling automation components of the ecosystem were deployed, Fig. 2. Technical descriptions of each component will be described in detail later.

Well Planning Module

To enable seamless collaboration of all stakeholders throughout the well design process, a native cloud-based solution was developed. In this ecosystem, engineering applications for each domain expert were made available online. This allowed each domain expert to prepare their individual deliverables in the shared environment with immediate access to relevant

Fig. 1 *The progressive levels of automation now possible in drilling operations[3].*

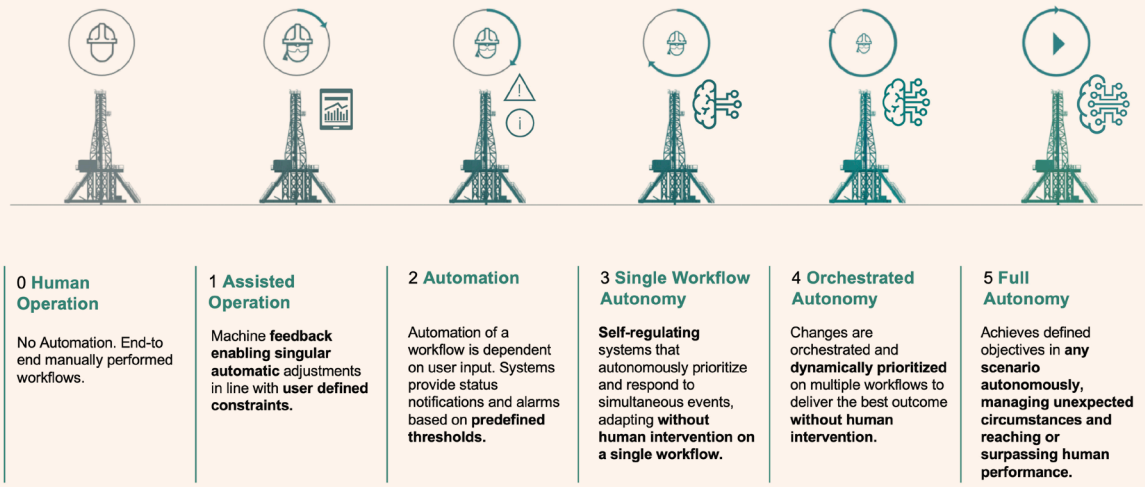

Fig. 2 *The well design and drilling automation components of the digital well construction[3].*

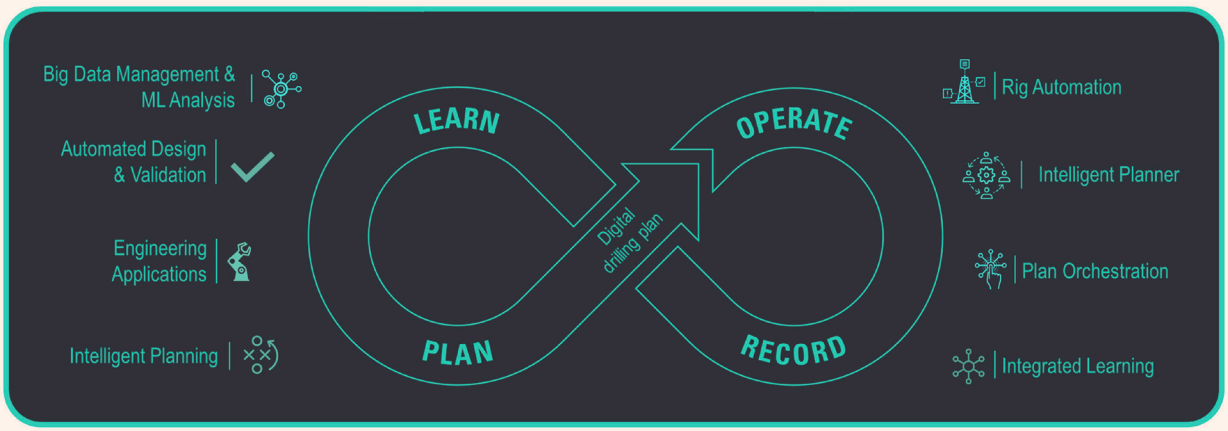

data as well as resources for automating most of the repetitive tasks.

As a result, collaboration and efficiency was greatly enhanced and team members were able to access scalable computational engines for activities such as automated trajectory design, wellbore stability analysis, intelligent casing seat selection, well barrier compliance, kick tolerance validation, as well as integration into industrial machine learning resources. In this method, each completed deliverable became an object in a network of digitally linked systems, which when synced, would force all related systems to update automatically to revalidate the design. With an online environment, project managers had far greater visibility over task tracking and project progress to ensure that the drilling program was delivered on time with all required validations from expert reviewers.

Once the well plan was completed, a traditional drilling program document was exported along with a digitalized drilling program (DDP), which could automatically be synced to a compatible automated drilling system, which also resides on the cloud. This DDP contained all information necessary to safely drill the well with automation. It was not restricted to basic limits and drilling parameters for each well interval, but was a comprehensive overview of well operations with specific details, recommendations, and reminders to assist with operations. In addition, drilling notes, drilling risks, reminders, checklists, etc., were included in the digital program and would be shared with the relevant parties throughout each step of the drilling operations.

Drilling Automation Module

Once the DDP was received at the rig, it was presented to the rig site experts for validation. Once accepted, the DDP was synced to the rig's automated drilling system,

which would define all recommendations, limits, and constraints for each interval of the well. From this point, the drilling automation module could be engaged to drill the well and ultimately unlock increased drilling performance, efficiency, precision, and safety.

The automation system's main focus was to bring autonomous functionality to all drilling steps between the removal of the slips after connection, until the slips were installed after the stand was drilled. Throughout these activities, the system not only enabled a "hands-off" operation — drilling, pre-connections/post-connections, working the pipe, friction test, etc. — but also enabled several integrity and performance-based workflows. This included intelligent rate of penetration (ROP) optimization, directional drilling workflows, and drilling dysfunction mitigation.

Together, these functionalities worked to deliver the well exactly as planned while precisely following all operator recommendations and limits while delivering improvements in the ROP, tool reliability, and consistency. As mentioned earlier, given the intelligent planning engine integrated into the drilling automation system, all functionalities could be leveraged on-demand and re-prioritized based on the system's interpretation of the drilling environment.

Figure 3 shows how the automated module operations can be split into four main categories. The "Stand Automation" feature automates all drilling actions executed by the driller in an entirely consistent manner with exact precision. The "ROP Optimization" feature leverages intelligent engines to identify the ideal parameters to maximize the drilling rate. This module works in tandem with the "Dysfunction Mitigation" feature to readjust parameters whenever drilling events such as stick-slip or drillstring shock and vibrations are encountered to avoid damage to the bit or downhole tools.

Finally, directional drilling can be augmented through "Automated Downlinking," and surveying to enable increased accuracy while minimizing the driller's intervention during critical operations. Due to its autonomous nature, the system could independently "replan" and implement each of the above workflows "on the fly," based on its interpretation of the drilling environment.

Richer Data

Over the past decade, oil and gas organizations have become increasingly conscious of the wealth of insight locked away in the data collected throughout all of the phases of well construction. Despite this awareness, value from data science projects is rare in drilling operations, and more often than not, such data is archived in the organization's databases and left nearly inaccessible due to the lack of structure and context.

Estimates of a major exploration and production organization predict that 80% of time spent on today's data science projects are spent looking for data while 20% is spent on cleaning, structuring, and using the data. Even when data can be properly accessed, often there is inadequate context recorded to properly apply models to extract meaningful insight from the data. This highlights that what is captured while drilling is critical; any missing or inadequate data could sabotage the data science project before it has even begun.

Comparatively, one of the most beneficial byproducts of implementing a comprehensive cloud-based solution is the centralization and normalization of data. With cloud-enabled drilling rigs capturing up to a thousand datapoints of highly contextualized information per second, data is synced to corporate data lakes where the cleaning and structuring begins immediately. Once

Fig. 3 *The four categories of the automated module operations[3].*

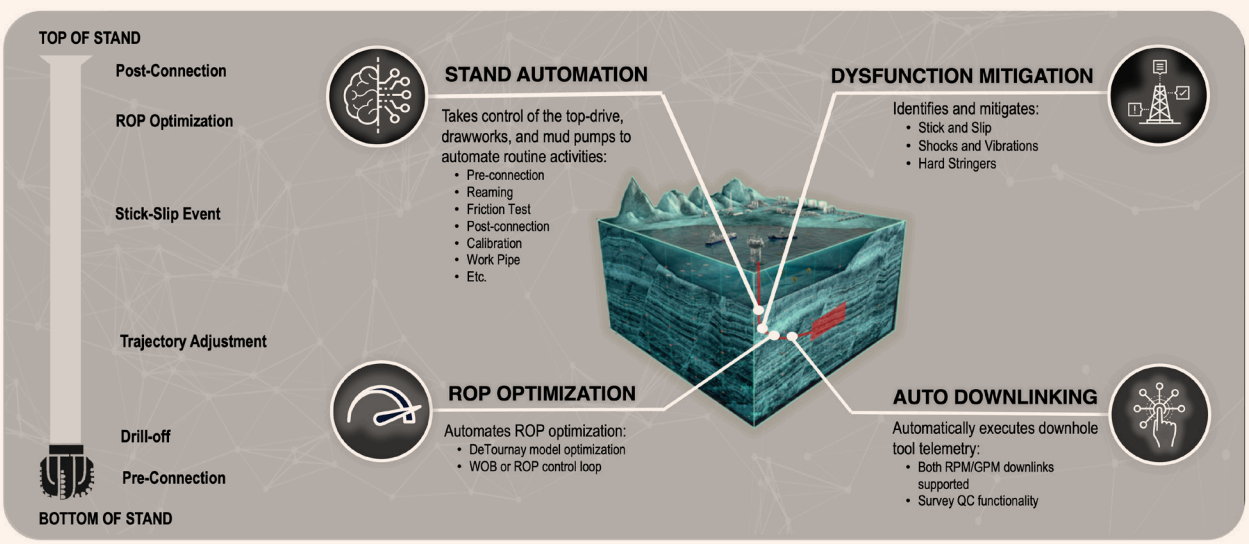

complete, the refined data becomes directly accessible on the online environment in real-time. Data scientists and experts are then free to tie-in directly to visualization software and industrial machine learning resources to extract insights ranging from drilling anomaly detection, parameter optimization, equipment reliability, trend analysis, etc.

Collaboration Strategies

Prior to deployment, the project stakeholders were made well aware of the grim statistics for the success rate of digital initiatives in the oil and gas industry. Despite innovative technologies and plans, countless digital projects have failed, not at inception and design, but at implementation where inadequate commitment and a lack of leadership oversight have negatively affected them even before they began. As such, it was well understood that the success of this transformation hinged on alignment at all levels.

Given the deep existing relationships among the stakeholders at various levels who had collaborated in the past, they met prior to the project implementation to define a way forward for the deployment. The shared work culture of constant optimization and the push for a digital progress simplified this collaboration, allowing the projects' leadership to jointly focus on the implementation challenges with a multilateral approach to problem solving.

Optimized Visibility

Transparency was immediately identified as a critical component for progress. As success depended on many individual teams, it was essential that all stakeholders were aware of their roles in the project. As a solution, an automated data reporting system was customized to allow automation specific insight to be extracted on a daily basis from exported rig data.

Automated reports could then be shared with all stakeholders involved with minimal manual input to track automation utilization, performance, and any issues within the system. Throughout the implementation process, field benchmarks would be updated to ensure that relevant, up-to-date comparisons were available. This would allow stakeholders to identify potential bottlenecks or system anomalies for fast resolution to maximize the value added with automation.

Staggered Approach

As with any sweeping modernization process, change is usually difficult. This is especially true for oil and gas operations with a heavy focus on precision solutions and risk avoidance. To streamline the implementation as much as possible, multiple familiarization sessions were held with the end users in preparation for deployment.

Once in operation, 24-hour support was made available both on the rig site and remotely for both well planning and drilling automation related activities. At each step of deployment, progress was governed through "stage gates," meaning that the functionality utilized and the support staff available would not change until specific metrics for adoption and competency had been achieved.

Each module was deployed separately with support teams for each. Once each module was successfully adopted, they were integrated together by connecting through the digital drilling program.

Digital Well Planning Results

As previously mentioned, the well planning solution was deployed in stages beginning with a benchmarking period, followed by a learning and optimization period. Throughout benchmarking, details were collected from experienced subject matter experts throughout the creation of the well plans. To remove any bias, categories for comparison were established for each well type. Deployment started with a few select individuals from each domain of expertise. This ensured that any software compatibility challenges could be identified and resolved before moving to the wider rollout across the organization. Once deemed ready, training began for a wider scope of engineers with a dedicated remote team available for support at all times throughout the learning curve.

After the first three months following deployment, gains in efficiency and a reduction in well plan delivery time became increasingly evident. Overall, a 23% to 25% reduction in well plan preparation time was observed with gains coming from various parts of the preparation process. Figure 4 shows the details of the savings breakdown. In addition, a reduction in planning risk was evident through automated tools such as automated offset well analysis, which augmented the engineer's analysis process. This also automated the trajectory design to ensure the design engineer had considered all risks and options, and engineering calculation validation to ensure that the well design integrity was evaluated at each step.

Once fully implemented, the connection between the planning solution and the rig's automated drilling system was established so that all limits, recommendations, and best practices could be directly communicated for execution. This minimized the risk of deviations from the plan caused by misinterpretation or negligence as all drilling operations would be executed with automation.

Drilling Automation Results

Prior to the deployment of the automation system, a comprehensive benchmarking analysis was conducted to identify the present performance of the candidate rigs as well as their ranking in comparison the nonautomated rigs in the project. The analysis covered a variety of metrics related to the areas in which automation was expected to introduce value. This included standard metrics such as drilling ROP, duration of pre-connection and post-connection activities, and spud-to-well total depth foot per day key performance indicators (KPIs). Additionally, automation specific KPIs such as downhole tool communication accuracy, bottom-hole assembly tool failure statistics, bit trips per section, and drilling dysfunction events are included. These were established on a single rig level as well as a fieldwide comparison for comparable well types.

As previously mentioned, the implementation would

Fig. 4 *Details of the well planning savings.*

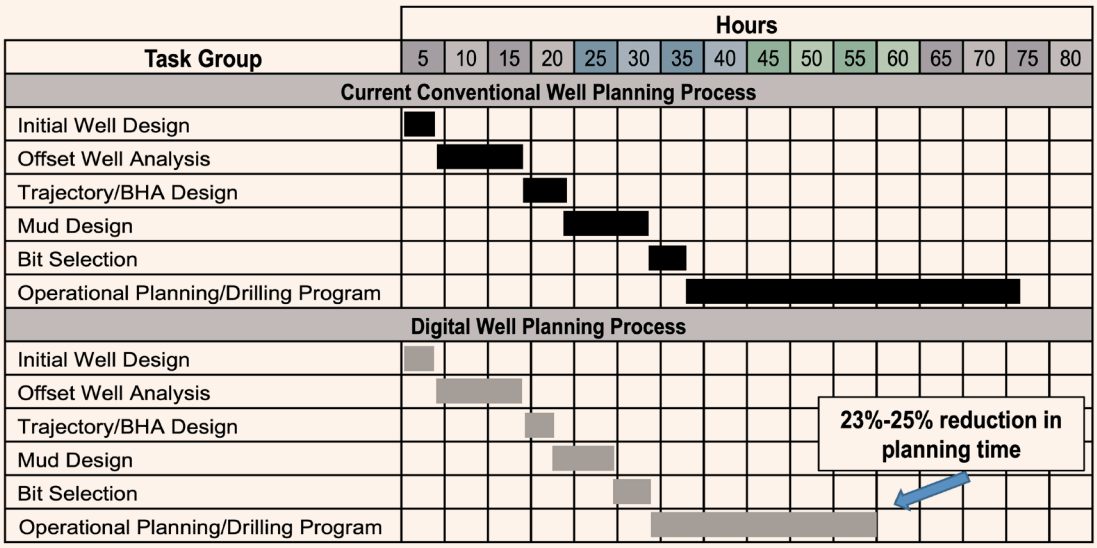

result in "full-stand" drilling automation with additional functionality for drilling trouble mitigation, ROP optimization, and directional drilling workflows.

Full-Stand Automation

Given the variability to human operation, wells are often drilled far differently than intended as per the engineering plan. Although clear practices and recommendations are laid out, it is nearly impossible for a driller to follow them all while simultaneously prioritizing crew safety and maintaining performance standards. Unfortunately, these discrepancies can sometimes result in far more catastrophic events than under achieving performance.

In fact, according to a report published in the *Journal of Petroleum Technology*[2], up to 80% of operational incidents are a direct result of human error or failure to adhere to the recommended best practices. As such, automation is an opportunity not only to accumulate time savings through more precise operations, but also to introduce a step change in adherence and consistency for crew safety and operational integrity.

As discussed earlier, all drilling operations between the removal of slips after the drillpipe connection to installing the slips prior to the next connection could automatically be performed by the automated drilling rig. This included all required post-connection, drilling, and pre-connection activities, including additional optional steps such as "friction test" and "working the pipe." For the first one and a half years after deployment, a step change in consistency as well as performance became immediately clear.

Evidence of this can be identified in Fig. 5a where all pre-connection sequences from a particular hole section on different wells are plotted to compare the automated and nonautomated operation. The figure shows the traveling block position during a reaming and backreaming sequence, before stopping for a connection. In total, 55 pre-connections are shown here; 38 performed with automation, and 14 performed by the driller (manually). As can be seen, each automated sequence is nearly indistinguishable from the next with near perfect precision. This is a distinct departure from the manual operated connections where variability is constant with parameters often exceeding the recommended practices increasing the risk of an operational incident.

Further evidence is presented in Fig. 5b, which summarizes the distribution of 533 pre-connections executed with automation in control. When compared to manual operations, the pre-connection time is decreased by 23% with a threefold increase in pre-connection consistency.

Fig. 5a *The pre-connection sequences from a particular hole section on different wells are plotted to compare the automated and nonautomated operation.*

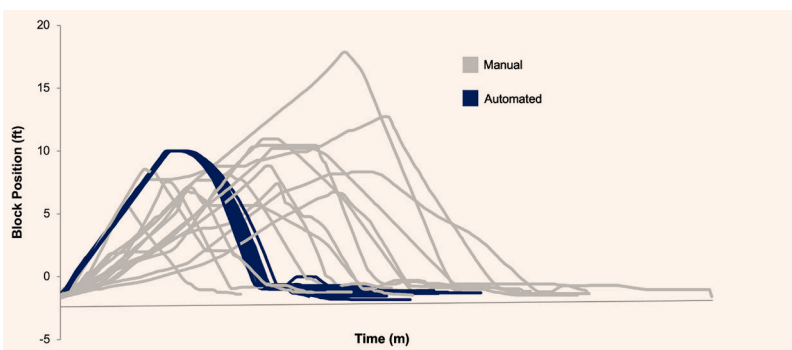

Fig. 5b *A summarization of the distribution of 533 pre-connections executed with automation in control.*

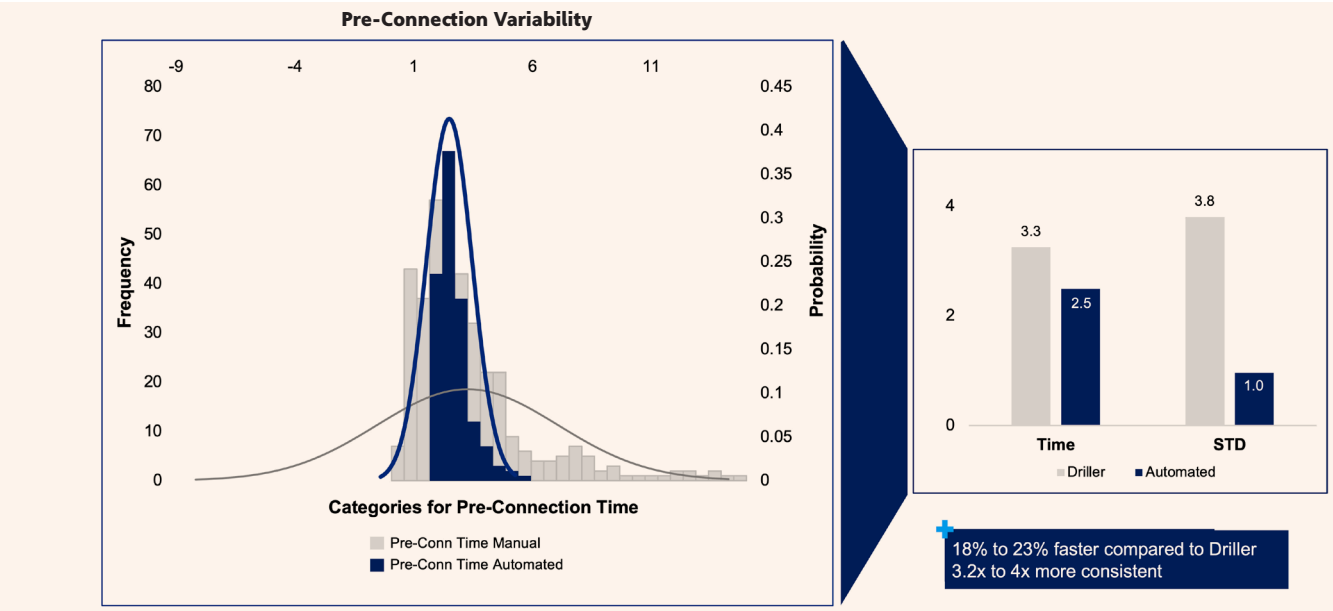

ROP Optimization

Under traditional drilling logic, the highest ROP is generally expected through maximizing the drilling parameters within the limits of the tools. Subsequently, in reality, one must recognize that not all formations are as receptive to this strategy. In addition, excessive parameters can often lead to premature tool failure and additional bit trips, which can cost more well time. In traditional drilling operations, this balance of performance and reliability relies exclusively on the driller's experience, thereby introducing inconsistency and hidden lost time due to poorly optimized parameters. As an alternative, the automation system relied on the intelligent ROP optimization algorithms, which constantly adjusted drilling parameters to identify the best combination of drilling parameters for maximizing ROP while remaining within the operator's recommended limits.

An excellent example of this can be seen in Fig. 6 in which the 16" hole sections in two wells were drilled 300 ft apart by the same rig. Well-1 was drilled with the automation system in control while Well-2 was drilled manually. In the manually drilled section, it is evident that parameters were conservative with the weight on bit (WOB) limited far below to maximum limit defined for the section. In the automated case, parameters were maximized throughout the section leading to an average ROP improvement of nearly 60%. Overall, the automated approach improved the average ROP by 16.4% over the span of one year in operation.

As a second contributor to performance, the increased visibility of rig operations afforded by a cloud-based drilling rig enabled office based personnel to become more engaged in performance optimization. Through the cloud-based drilling monitoring interface, drilling engineers working remotely were able to identify unnecessary limits put on ROP through a specific interval of the well.

After an investigation, a team of subject matter experts recommended the limit be increased to a safe margin, which ultimately led to performance doubling the field average and resulted in a new drilling strategy for the remaining, non-automated rigs.

Drilling Dysfunction Mitigation

When evaluating performance, the go-to KPI generally examined tends to be the average ROP. This doesn't always tell the whole story. Premature failure of the bit or downhole tools can easily lead to more than a day of nonproductive time to replace the tool as well as the additional cost of the replacement equipment. As such, it is critical that while drilling, dysfunctions such as drillstring shocks and vibrations, as well as stick and slip, are mitigated to avoid premature failure.

To manage this, most drilling organizations have detailed mitigation best practices in place for the driller to follow in case of an event being encountered. In practice, mitigation strategies are often implemented late and often only partially implemented. In addition, once the drilling dysfunction is passed, the driller often fails to return to optimization practices in a timely manner to maximize performance.

To combat premature tool failure, the automation system incorporates a drilling dysfunction mitigation system, which would detect events such as shock and vibration, stick and slip, and hard stringers. Once detected, it would autonomously define a custom mitigation sequence based on the nature and severity of the event and independently "replan" the drilling steps

Fig. 6 *Drilling with the same rig, Well-1 was drilled with the automation system in control while Well-2 was drilled manually.*

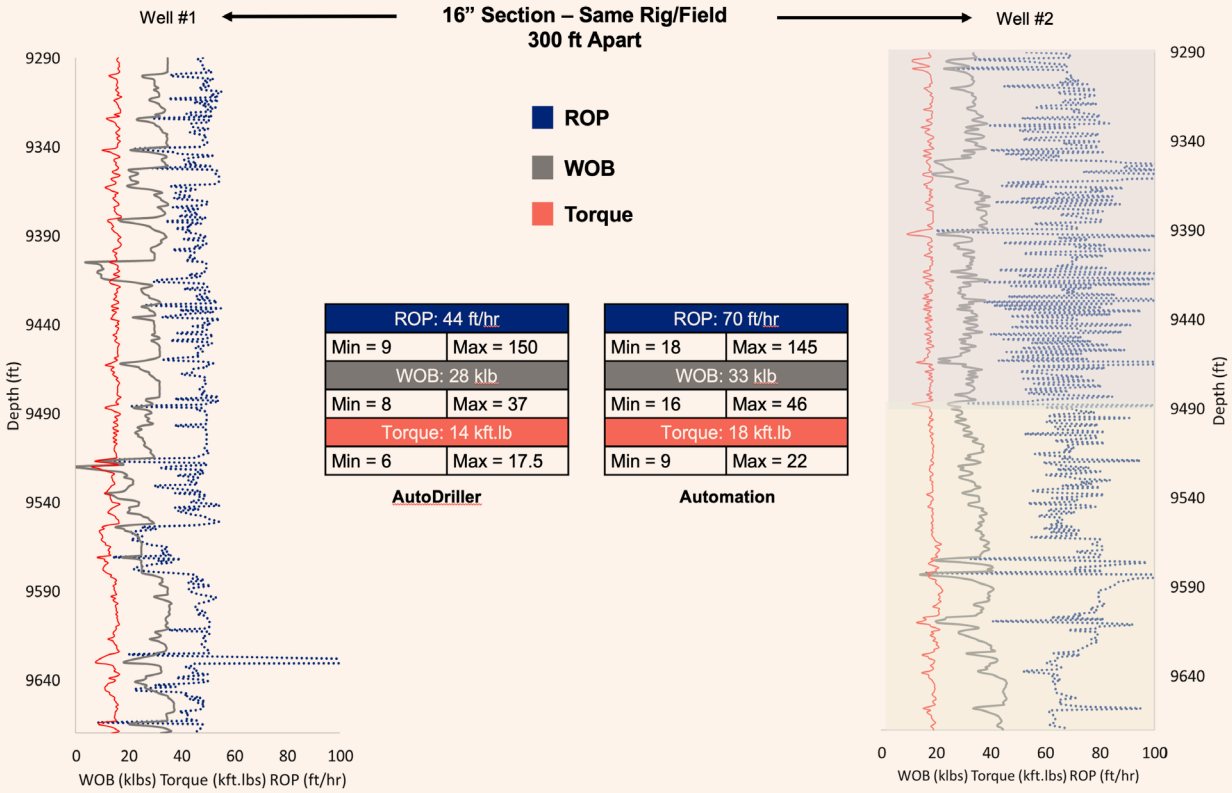

to accommodate execution.

An example of this balance of mitigation and performance is displayed in Fig. 7, which documents a stick-slip event encountered while drilling. It can be seen that as soon as the torque fluctuation reaches a threshold limit (shown in red), the automation system immediately reduces the WOB recommendation to mitigate the event. As the initial WOB reduction was not sufficient to mitigate the event, it continues to reduce the recommendation four additional times before the torque fluctuation becomes negligible.

Immediately once the event has been mitigated, the system returns to optimization and increases the recommendation to balance on the limit of performance and dysfunction avoidance. In the case that the event could not be successfully mitigated, the system would pick up the string off the bottom and briefly stop the rotation to dissipate energy before returning to the bottom to continue drilling.

In this example, the first 5⅞" section was drilled in a single run for the first time in the region. This was achieved by preserving the tools with automation long enough to finish the section. In addition, by straddling the limit of performance and dysfunction mitigation, the highest average ROP was also achieved. While in nonautomated systems, the driller suffers from exhaustion of perpetually adjusting parameters to balance at the limit. Moreover, the automation system can perform the optimization sequence hundreds of times as often as necessary to ensure that the optimal selections are chosen.

Overall, after one year in operation, a stark contrast was evident in the frequency of tool failures when comparing wells drilled with automation with wells drilled manually. As seen in Fig. 8, when comparing six consecutive wells, the total nonproductive time per well showed a dramatic reduction following the full deployment of automation, even in similar well types with identical tools.

Directional Drilling Workflows

As the majority of modern directional drilling tools communicate through telemetry (patterned parameter pulses), precise control over the drilling parameters (revolutions per minute and flow rate) is key to maintaining accurate directional control. In traditional drilling operations, the driller or directional driller is forced to manually manipulate the parameters in a specific sequence, which the downhole tool will recognize as a command. As a result of human inconsistency, such downlinks can and do often fail, forcing the driller to stop drilling, pick up off the bottom, and repeat the downlink, resulting in up to 20 minutes of lost time, Fig. 9.

In addition, downlinks while drilling presents

Fig. 7 *The stick-slip mitigation example.*

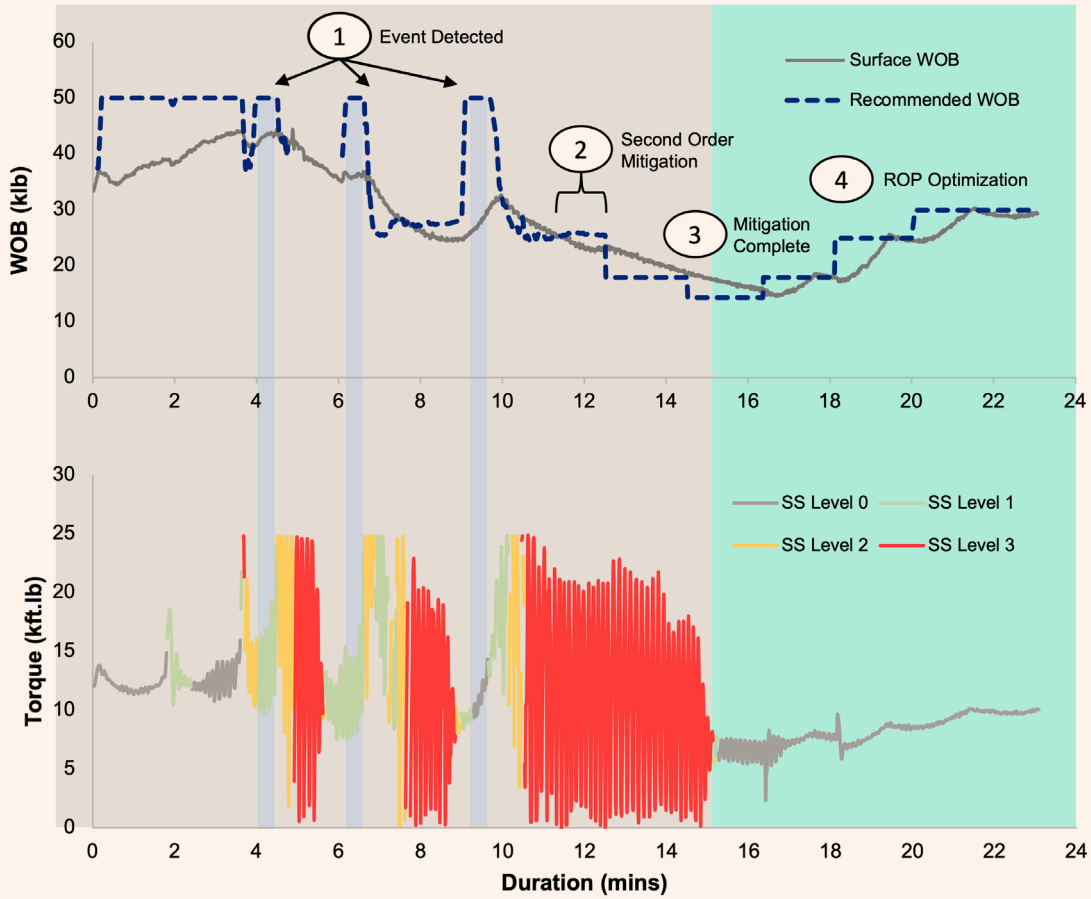

Fig. 8 *The total nonproductive time by well.*

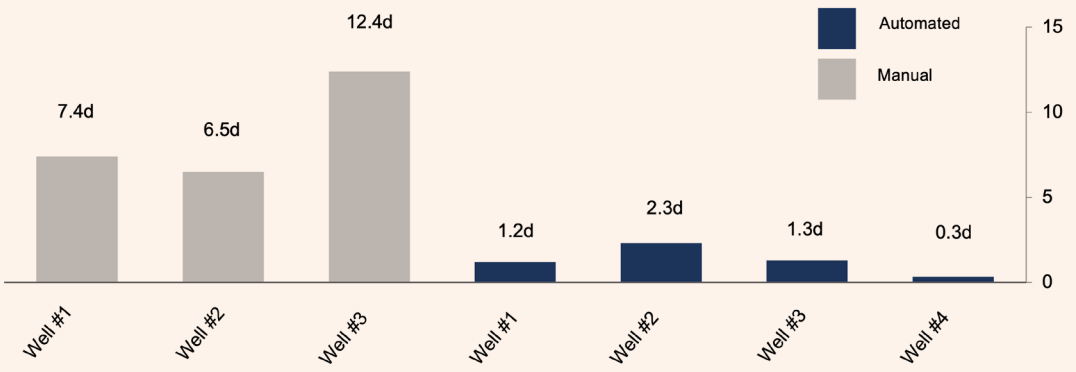

challenges for supervision. Throughout the downlinking process, the driller is occupied with frequent parameter changes and usually struggles to remain attentive to drilling operations and personnel on the rig floor. This increases the chance of safety incidents or injury. Alternatively, with automated downlinks, the command is selected from the directional driller's user interface, the driller approves the request and the system manipulates the revolutions per minute or flow rate with machine precision. As a result of the increased accuracy, it is rarely required to stop drilling while executing the sequence.

Fig. 9 *The downlinking process comparison of manual and automated drilling.*

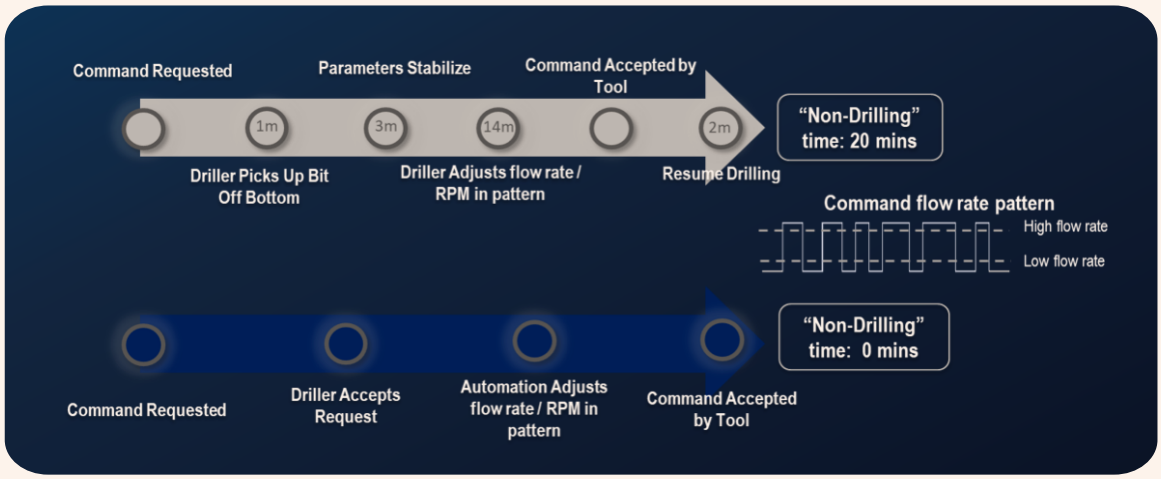

Throughout the past one and a half years since deployment in this particular project, more than 1,300 downlinks have been sent via automation with an overall success rate of 95%. This constitutes a 9% increase as compared to the field average success of 87% when the downlinks are performed manually, Fig. 10. In addition, by automating downlinks, the driller was able to perform 18% more downlinks while drilling on the bottom, contributing to less delays as a result of directional operations. Ultimately, the increased precision enabled an improved level of directional control, thereby improving the adherence to the planned trajectory, effectively maximizing wellbore quality and improving production capacity through optimized reservoir contact.

Fig. 10 *The automated downlink results compared to the field benchmark.*

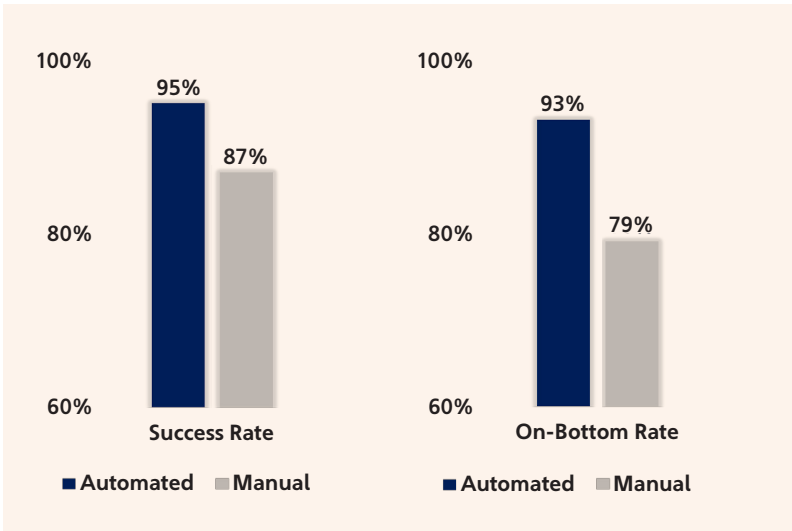

Way Forward

Throughout this proof of concept, there has been undoubtable evidence for both parties in the partnership that digitalizing the well construction process brings unmistakable value. As such, there is a deeper appetite to continue expanding the implementation and integration of digital technology into a wider scope of oil and gas drilling operations. In the immediate future, the next steps will focus on bringing deeper integration of the plan orchestration to the rig.

This means engaging multiple stakeholders across different disciplines to support operations in real-time with a suite of visualizations and intelligent tools to allow better collaboration. Advanced performance computations as well as drilling trouble detection (sticking trend, washout detection, etc.) will assist the driller and well site leader to make better decisions while offering them deeper insight on the well plan. The rig site management will also be able to leverage the cloud architecture to better record lessons learned and flag events for deeper analysis.

In the long-term for automation, the degree of autonomous drilling will expand to cover a wider range of the drilling operations, including full section automation before eventually moving into full autonomy for nearly all drilling operations. This includes additional workflows such as automated directional steering and automated tripping as well as an increased level of independence and ability to manage dynamic conditions.

Rig site and office teams will become increasingly interlinked with added opportunity for remote work. Altogether, it is clear that the value-added increases exponentially as digital modules become further interlinked, closing the space between teams.

Conclusions

As market conditions result in an increasing need to streamline operations, modern oil and gas organizations must continually be on the lookout for opportunities

to increase efficiency and productivity. This article outlines persuasive evidence for an integrated approach to well construction where stakeholders are able to collaborate more efficiently, and workflows from planning to execution can be automated. Through the digital strategies presented here, value addition will only accelerate as the distance between the office and the rig site continues to shrink.

This is not to say that it is without challenges. In a traditionally conservative industry, it is especially difficult to fully implement a system that aspires to radically change the way of operating. As such, effective change management strategies are essential in ensuring the long-term sustainability of the system. Moving forward, it is critical that the system continues to develop with the release of new functionalities, and planning operational integration. Overall, this exercise has shown convincing evidence that the future is digital for drilling.

Acknowledgments

This article was prepared for presentation at the SPE Middle East Oil and Gas Show and Conference, Manama, Kingdom of Bahrain, November 28-December 1, 2021.

References

1. Allen, H.G. and Scott, P.: "Semi-Automatic Drilling Rig," SPE paper 1378, presented at the SPE Automation Symposium, Hobbs, New Mexico, April 28-29, 1966.

2. Whitfield, S.: "Human Error: The Big Hurdle to Safer Facilities," *Journal of Petroleum Technology*, 2017.

3. Goodkey, B., Hernandez, G., Nunez, A., Corona, M., et al.: "Drilling in the Digital Age: Harnessing Intelligent Automation to Deliver Superior Well Construction Performance in Major Middle Eastern Gas Field," SPE paper 203251, presented at the Abu Dhabi International Petroleum Exhibition and Conference, Abu Dhabi, UAE, November 9-12, 2020.

4. Ouahrani, L., Haris, A.N., Suluru, S., Chiha, A., et al.: "Invisible Lost Time Measurement and Reduction Contributes to Optimizing Total Well Time by Improving ROP and Reducing Flat Time," SPE paper 192319, presented at the SPE Kingdom of Saudi Arabia Annual Technical Symposium and Exhibition, Dammam, Saudi Arabia, April 23-26, 2018.

About the Authors

Ernesto S. Gomez

B.S. in Petroleum Engineering, University Central de Venezuela

Ernesto S. Gomez is a Drilling Engineer working in Saudi Aramco's Gas Drilling Engineering Department. He has extensive drilling experience in both onshore and offshore deep gas drilling. Ernesto's experience includes extended reach directional drilling in heavy oil wells, cost control and budget analysis, oil and gas well design, generating of best drilling practices guides, on-site rig supervision, end-of-well reports and drilling operations logistics.

He has been in the oil and gas industry for over 22 years. Before joining Saudi Aramco in 2008, Ernesto gained his experience working in onshore extended directional drilling campaigns in southeast Venezuela, where he worked as an on-site Drilling Supervisor for delineation and stratigraphic wells.

Ernesto received his B.S. degree in Petroleum Engineering from the University Central de Venezuela, Caracas, Venezuela.

Ebikebena M. Ombe

M.S. in Offshore and Ocean Technology (Subsea Engineering Option), Cranfield University

Ebikebena M. Ombe is a Drilling Engineer with 16 years of oil and gas drilling industry experience. He works with Saudi Aramco's Gas Drilling Engineering Department, where he is responsible for the design, drilling and completion of gas development wells for Saudi Aramco.

Before joining Saudi Aramco in 2014, Ebikebena worked as a Well Engineer for Shell. While at Shell, he worked with both the front end well design group and the well delivery department, and was involved with the design and construction phases of numerous oil and gas drilling and workover projects. Ebikebena also worked as the regional wells directional survey focal point for Shell's Sub-Saharan Africa drilling operations.

He received his B.S. degree in Metallurgical and Materials Engineering from the Obafemi Awolowo University, Ile-Ife, Nigeria, and his M.S. degree in Offshore and Ocean Technology (Subsea Engineering Option) from Cranfield University, Bedford, U.K.

Rafael Carvalho

B.S. in Electronics Engineering, Instituto Tecnologico de Aeronautica

Rafael Carvalho has worked the last 15 years in Schlumberger, holding different positions on the Well Construction Domain. He started his career as a Field Engineer and moved up the ranks as Well Site Supervisor, Drilling Engineer, Senior Drilling Engineer, and Drilling Manager within the Schlumberger Integrated Project Management business line.

Over the last three years, driven by the Industry Digital Transformation, Rafael has been assigned to lead the deployment of digital automation solutions on all Schlumberger lump-sum turnkey projects. Recently, he has been assigned to oversee the development of DrillOps Rig Operations Solutions portfolio.

Rafael received his B.S. degree in Electronics Engineering from the Instituto Tecnologico de Aeronautica, Sao Jose dos Campos, Brazil.

Brennan Goodkey

B.S. in Mechanical Engineering, University of Alberta

Brennan Goodkey has spent the past five years working for Schlumberger in a variety of positions in upstream oil and gas. He started his career in Offshore Seismic research in the Arctic Circle before transitioning to Well Construction in the Middle East as a Field Engineer, and eventually progressing to Well Site Supervisor and Drilling & Well Engineer.

Brennan was a key contributor in the deployment of the first drilling automation system in Saudi Arabia, and he currently works for Schlumberger USA in a product management role focusing on global DrillOps Rig Operations Solutions.

Brennan received his B.S. degree in Mechanical Engineering from the University of Alberta, Edmonton, Alberta, Canada.

A First Attempt to Predict Reservoir Porosity from Advanced Mud Gas Data

Dr. Fatai A. Anifowose, Dr. Mokhles M. Mezghani, Saleh M. Badawood and Javed Ismail

Abstract /

Porosity, a critical property of petroleum reservoirs, is a key controlling factor of the reservoir storage capacity. It has been conventionally measured from core plugs. Empirical correlations, statistical, and machine learning methods have been employed for indirect estimation of porosity. The results obtained from these approaches are available only after acquisition of drilling and wireline logs. Obtaining porosity estimates in real-time, ahead of wireline logging, can help in making critical decisions and enabling early assessment of reservoir quality.

We present the results of a machine learning approach to predicting porosity from advanced mud gas data. Data sets integrating advanced mud gas data with porosity were gathered from seven wells to prove this concept. The mud gas data includes light and heavy flare gas components. Optimized artificial neural network (ANN) models were applied to the data sets and multivariate linear regression (MLR) models were used as benchmarks. Each well data set was split into training and validation subsets using a randomized sampling approach with the ratio of 70:30. A 100 parts per million (ppm) cutoff was applied to the total normalized gas.

The ANN models consistently outperformed the MLR models in all the data sets. The ANN models have training and validation correlation coefficients of up to 0.89 and 0.88, respectively, compared to an average of 0.79 and 0.77 for the MLR models. The training and validation mean squared errors (MSEs) for the ANN models are as low as 0.0135 and 0.021, respectively, compared to those of the MLR models in the range of 0.0007 and 0.03, respectively. These results indicate the nonlinearity of the relationship between porosity and the gas components. Furthermore, it can be deduced that the approach is feasible, and better results are achievable. The randomized sampling ensures that each data point has an equal chance to be used for either training or validation without bias. The cutoff applied to the normalized total gas is a standard practice to eliminate the background gas effect in the mud gas data.

This study provides an opportunity to utilize mud gas data beyond the traditional fluid typing and petrophysical correlation purposes. The presented approach has the capability to complement existing reservoir characterization approaches in providing reservoir quality assessments at the early stage of exploration. We plan to apply state-of-the-art machine learning models and perform sensitivity analysis on the gas components in the future to increase the accuracy.

Introduction

Reservoir rock properties are the various parameters that describe a reservoir. One of those that are of most interest to geologists and reservoir engineers is porosity. Reservoir rock porosity, denoted by ϕ, is the fraction of the rock volume that is occupied by the pore volume. It is mathematically defined as:

$$\varphi = \frac{V_p}{V_b} \quad (1)$$

where V_p is the pore volume and V_b is the bulk volume.

Expressing the bulk volume in terms of the two constituents of a rock, pore and grain, we have:

$$V_b = V_p + V_g \quad (2)$$

where V_g is the grain volume.

Combining Eqns. 1 and 2, we can develop a more comprehensive definition of porosity as follows:

$$\varphi = \frac{V_p}{V_b} = \frac{V_b - V_g}{V_b} \quad (3)$$

A method of determining porosity is by laboratory measurements of routine core analysis. Porosity is also estimated from wireline logs. The logs used to evaluate porosity based on theoretical or empirical considerations

are sonic, density, and neutron. Porosity, along with other reservoir properties such as permeability, rock compressibility, and total organic content, are used to determine reservoir quality.

While reservoir porosity has been estimated using empirical correlations[1], statistical correlations[2], and machine learning methods[3], the need to obtain it in real-time, ahead of wireline logging, is crucial and could help in making critical decisions and enable early assessment of reservoir quality.

This work focuses only on mud gas data at this stage of our work to achieve a more objective and possible real-time porosity prediction. Since there is no existing equation relating the mud gas components with reservoir porosity, this is a typical opportunity for machine learning application. This work is the first attempt to achieve this objective.

As a quick way to prove the feasibility of this concept, we implemented an artificial neural network (ANN) model as a nonlinear approach and a multivariate linear regression (MLR) as a linear approach to benchmark the performance of the ANN model. MLR is the method that estimates the coefficients of the linear equation involving multiple independent variables that best predict the value of a quantitative dependent variable. Details of the MLR algorithm can be found in Alexopoulos (2010)[4]. ANN is a nonlinear and machine learning-based method that emulates the brain and nervous system to model complex problems. Details of the ANN algorithm can be found in Walczak and Cerpa (2003)[5].

Mud gas data is acquired from the mud logging assembly while drilling. One of the purposes of the drilling mud pumped down at high pressure to the formation through the drillpipe is to convey the drill cuttings and other debris from the wellbore to the surface. The returned mud, mixed with liberated gases, is collected at the surface in the separator tank where it is degassed using an agitator. The gas mixture that is extracted from the mud is conveyed through a vacuum pipeline to the logging unit to be separated and measured. The logging unit is composed of the gas sampler, chromatograph, and spectrometer that separate and measure the different gas components ranging from the light to the heavy, as well as the organic and inorganic.

Methodology

Mud gas and wireline data sets from three wells were used to test the feasibility of this approach. We used the mud gas parameters from mud logging data as input and neutron porosity (NPHI) from wireline as the target parameter. The mud gas data includes 15 light and heavy flare gas components measured in parts per million (ppm), Table 1.

Table 1 *The 15 light and heavy flare gas components.*

Mud Gas Parameter	Full Name
C1	Methane
C2	Ethane
C2S	Ethane + Ethene
C3	Propane
iC4	Iso-Butane
C4	Normal Butane
iC5	Iso-Pentane
C5	Normal Pentane
C6	Hexane
C7	Heptane
C8	Octane
C6H6	Benzene
C7H8	Toluene
C7H14	Cycloheptane
TNHC	Total Normalized Hydrocarbon

From Table 2, we observe a positive linear correlation between the gases and NPHI, which agrees with the hypothesis that an increase in the volume of gas liberated from the wellbore should correspond to increase in the porosity of the rock. Given the relatively low correlation of the mud gas parameters, one of the objectives of this study is to prove the efficacy of the machine learning methodology in overcoming the limitation of the MLR algorithm. The ANN algorithm is expected to discover the hidden pattern and nonlinear relationship between the inputs and the target parameters.

As a first attempt at this new approach to porosity prediction, we use the within well training and validation method rather than the interwell. With this

Table 2 *The linear correlation of the gas components with NPHI for all wells.*

Well	C1	C2S	C2	C3	IC4	NC4	IC5	NC5	C6	C7	C8	C6H6	C7H8	C7H14	THC
1	0.35	0.32	0.39	0.38	0.44	0.40	0.47	0.36	0.17	0.37	0.30	0.32	0.35	0.40	0.37
2	0.66	0.57	0.56	0.48	0.49	0.46	0.46	0.44	0.41	0.44	0.41	0.42	0.43	0.38	0.60
3	0.29	0.30	0.29	0.27	0.29	0.29	0.28	0.27	0.21	0.23	0.23	0.18	0.09	0.19	0.27

method, each well's data set is split into training and validation subsets using a randomized sampling approach with the ratio of 70:30. A 100 ppm cutoff was applied to the total normalized gas to remove the effect of the noise as a result of the background gas from the data sets. The models' parameters were optimized to relate the mud gas variables to the NPHI in the most effective manner.

To evaluate the performance of the models, we used two complementary criteria: correlation coefficient, R, and mean squared error (MSE). The correlation coefficient measures the degree of relative trend between the actual and the predicted variables. The higher the value, the closer the trend. Equation 4 shows the calculation:

$$R = \frac{\sum(x_i-\bar{x})(y_i-\bar{y})}{\sqrt{\sum(x_i-\bar{x})^2\sum(y_i-\bar{y})^2}} \quad 4$$

where x_i are the actual NPHI values, is the mean of the actual NPHI values, y_i are the predicted NPHI values, and is the mean of the predicted NPHI values.

The MSE is the average of the squares of the difference between the actual and predicted NPHI values. MSE is a risk function, corresponding to the expected value of the squared error loss. The estimation can be seen in Eqn. 5:

$$MSE = \frac{1}{n}\sum_{i=1}^{n}(y_i - \bar{y}_i)^2 \quad 5$$

where n is the number of data points, y_i are the actual NPHI values, and are the predicted NPHI values.

Combining the R and MSE performance metrics provides the opportunity to detect instances of possible underfitting or overfitting of the models.

Results and Discussion

The metrics presented in Table 3 compares the performance of the MLR and ANN models. The same comparative performance is also shown in Figs. 1 to 3. The results show that the ANN models consistently outperformed the MLR models on all three wells, Well-1, Well-2, and Well-3.

Table 3 *A comparison of the performance of the MLR and ANN models using the R and MSE performance metrics.*

Wells	Models	Training		Validation	
		R	MSE	R	MSE
1	MLR	0.60	0.00302	0.60	0.05645
	ANN	0.84	0.00135	0.81	0.0424
2	MLR	0.63	0.00790	0.63	0.08863
	ANN	0.86	0.00331	0.84	0.06290
3	MLR	0.79	0.00078	0.77	0.02786
	ANN	0.89	0.0004	0.88	0.02106

The ANN models have training and validation correlation coefficients of up to 0.89 and 0.88, respectively, compared to an average of 0.79 and 0.77 for the MLR models. The training and validation MSEs for the ANN models are as low as 0.0135 and 0.021, respectively, compared to those of the MLR models in the range of 0.0007 and 0.03, respectively.

The performance of the ANN models indicates that its nonlinear and hidden pattern discovery capabilities are more feasible for predicting porosity from mud gas data despite the relatively weak linear correlations. It can be deduced that the novel approach for predicting porosity in real-time while drilling using only mud gas data is feasible. The randomized sampling ensures that each data point has an equal chance to be used for either training or validation without bias.

The cutoff applied to the normalized total gas is a standard practice in the mud logging community to remove the background gas effect in the mud gas data.

Conclusions

This study confirms that there is ample room in which to utilize mud gas data for reservoir characterization beyond the traditional fluid typing and petrophysical correlation purposes. ANN models were successfully used in this study to predict reservoir porosity from mud gas data. The MLR models were used as a benchmark to prove that machine learning approaches are capable of discovering hidden and nonlinear patterns in complex problems that linear models are not capable of handling.

Despite the weak linear relationships between the mud gas parameters and porosity, the ANN models consistently outperform the MLR. This leads to the following conclusions:

- The machine learning approach based on ANN is feasible where no prior existing derived relationships existed.
- This novel approach to predict porosity in real-time has the capability to complement existing reservoir characterization approaches in providing reservoir quality assessments at the early stage of exploration.
- The machine learning methodology is capable of overcoming the limitation of linear models in handling complex problems.

In our continued studies, we plan to apply state-of-the-art machine learning models and perform sensitivity analyses on the gas components to increase the prediction accuracy of the porosity.

References

1. De Mello Silva, F.G., Beneduzi, C.F., Nassau, G.F. and de Bittencourt Rossi, T.: "Using Sonic Log to Estimate Porosity and Permeability in Carbonates," paper presented at the 16th International Congress of the Brazilian Geophysical Society, Rio de Janeiro, Brazil, August 19-22, 2019.

2. Rafik, B. and Kamel, B.: "Prediction of Permeability and Porosity from Well Log Data Using the Nonparametric Regression with Multivariate Analysis and Neural Network, Hassi R'Mel Field, Algeria," *Egyptian Journal of*

Petroleum, Vol. 26, Issue 3, September 2017, pp. 763-778.

3. Gamal, H. and Elkatatny, S.: "Prediction Model Based on an Artificial Neural Network for Rock Porosity," *Arabian Journal for Science and Engineering*, 2021.

4. Alexopoulos E.C.: "Introduction to Multivariate Regression Analysis," *Hippokratia*, Vol. 14, Supplement 1, December 2010, pp. 23-28.

5. Walczak, S. and Cerpa, N.: "Artificial Neural Networks," in *Encyclopedia of Physical Science and Technology*, 3rd edition, (ed.) Meyers, R.A., Academic Press Inc., 2003, pp. 631-645.

Fig. 1 *The training and testing comparison of the MLR and ANN models on the porosity prediction for Well-1.*

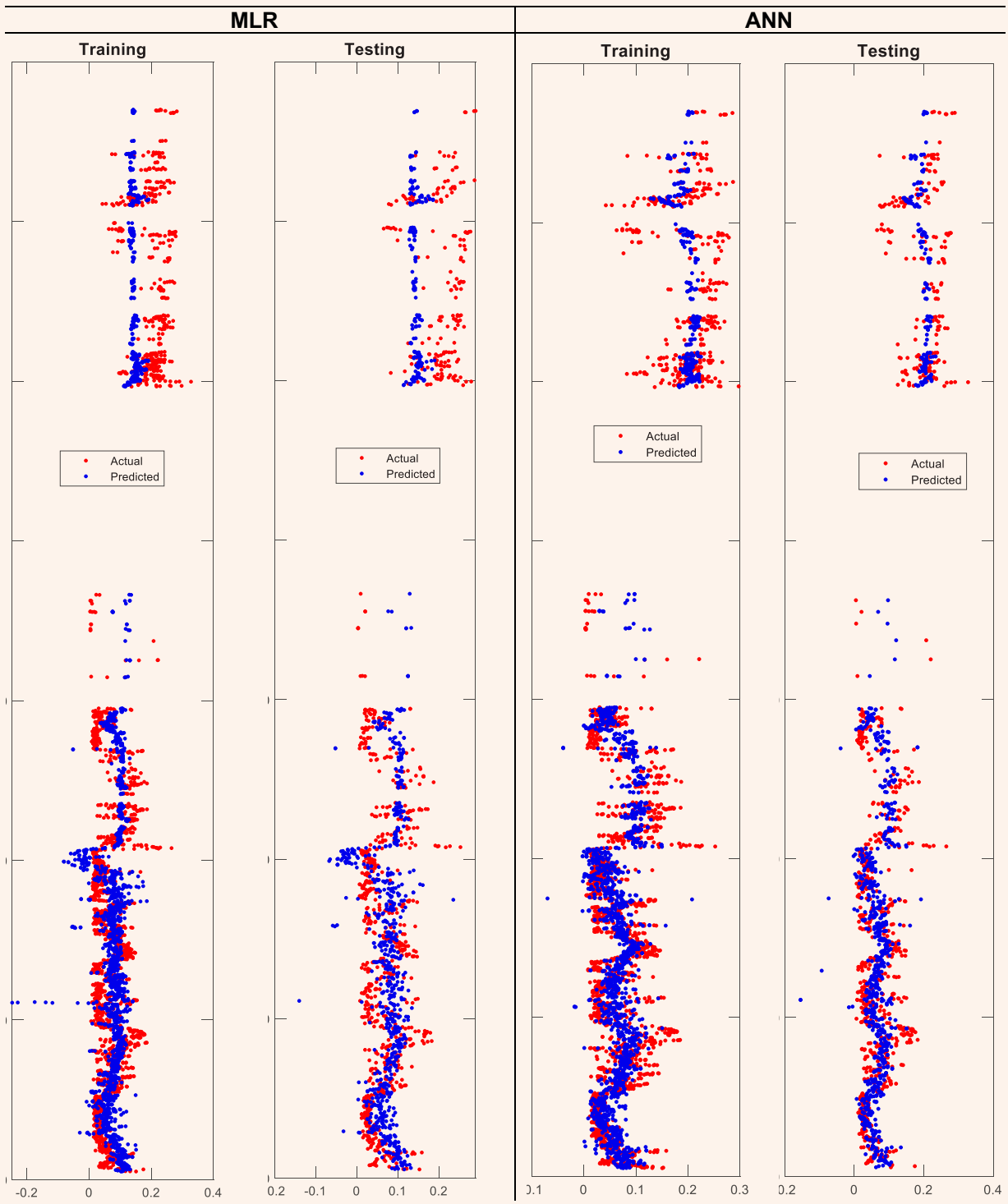

Fig. 2 *The training and testing comparison of the MLR and ANN models on the porosity prediction for Well-2.*

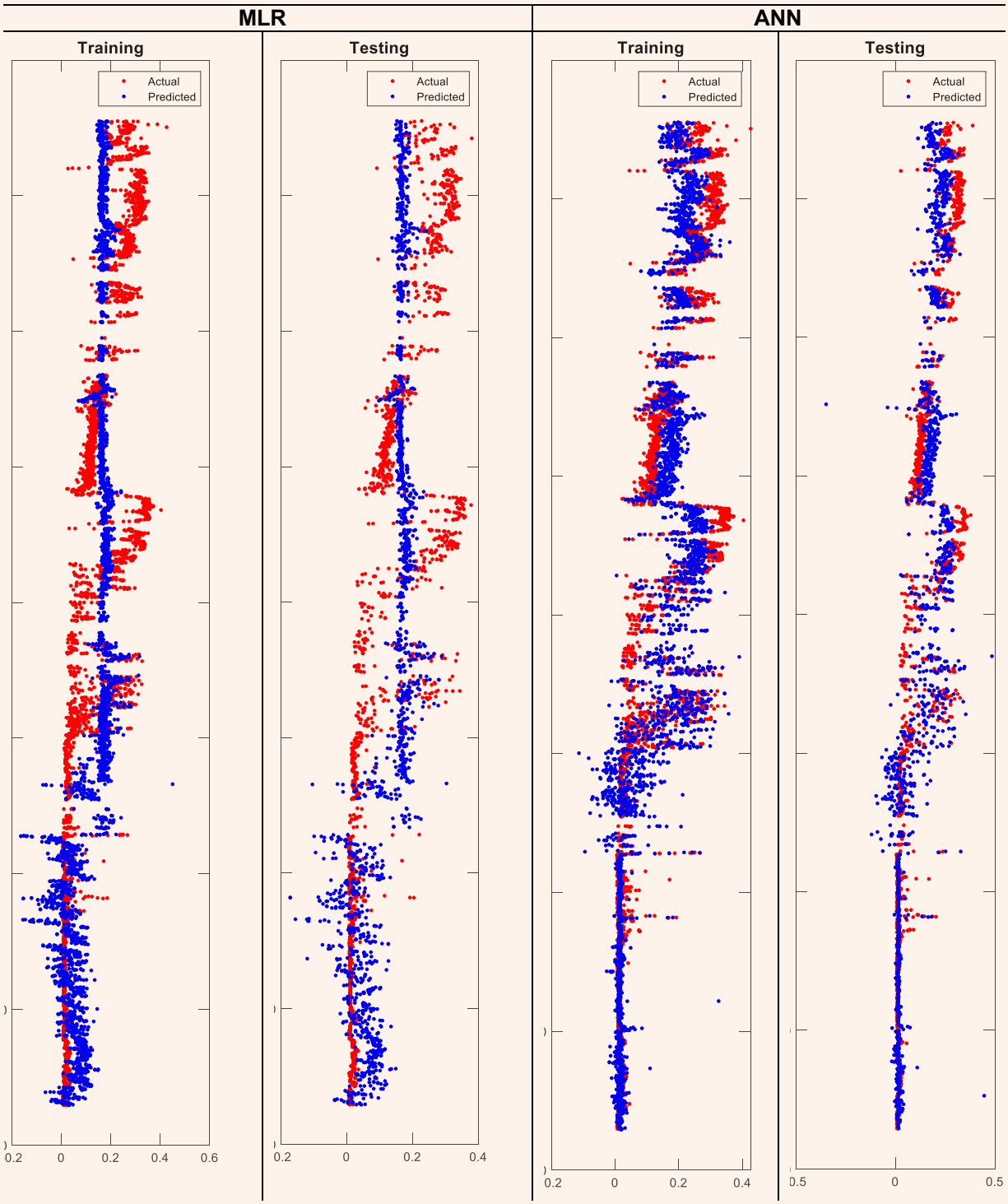

Fig. 3 *The training and testing comparison of the MLR and ANN models on the porosity prediction for Well-3.*

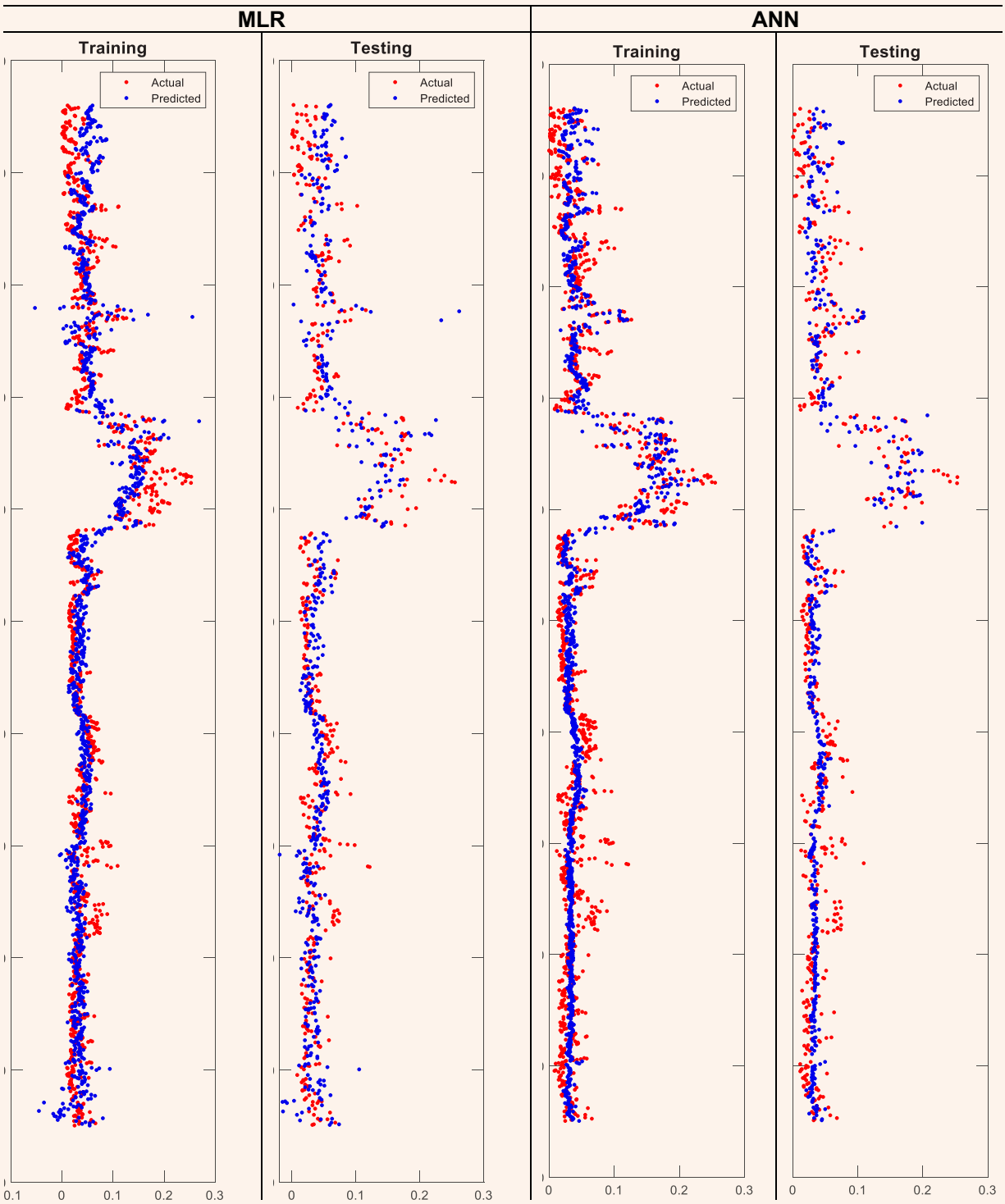

About the Authors

Dr. Fatai A. Anifowose

Ph.D. in Computer Science, University of Malaysia

Dr. Fatai A. Anifowose is a Geologist working in the Geological Operations Department of Saudi Aramco's Exploration and Petroleum Engineering Center – Advanced Research Center (EXPEC ARC). Before joining Saudi Aramco in 2015, he was a Research Engineer at the Center for Integrative Petroleum Research (formerly Center for Petroleum and Minerals), at the Research Institute of King Fahd University of Petroleum and Minerals (KFUPM) in Dhahran.

Fatai's research work focuses on automating geological, petrophysical, and petroleum engineering workflows and creating opportunities for machine learning applications to increase accuracy, improve efficiency, and enhance productivity.

He has published over 70 papers, presented over 30 presentations, and filed several patents. Fatai received the 2021 Society of Petroleum Engineers' Regional Data Science and Engineering Analytics and Service award.

In 2009, he received his M.S. degree in Information and Computer Science from KFUPM, Dhahran, Saudi Arabia. In 2014, Fatai received his Ph.D. degree in Computer Science from the University of Malaysia, Sarawak, Malaysia.

Dr. Mokhles M. Mezghani

Ph.D. in Applied Mathematics, Paul Sabatier University

Dr. Mokhles M. Mezghani joined Saudi Aramco in 2005 as a Research Science Consultant. He currently works in the Geology Technology Division of Saudi Aramco's Exploration and Petroleum Engineering Center – Advanced Research Center (EXPEC ARC). Before joining Saudi Aramco, Mokhles worked as a Research Engineer at IFP, France, on history matching and the integration of well testing, production, and 4D seismic data.

He is currently developing a suite of tools to enhance and automate the reservoir characterization and geological modeling processes. Some of Mokhles' major accomplishments include: development of a 2.5D unstructured grid for GigaPowers accounting for complex wells; software for capillary pressure estimation from conventional log data; a platform for automated thin section analysis based on image processing; an automated workflow for core description based on high resolution digital core images; and a UAV-based remote sensing platform for outcrop modeling.

Previously, his work was centered on fluid flow simulation, geological modeling, and history matching and optimization.

Mokhles received his Ph.D. degree in Applied Mathematics from the Paul Sabatier University, Toulouse, France.

Saleh M. Badawood

B.S. in Geology, University of Houston

Saleh M. Badawood is a Charge System Analyst specializing in basin modeling and petroleum system analysis. He currently works in the Regional Resource Assessment Division of Saudi Aramco's Exploration Resource Assessment Department. Saleh has over 10 years of experience in regional geology. In addition, he has experience in reserve assessment, geosteering, and well site geology.

Additionally, he acquired training in petroleum systems basin modeling from Jacobs University, Bremen, Germany.

Saleh is a member of the American Association of Petroleum Geologists (AAPG) and Society of Petroleum Engineers (SPE).

He received his B.S. degree in Geology from the University of Houston, Houston, TX.

Javed Ismail

M.S. in Petroleum Geochemistry, University of Newcastle

Javed Ismail is a Senior Geological Consultant and Charge Subject Matter Expert working in the Regional Resource Assessment Division of Saudi Aramco's Exploration Resource Assessment Department. His specialties include basin modeling and petroleum geochemistry.

Javed has over 25 years of industry experience, including work at BP and Robertson-FUGRO.

He received his B.S. degree (first class) in Geology from the University of Leeds, Leeds, U.K., and an M.S. degree in Petroleum Geochemistry from the University of Newcastle, Newcastle, U.K.

Three-Phase Saturation Evaluation Using Advanced Pulsed Neutron Measurement

Ilies Mostefai, Marie Van Steene and Ali Almulla

Abstract /

Accurately monitoring saturation change mechanisms requires adequate surveillance methods and techniques. We present a methodology to evaluate three-phase saturation using an advanced pulsed neutron measurement. This is a complex reservoir monitoring situation, where gas saturation must be monitored in addition to oil saturation, in a variable water salinity environment.

An advanced pulsed neutron logging tool provides a robust thermal neutron measurement (hydrogen index) for gas quantification. A formation capture cross section (sigma) was not used for water saturation because of its sensitivity to water salinity, which changes vertically and laterally in the subject field. The apparent volume of oil from the tool's improved precision carbon/oxygen (C/O) method provided a salinity independent indicator of oil saturation. Since this C/O apparent oil volume combines the carbon contributions from oil and gas, elemental modeling provided the apparent oil volume response to gas. The lithology information and porosity from an initial formation evaluation were also entered in a linear solver to resolve water, oil, and gas volumes.

This methodology was applied in wells where all three fluid saturations (water, oil, and gas) were expected to change over time. Surveys were taken at regular intervals over a span of several years. With the improved precision of the advanced pulsed neutron measurement, it was possible to precisely map the saturation changes with time in the field and identify variations in the fluids' volumes down to a few porosity units. This information was critical in understanding fluid movements inside the reservoir.

This is the first implementation of this technique. The precision brought by the advanced pulsed neutron tool provides superior results for monitoring a complex fluid mixture.

Introduction

The pulsed neutron carbon/oxygen (C/O) technique[1] is one monitoring technique used for water saturation monitoring that does not require prior knowledge of the water salinity in the zone of investigation. Neutron capture cross section (sigma) is acquired in parallel because it can provide additional information about the water salinity. Subsequently, it cannot be used for water saturation evaluation because the salinity in the zone of investigation is changing and unknown.

The C/O technique provides information about the oil phase because it is sensitive to the carbon. Moreover, to solve the three-phase fluid system, another measurement besides C/O is required. The hydrogen index measurement from the pulsed neutron thermal porosity is sensitive to the gas phase. Consequently, until recently, it could not be used as a quantitative measurement when gas is present in the borehole. Recent advances in pulsed neutron technology have enabled enhanced precision C/O measurements and quantitative thermal neutron porosity, even in the presence of gas in the borehole. Those advances have also enabled quantitative reservoir water saturation monitoring in three-phase systems.

Technological Advances

Rose et al. (2015)[2] recently introduced a new slim pulsed neutron tool. Based on recent technological advances, the tool uses a high performance pulsed neutron generator with a very high neutron output for greater measurement precision and a state-of-the-art scintillator, photomultiplier, and acquisition electronics. An optimized pulsing scheme permits clean separation of inelastic domains and captured gamma rays. There is simultaneous acquisition of time and energy domain data. Other advantages over previous generation technologies include much improved borehole compensation for the sigma and thermal neutron porosity (TPHI). By making use of the data acquired shortly after the neutron burst, precise measurements can be obtained even when the borehole is filled with gas or when there are many changes in completion configuration. The thermal neutron porosity from the new pulsed neutron tool is a quantitative measurement, enabling quantitative gas evaluation.

Finally, the C/O measurements from this tool benefit from a large improvement in spectral precision in the capture and inelastic domains, which allows it to deliver a precise full spectrum-based (yield) C/O ratio. The

spectral precision is much improved compared to that of the current technology, and allows eliminating the use of window data and alpha processing, as well as reducing the number of passes (in this case a reduction from 5 to 3 passes), which provides significant gains in logging efficiency. This increase in precision is essential when evaluating small oil saturation changes vs. time.

The current technology pulsed neutron tool's C/O measurement reads too high in the presence of gas in the borehole; this could be due to imperfections in the tool background measurement in the presence of gas. The "gas correction" in the current C/O technology processing was empirically derived based on early pulsed neutron data acquired in a steamflooded field where the apparent C/O volume of oil was too high in steam zones and didn't match core oil saturation without correction[5].

The presence of gas in the borehole or in the formation, including in the presence of carbon dioxide (CO_2) gas, has a minimal effect on the new pulsed neutron tool's spectral answers. For the capture spectra, there is some contribution to the spectrum of the hydrogen in the gas but it will not impact the lithology interpretation because hydrogen is not used in the closure. For the inelastic spectra, because the presence of gas in the borehole has a significant impact on the spectral shape, a special tool background standard is introduced in the spectral analysis processing to account for the borehole gas impact.

Data Interpretation Workflow

The three-phase saturation interpretation described in this article is a two-step process. The first step is to compute the apparent oil volume from the C/O data. It is an apparent oil volume because it also includes the carbon and oxygen responses of any hydrocarbon gas or CO_2 present in the formation. The standard C/O processing typically considers only the presence of oil and water because it has reduced sensitivity to fluids with low carbon density.

The next step is to account for the carbon contribution in the gas or in the CO_2, depending on the type of fluid present in the formation. The most straightforward way to account for the gas presence on the carbon measurement would be to use the carbon yield after subtraction of the inorganic carbon contribution from the matrix — total organic carbon dry weight. Accounting for the carbon in hydrocarbon gas using this method is discussed in Craddock et al. (2013)[4] but is not used in this work.

To compute a hydrocarbon gas response for the C/O apparent oil volume ($VUOI\_YLD_{gas}$), the response endpoint for hydrocarbon gas can be computed by dividing the carbon density value of the gas with the carbon density value of the oil, which would be very low.

Deriving the C/O volume of oil's response to CO_2 is more complicated because the CO_2 is contributing to both the carbon and the oxygen yields, both of which are used in the C/O ratio. This means that the same method as for the hydrocarbon gas cannot be used. To include the effect of oxygen in the calculation of the response to CO_2 of the C/O volume of oil, we ran three different nuclear modeling runs in 30 pu limestone, respectively assuming water, oil, and CO_2 in the pore space. For each of these three scenarios, we computed the ratio of carbon and oxygen number densities. The $VUOI\_YLD_{CO^2}$ (the C/O volume of oil response to a 30 pu limestone rock filled with CO_2) endpoint was computed based on the difference in the number density ratios' dynamic range between the oil and CO_2 compared with the water point. The endpoint was calculated as 0.27.

Once the gas endpoints are computed, we solve for the volumes of oil, water, and gas using a linear simultaneous solver. We require solving the following system of linear equations:

$$1 = V_{water} + V_{oil} + V_{gas} + V_{minerals} \quad (1)$$

$$TPHI = V_{oil} * TPHI_{oil} + V_{water} * TPHI_{water} + V_{gas} * TPHI_{gas} \quad (2)$$

$$VUOI\_YLD = V_{oil} * VUOI\_YLD_{oil} + V_{water} * VUOI\_YLD_{water} + V_{gas} * VUOI\_YLD_{gas} \quad (3)$$

where:

- $VUOI\_YLD_{oil}$, $VUOI\_YLD_{water}$, and $VUOI\_YLD_{gas}$ are the responses of the C/O measurement to a rock filled with oil, with water, or with CO_2, respectively.
- $TPHI_{oil}$, $TPHI_{water}$, and $TPHI_{gas}$ are the C/O measurement responses to a rock filled with oil, with water, or with CO_2, respectively.
- V_{water}, V_{oil}, and V_{gas} are the volumes of water, oil, gas, and $V_{minerals}$ are the minerals' volumes in the matrix.

The measurement inputs to the solver are the apparent oil volume from the C/O processing (VUOI_YLD in Eqn. 3) and the thermal neutron porosity from the new pulsed neutron tool (TPHI in Eqn. 2), together with their uncertainties. The porosity and mineral volumes are fixed and taken from the open hole formation evaluation performed at the time the well was drilled, Eqn. 1.

Endpoints linking the measurements to their response in pure fluids are also required inputs. Because the measurement inputs have no or little sensitivity to water salinity, the volume of water that is solved for includes both low and high salinity waters. The sigma measurement can be used to calculate the salinity of the water volume.

As with the traditional interpretation of C/O measurement, it is necessary to account for carbon present in the borehole. Fluids containing carbon can be present in the borehole both in static and flowing conditions. The current pulsed neutron tool uses shielding to focus the near detector toward the borehole while the far detector is focused toward the formation[5]. This enables

a good measurement of carbon in the borehole. The new tool does not have shielded detectors, so the borehole carbon measurement has a higher uncertainty, which can affect the fluids' volumes analysis. It is also difficult to resolve the borehole fluid volumes with conventional production logging measurements ($n-1$) because accurate measurements are required to solve for n fluid volumes.

The method we present works both in open hole and in cased holes because the measurements are robust in both environments. One could consider adding the resistivity measurement in the wells logged in Fiberglas casing and in open hole. Although, this would require solving for water salinity and the Archie parameters — cementation and saturation exponents. The saturation exponent could be changing with time, which would require the control of one more variable.

The method described here is based on the assumptions of lithology, porosity, and fluids density. Although the lithology and the porosity are not expected to change with time, the density of the fluids could change. Cement quality could also be degrading with well production. The deterioration of cement quality can affect the C/O measurement and the neutron porosity measurement if the deterioration is severe.

Field Examples

The three examples of application of the workflow described are discussed next.

Well-1

Well-1 is a cased well with Fiberglas casing. The C/O processing is done as if the well was an open hole well, with a bit size set to the casing's internal diameter. Because the well is cased, the pulsed neutron data was acquired only in shut-in mode. Figure 1 shows the time-lapse data for Well-1. Outputs of the new pulsed neutron tool (sigma, neutron porosity, and far detector C/O ratio) and the apparent volume of oil from the C/O processing are shown in the left of Fig. 1. Because gas was present in the borehole during the first time-lapse C/O pass, it resulted in an increase of the far detector C/O ratio. The interpreted volumes of gas, oil, and water are shown on the right in Fig. 1 for a selected subset of acquisition times.

From acquisition time to acquisition time, there are nearly no changes in the formation below X210 ft, and the data repeats well from pass to pass. The maximum reading difference in that zone in sigma is 0.5 cu and for TPHI it is 1.5 pu. Large variations in sigma and neutron porosity are seen above X210 ft. This is due to their high sensitivity to the presence of gas in the formation. The neutron porosity obtained in

Fig. 1 *The time-lapse data for Well-1. The fluid volumes' interpretation shows a decrease in the gas volume in one pocket at the top of the reservoir at X160 ft. There is no gas in the lower part of the reservoir below X210 ft.*

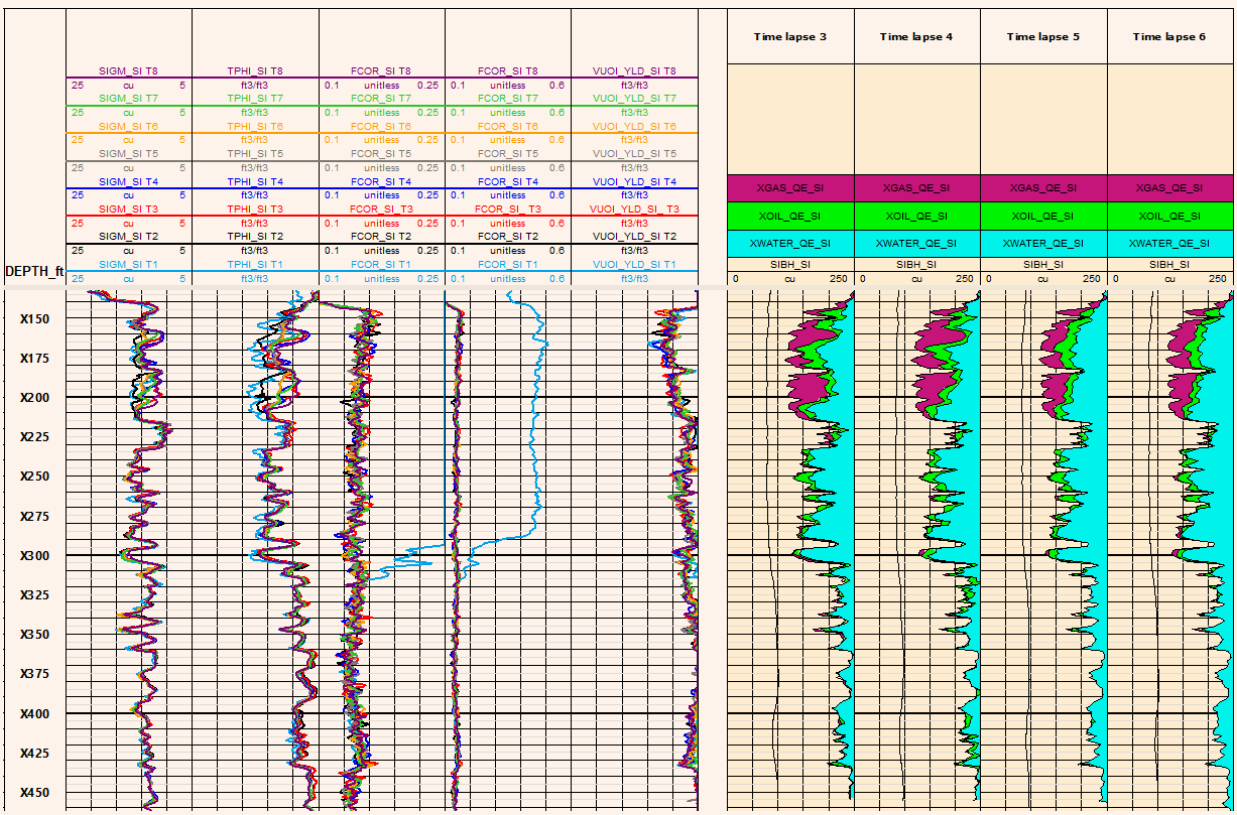

time-lapse pass 1 is not affected by the presence of the gas in the borehole. Little change is observed on the far detector C/O ratio above X210 ft, indicating that although the nature of the fluid inside the reservoir could be changing, the total carbon content does not change much.

The fluid volumes' interpretation shows for a decrease in the gas volume in one pocket at the top of the reservoir at X160 ft. There is no gas in the lower part of the reservoir below X210 ft.

We conducted a conservative uncertainty analysis on the far detector C/O data, assuming that nothing changed over the analysis section, neither in the borehole nor in the formation, and comparing data acquired at different times, with different tools, over a span of more than two years. In Well-1, the analysis is limited to the depths below X216 ft, because this is where the least change with time is expected. The maximum variation in 50% of the data is 0.015, which is 12.5% of the dynamic range at 25 pu; for 90% of the data, it is 0.023, corresponding to 19% of the dynamic range.

Well-2

The data for Well-2 is shown in Fig. 2, where a selected subset of acquisition times' volume interpretation is shown. Outputs of the new pulsed neutron tool (sigma, neutron porosity, and far detector C/O ratio) and the apparent volume of oil from the C/O processing are shown on the left. The interpreted volumes of gas, oil, and water are shown on the right for a selected subset of acquisition times. Well-2 is an open hole well. Data in this well was acquired only in shut-in conditions. Gas was present in the borehole across part of the reservoir in time-lapse passes 3, 5, 6, and 7. It was also present in the borehole above the top of the reservoir at other times.

In this well, no changes with time in sigma and neutron porosity are recorded below X250 ft. In this zone, the maximum change between acquisitions is 0.5 cu for sigma and 2.5 pu for the neutron porosity. Some changes are recorded with time between X250 ft and X165 ft. Large changes are observed above X165 ft and are linked to the change in the gas fraction present in the formation. The presence of gas in the borehole doesn't disturb the sigma and neutron porosity readings.

For the far detector C/O ratio, acquisitions with gas in the borehole must be considered separately from acquisitions without gas in the borehole. For acquisitions without gas in the borehole, changes in the C/O ratio with time are observed only above X165 ft. The

Fig. 2 *The time-lapse data for Well-2. The gas volume in the reservoir zone at X170 to X260 ft decreased over time. Moreover, the bulk of the gas is present above X150 ft. Small variations of the oil volume are observed with time.*

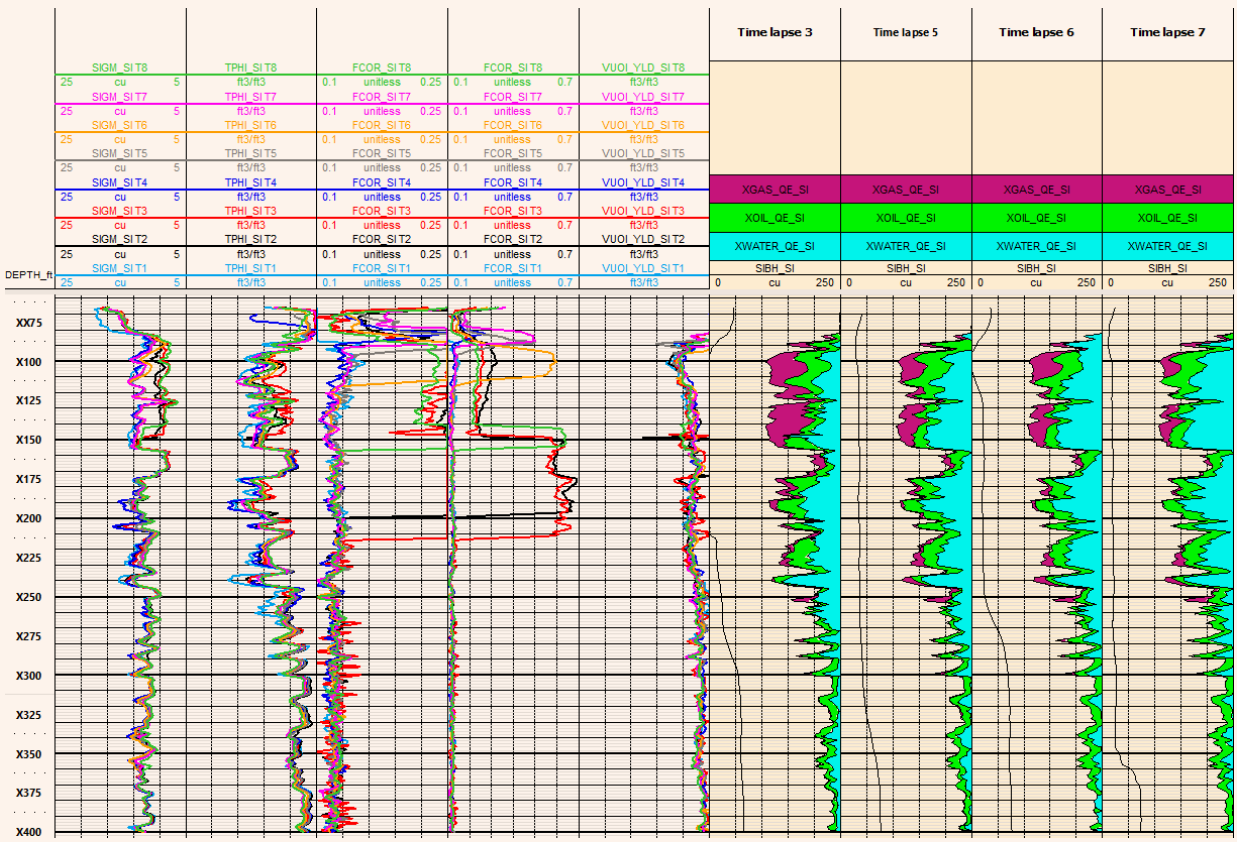

presence of gas in the borehole has a large impact on the C/O ratio and must be accounted for before interpreting the C/O ratio quantitatively.

As highlighted previously, the best way to perform the correction is to measure the C/O ratio of the borehole contribution. In the absence of this direct measurement, the nature of the fluids in the borehole and their borehole C/O contribution must be estimated. This process implies a higher uncertainty on the calculated fluid volumes than for acquisitions with water in the borehole.

Figure 2 also shows that the gas volume in the reservoir zone at X170 to X260 ft decreased over time; however, the bulk of the gas is present above X150 ft. Small variations of the oil volume are observed with time.

The same uncertainty analysis was conducted as in Well-1. In Well-2, the analysis is limited to the depths below X156 ft. The maximum variation in 50% of the data is 0.011, which is 11% of the dynamic range at 27 pu. The variation for 90% of the data is 0.019, corresponding to 19% of the dynamic range.

Well-3

Well-3 is a steel cased well. It is perforated in the zone X135 to X175 ft. Pulsed neutron data and borehole holdup measurements were acquired both in shut-in and in flowing modes. The pulsed neutron data and its interpretation results are shown in Fig. 3, with a similar format to previous presentations, except that both shut-in and flowing data sets are presented.

Outputs of the new pulsed neutron tool (sigma, neutron porosity, and far detector C/O ratio) as well as the apparent volume of oil from the C/O processing are shown on the left. The interpreted volumes of gas, oil, and water are shown on the right for a selected subset of acquisition times. Both flowing and shut-in data are shown. In time-lapse passes 2 and 3, gas is present at X140 ft, and some oil in the borehole in flowing mode had to be accounted for during the C/O processing. An increase in the oil volume of up to 5 pu is seen in the flowing pass in the interval X180 to X195 ft in the time-lapse passes 2 and 3 data sets compared with time-lapse pass 1.

There are very few changes with time on all measurements below X200 ft. In this zone, the maximum change between acquisitions is 0.5 cu for sigma and 0.3 pu for the neutron porosity. Some changes can be observed on the sigma at X215 ft after time-lapse pass 1. An anomaly can be observed on the sigma and far detector C/O ratio at X160 ft, at the base of the perforations. It is observed in both the flowing and shut-in passes and is present only after the time-lapse pass 1. No recent cement bond long is available, so it is not possible to verify cement quality deterioration, but it is possible that this anomaly is due to cement damage after large fluid production. The C/O data cannot be used quantitatively over this zone. Another anomaly at X150 ft started developing in time-lapse passes 2 and 3 compared with time-lapse pass 1. It mostly affects the far detector C/O ratio, although the sigma also shows a slight increase.

Fig. 3 *The time-lapse data for Well-3. Anomalies possibly related to cement condition are observed at X150 ft and X160 ft after time-lapse pass 1.*

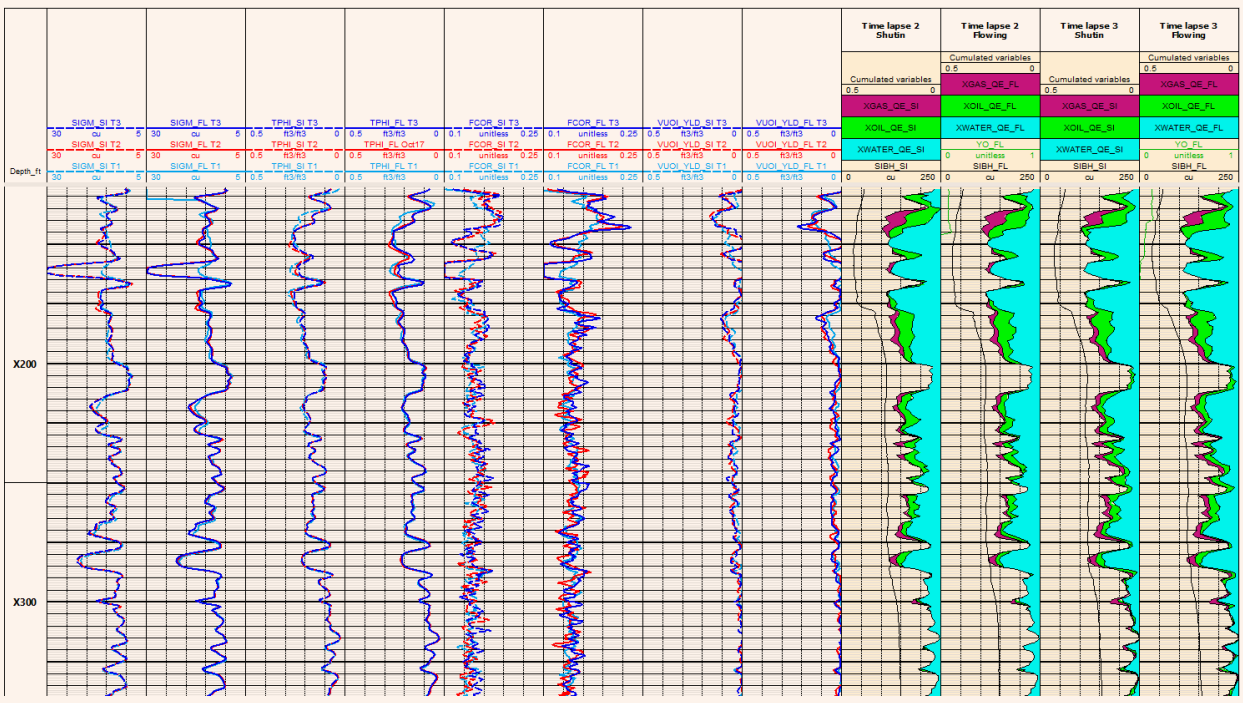

In time-lapse passes 2 and 3, gas is present at X140 ft, and some oil in the borehole in flowing mode had to be accounted for during the C/O processing. An increase in the oil volume of up to 5 pu is seen in the flowing pass in the interval of X180 to X195 ft in time-lapse passes 2 and 3 compared with time-lapse pass 1.

The same uncertainty analysis was conducted as in Wells 1 and 2. In Well-3, the analysis is limited to the depths below X170 ft. The maximum variation in 50% of the data is 0.017, which is 12.5% of the dynamic range at 28 pu. The variation for 90% of the data is 0.03, corresponding to 22% of the dynamic range.

Conclusions

Three field examples acquired in time-lapse series and in different conditions demonstrate the robustness of the new pulsed neutron measurement, in terms of repeatability and suitability to monitor saturation variations of three fluid phases in the reservoir. The gas phase monitoring was enabled by a quantitative neutron porosity measurement, providing quantitative results even in the presence of gas in the borehole. The precise C/O data enabled the monitoring of the oil volume inside the reservoir.

For each example, we conducted a conservative uncertainty analysis on the far detector C/O data, assuming that nothing changed over the analysis section, neither in the borehole nor in the formation, and comparing data acquired at different times, with different tools, over a span of more than two years. Depending on the completion type, the maximum variation in 50% of the data was included between 0.011 and 0.017 — 11% to 12.5% of the dynamic range. The maximum variation in 90% of the data was included between 0.019 and 0.03 — 19% to 22% of the dynamic range.

For the sigma measurement, the maximum variation was 0.5 cu and for the thermal neutron porosity, it is between 0.3 pu and 2.5 pu, depending on the borehole status and condition.

It is noted that an accurate borehole holdup measurement is required to interpret the C/O data when the fluids in the borehole vary. It can be a source of uncertainty when three-phases are simultaneously present in the borehole.

Acknowledgments

The authors would like to sincerely thank David Rose (Schlumberger Houston Formation Evaluation Center) and Tong Zhou (who was working at Schlumberger Houston Formation Evaluation Center at the time of this work) for their continuous support in the acquisition and interpretation of the new pulsed neutron tool data.

This article was presented at the International Petroleum Technology Conference, Riyadh, Kingdom of Saudi Arabia, February 21-23, 2022.

References

1. Morris, F., Grau, J., Hemingway, J., Plasek, R., et al.: "Introduction of Enhanced Carbon-Oxygen Logging for Multi-Well Reservoir Evaluation," paper presented at the SPWLA 40th Annual Logging Symposium, Oslo, Norway, May 30-June 3, 1999.
2. Rose, D., Zhou, T., Beekman, S., Quinlan, T., et al.: "An Innovative Slim Pulsed Neutron Logging Tool," paper presented at the SPWLA 56th Annual Logging Symposium, Long Beach, California, July 18-22, 2015.
3. Badruzzaman, A., Skillin, R.H., Zalan, T.A., Badruzzaman, T., et al.: "Accurate Oil Saturation Determination Using Carbon/Oxygen Logs in Three-Phase Reservoirs," paper presented at the SPWLA 39th Annual Logging Symposium, Keystone, Colorado, May 26-28, 1998.
4. Craddock, P.R., Herron, S.L., Badry, R., Swager, L.I., et al.: "Hydrocarbon Saturation from Total Organic Carbon Logs Derived from Inelastic and Capture Nuclear Spectroscopy," SPE paper 166297, presented at the SPE Annual Technical Conference and Exhibition, New Orleans, Louisiana, September 30-October 2, 2013.
5. Scott, H.D., Stoner, C., Roscoe, B.A., Plasek, R.E., et al.: "A New Compensated Through-Tubing Carbon/Oxygen Tool for Use in Flowing Wells," paper presented at the SPWLA 32nd Annual Logging Symposium, Midland, Texas, June 16-19, 1991.

About the Authors

Ilies Mostefai

M.S. in Electrical Engineering, University Ferhat Abbas

Ilies Mostefai is Petroleum Engineer Specialist working in Saudi Aramco's Reservoir Description and Simulation Department, where he heads the Saturation Monitoring team in the Reservoir Surveillance Petrophysics Unit. Ilies focuses on saturation monitoring techniques such as pulsed neutron and time-lapse resistivity.

Prior to joining Saudi Aramco, he enjoyed a career of 19 years at Schlumberger, holding various positions from Wireline Field Engineer to Petrophysics Domain Champion, including petrophysics software support.

Ilies received his M.S. degree in Electrical Engineering from University Ferhat Abbas, Setif, Algeria.

Marie Van Steene

M.S. in Mechanical Engineering, Universite Libre de Bruxelles

Marie Van Steene is a Principal Petrophysicist and is presently the Petrophysics Domain Champion for Schlumberger Drilling & Measurements in Saudi Arabia. She started in 2000 with Schlumberger as a Wireline Field Engineer. Marie has worked in Australia, New Zealand, and India. In 2006, she started working as a Petrophysicist in Malaysia. Marie then worked in Egypt and Kuwait, before moving to Saudi Arabia in 2016.

Her interests include formation evaluation in open holes and cased holes. Marie has been a leader of the Schlumberger dielectric and nuclear magnetic resonance special interest groups for several years.

She is currently the Vice President of Technology in the Society of Petrophysicists and Well Log Analysts Saudi Arabia Chapter committee.

In 2000, Marie received her M.S. degree in Mechanical Engineering from Universite Libre de Bruxelles, Brussels, Belgium.

Ali Almulla

B.S. in Geophysics, King Fahd University of Petroleum and Minerals

Ali Almulla joined Schlumberger in 2017, after two years as a Wellsite Geologist. He is currently working as a Petrotechnical Engineer with the Kingdom's Petrophysics team, supporting the wireline operation with a focus on reservoir saturation techniques.

In 2015, Ali received his B.S. degree in Geology from King Fahd University of Petroleum and Minerals (KFUPM), Dhahran, Saudi Arabia.

Resin Systems as an Evolving Solution within the Industry to Replace Conventional Remedial Cementing while Eliminating the Sustained Casing Pressure (SCP)

Wajid Ali, Faisal A. Al-Turki, Athman Abbas, Dr. Abdullah S. Al-Yami, Dr. Vikrant B. Wagle and Abdullateef A. Dahmoush

Abstract /

Sustained casing pressure (SCP) has been a major challenge in terms of well integrity management, all around the world. Cement is the main element that provides isolation and protection for the well. The cause for pressure buildup in most cases is a compromise of cement sheath integrity that allows fluids to migrate through microchannels from the formation to the surface. This article presents lab work and field application that support the efficiency and reliability of an innovative resin system in enhancing the wellbore's integrity.

This article also presents the development for potential wellbore isolation issues for casings utilizing surface treatments. Due to the solids-free nature and enhanced bonding characteristics, the resin system was utilized. The preparation for this job was unique due to the extremely limited injectivity rate. It was not possible to perform the job by utilizing the conventional cementing equipment, therefore, a specialized high-pressure pump with a very low pump rate capability was utilized for this unique pumping methodology. Multiple treatments were mixed and pumped as planned to achieve the desired set of results. Lab testing included thickening time tests, rheology, contamination, and compatibility testing.

Globally, conventional cement systems are often ineffective in potential remedial operations because of the high concentration of solids present within these systems. Therefore, the resin system is the best choice for this kind of potential remediation. The carefully timed setting ensured the optimum penetration and placement before the resin cured up, and ensured the potential channel became permanently sealed. The proposed solution in this article can add great value to restore the well's integrity and to save on the rig's operational cost.

The resin system is evolving as an emerging solution within the industry, replacing conventional cement in many potential crucial remedial applications. This article highlights the necessary laboratory testing, field execution procedures, and treatment evaluation methods so that this technology can be a critical resource for such potential remedial operations in the future.

Introduction

The key roles of primary cement jobs are to support casing strings and to prevent fluid movement through the annulus or into exposed permeable formations. The cement slurry must efficiently displace drill cuttings and mud from the annulus and then transition from a liquid phase to a solid phase. The resulting cement sheath should be able to withstand any future stress cycles encountered during the life of the well.

Proper cement density, composition, pre-job hole conditioning, and placement techniques must all be adequately designed to obtain a successful primary cement job[1]. The petroleum industry has long recognized that the following three factors can all contribute to a loss in annular pressure seal:

- Improper mud displacement during primary cementing.
- Formation fluids influx as the cement transitions to a solid.
- Cement sheath stress cracking during the life of a well.

If a successful primary cement job is not obtained or excessive stress damages the cement sheath during the wellbore's productive life, a costly remedial workover program may be necessary to address sustained casing pressure (SCP) or other safety issues.

Casing-casing annulus (CCA) pressure buildup is defined as the development of undesired pressure between two casing strings that is observed from casing spool outlet gate valves. The source of this pressure can be either from expansion of fluid in the annulus, due to heat when wells are put on production or from formation

where the cement sheath is cracked allowing fluids to communicate to surface[2].

This article discusses the remedial jobs that were performed on an offshore well to remediate the SCP, where a solids-free system was utilized to penetrate through the preexisting micro-channels to establish a dependable barrier against the formation fluid's influx. The resin additives are 100% made in the Kingdom, which assures their immediate availability.

Fluid Selection Methodology

A solids-free fluid with excellent bonding properties was required to be placed in the annular space to provide a dependable barrier to ensure the integrity and long-term zonal isolation. Tight injectivity conditions made the utilization of conventional cement slurry undesirable since particle laden fluids had a limited chance of penetrating and reliably sealing off the flow path. Due to solids-free nature and better bonding characteristics in comparison to conventional cement, an epoxy resin system was utilized to repair the CCA pressure by injecting the resin directly into the CCA from the surface. The carefully timed setting of resin ensured the optimum penetration and placement before the resin cured up and ensured the leak is permanently sealed.

The resin system is a compound that begins in a viscous (liquid) state and hardens with temperature and/or time. It comprises of epoxy resin(s) that crosslink when a crosslinker is introduced into the system[3-7]. The density of the base resin ranges from 66 lbm/ft^3 to 69 lbm/ft^3. With the addition of lightweight additives or weighting agents, the density can be adjusted based on the requirement. Table 1 lists the three major components of the resin. The mechanical properties of this product can be tailored to meet a variety of wellbore challenges. The resin system can withstand

Table 1 *The three components of the epoxy resin system.*

Additive	State	Function
Resin-1	Liquid	Resin blend used in all formulation
Resin-2	Liquid	Base resin component to reduce viscosity
Crosslinker	Liquid	Curing agent to control the resin's setting time

Fig. 1 *A schematic of the planned wellbore.*

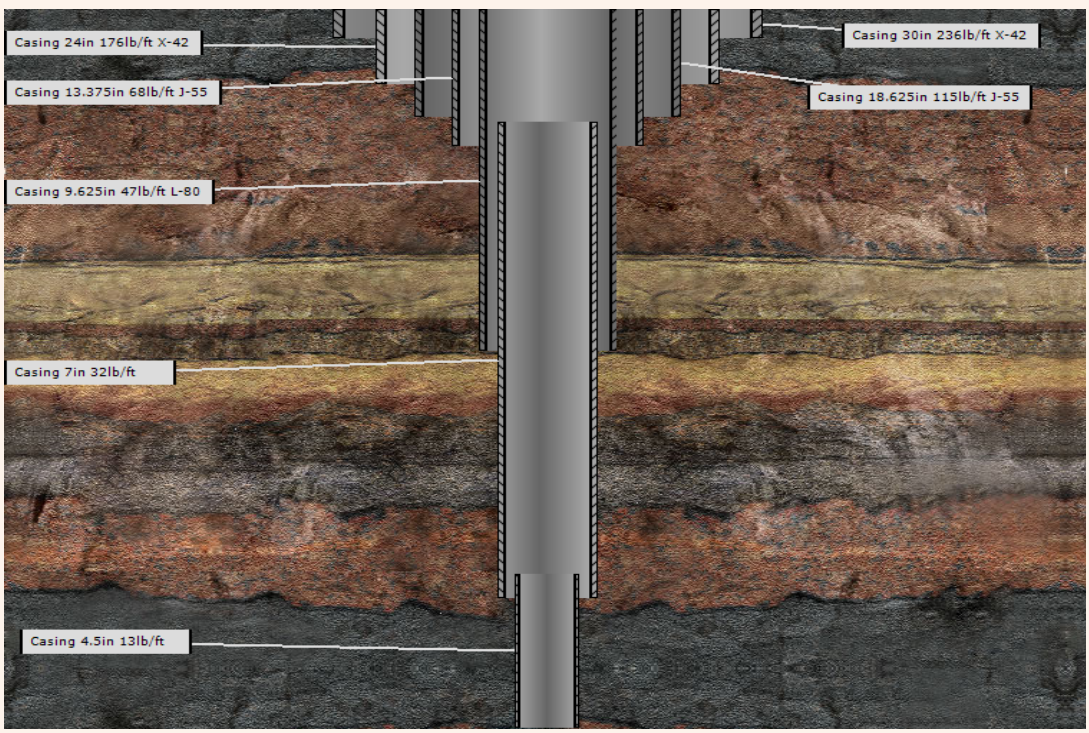

impurities in the wellbore and achieve a set state with high bond strength.

Case History

Well Information

The well was planned to be drilled as a vertical offshore well, Fig. 1, to evaluate the oil column and oil-water content for different reservoirs.

A few weeks after cementing the 7" liner, some pressure buildup was noticed inside two of the CCAs; the 13⅜" × 18⅝" CCA and 24" × 30" CCA. Once the pressure value became stable, at approximately 100 psi, then the sustained pressure in both annuli was bled off completely. Further on, both annuli were shut-in to observe the pressure buildup trend. While observing the pressure buildup trend in the annuli for a few days, it was finally concluded that three annuli were demonstrating the SCP with the following values:

- 30" casing × 24" casing — 90 psi maximum value.
- 24" casing × 18⅝" casing — 100 psi maximum value.
- 18⅝" casing × 13⅜" casing — 150 psi maximum value.

Since it wasn't possible to access any of above mentioned CCAs through downhole, it was decided to cure the CCA by injecting the suitable product directly into the CCA from the surface.

Laboratory Testing

The next step was to design a resin system with low

Table 2 *Formulations of the resin system.*

Cement/Additive	Unit	Concentration
	Formulation-1	
Resin-1	Grams	80.00
Resin-2	Grams	20.00
Curing Agent	Grams	4.00
	Formulation-2	
Resin-1	Grams	80.00
Resin-2	Grams	20.00
Curing Agent	Grams	5.00
	Formulation-3	
Resin-1	Grams	80.00
Resin-2	Grams	20.00
Curing Agent	Grams	6.00

Table 3 *The physical properties of various formulations of the resin system.*

Property	Formulation 1	Formulation 2	Formulation 3
Slurry Density (pcf)	66	66	66
Time to 100 Bc (hours)	4:44	3:50	3:15
300 rpm	95	97	100
200 rpm	64	65	68
100 rpm	28	29	30
60 rpm	15	17	18
30 rpm	6	6	6
6 rpm	3	3	3
3 rpm	2	2	2

rheology — to maximize the penetration ability — and adequate gel time (to place the resin inside the CCA without delayed or premature setting). The same set of lab equipment was used for this testing as is normally used to test the cement slurry. Three formulations with different concentrations of crosslinker were designed, Table 2 and Table 3.

While preparing the resin system, it was necessary to precisely add the crosslinker quantity to achieve the desired setting time of the resin. Additionally, the mixing of components was conducted at low shear conditions (< 2,000 rpm) to avoid the generation of any excessive heat.

It should be noted that the mentioned formulations were designed for reference only. Knowing the criticality of the job, the actual formulation to be used for the job was to be finalized based on the confirmation testing — to be performed on-site under actual ambient temperature conditions.

Table 4 *The maximum allowable squeeze pressure value.*

CCA	psi
30″ × 24″	600
24″ × 18⅝″	900
18⅝″ × 13⅜″	900

Table 5 *The collapse and burst ratings of the casings.*

Casing Details	Burst (psi)	Collapse (psi)
30″, 236 ppf, X-42	1,840	549
24″, 176 ppf, X-42	2,110	776
18⅝″, 115 ppf, J-55	3,070	1,550
13⅜″, 68 ppf, J-55	3,450	1,950

Fig. 2 *An image of the tanks used for preparing the resin system.*

Fig. 3 *An image of the high-pressure, low rate pumps.*

Fig. 4 *The control panel for the high-pressure, low rate pump.*

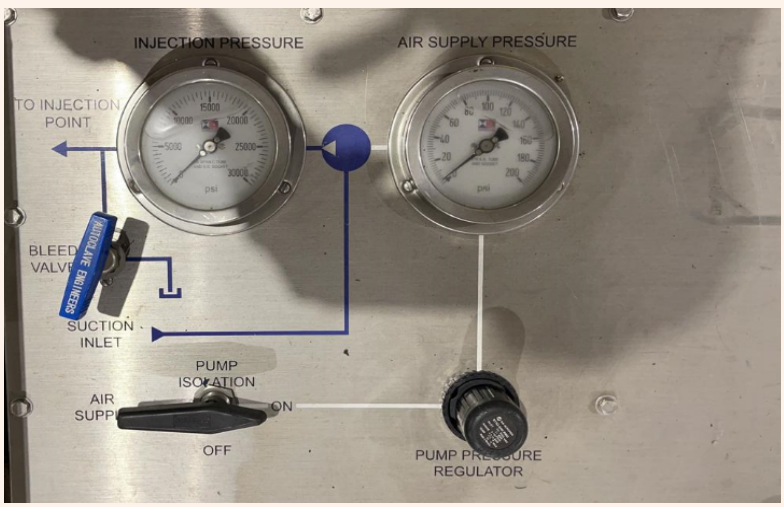

Treatment Execution

The first and foremost step toward treatment execution was to define the "maximum allowable squeeze pressure value" for each CCA. The values are defined, Table 4, keeping in mind the collapse and burst pressure ratings, Table 5.

As per the plan, the confirmation testing was performed on-site to confirm the setting time of the resin system as per actual ambient conditions prevailing on-site. The final recipe was chosen accordingly, keeping in mind the job time.

Figure 2 is an image of the tanks used to prepare the resin mixture. High-pressure, low rate pumps, Figs. 3 and 4, were utilized to pump the mixture. Special care was taken during the preparation and transfer of the resin to avoid the generation of excessive heat, which could result due to high agitation speed.

The injectivity test was performed using non-cured

resin, i.e., a mixture of resin-1 and resin-2, to confirm the fluid in-take potential of each of the CCAs. The results confirmed the potential of injectivity, therefore, further preparations were started to mix and squeeze the resin.

The next day, the first squeeze job was performed (one job on each CCA) to remediate the SCP. Figure 5 is a chart of the first squeeze job on all the CCAs. Table 6 is a summary of the resin volume injected during the squeeze treatment.

A solvent was utilized to clean the unset resin system from the equipment. Cleaning was begun as soon as the resin was drained out of the tanks. The solvent was directly added to the mixing tanks. It was ensured that the solvent cleaning fluid must contact all surfaces that contacted the resin system. Then, the solvent was moved through the pump to clean the high-pressure discharge pumps.

Post-Job Evaluation

The job was meticulously designed and executed flawlessly. For more than one year now, there has been zero SCP inside any CCA. The well's annuli pressures are under observation to validate the job's success. The combination of technology and deployment technique added great value to restore the well's integrity and to save the rig operation cost.

During the post-job evaluation session, it was also decided to pump cured resin (with a quite low amount of crosslinker) during the injectivity test. This may help to reduce the number of following treatments to completely seal the micro-channels.

Conclusions

1. Conventional cement does not always endure the mechanical stresses imposed by wellbore conditions, and it often falls short in providing permanent isolation beyond the production life of the well8.
2. Enhancing cement strategies and utilizing mechanical isolation packers should help in maintaining the well's integrity for the entire life cycle.
3. Resin should be preferred to remediate over conventional cements. The low rheology of the resin allows its deeper penetration with maximum injected volume. Also, the mechanical properties of resin allow for better wellbore integrity compared to conventional solutions.

Way Forward

Further planning and discussions are in progress to deploy the product for downhole CCA repair, i.e., by milling the casing and accessing the CCA, where feasible.

Fig. 5 *A chart of the first squeeze job on all CCAs.*

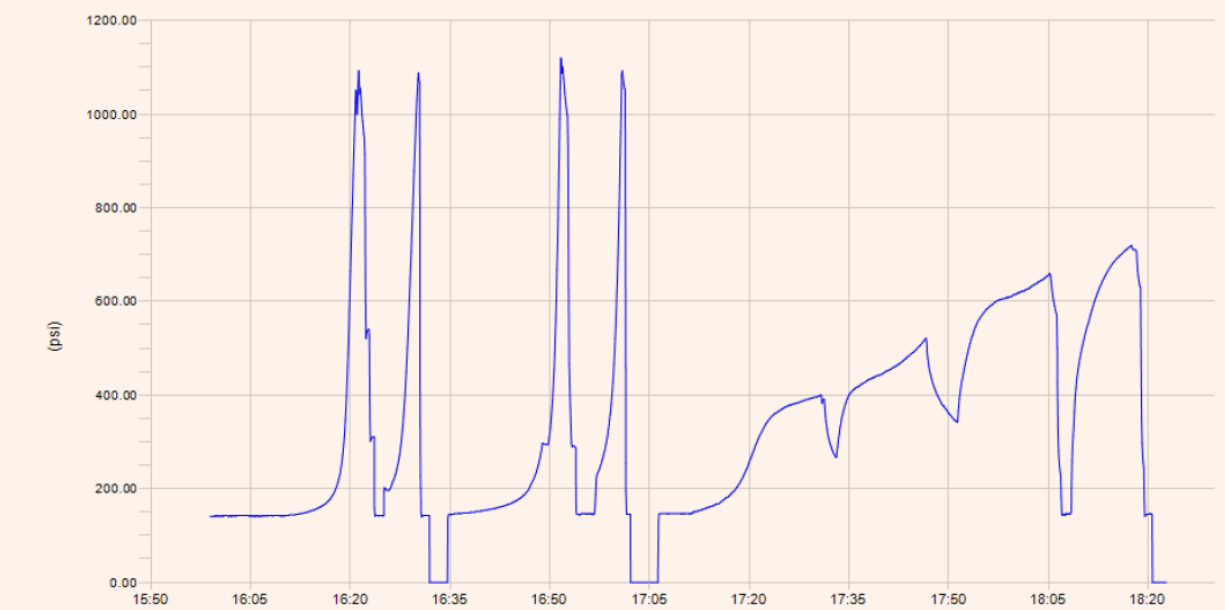

Table 6 *A summary of the cross-linked resin injection.*

	30" Casing × 24" Casing		24" Casing × 18⅝" Casing		18⅝" Casing × 13⅜" Casing	
Job #	**Volume (gal)**	**Max Squeeze Pressure (psi)**	**Volume (gal)**	**Max Squeeze Pressure (psi)**	**Volume (gal)**	**Max Squeeze Pressure (psi)**
1	7.00	600	9.00	900	7.0	900
2	6.20	600	1.30	900	2.50	900
3	0.50	600	0.75	900	1.50	900
4	2.25	600	—	—	—	—
5	0.53	600	—	—	—	—
6	0.26	600	—	—	—	—

References

1. Al-Yami, A.S., Alqam, M.H., Riefky, A. and Shafqat, A.U.: "Self-Healing Durable Cement; Development, Lab Testing, and Field Execution," SPE paper 189397, presented at the SPE/IADC Middle East Drilling Technology Conference and Exhibition, Abu Dhabi, UAE, January 29-31, 2018.
2. Alsubhi, A.M., Abduljabbar, A.M., Agazade, K. and Alyami, A.S.: "Well Integrity Improvement: CCA Preventive Actions in HPHT Offshore Gas Wells in the Arabian Gulf," SPE paper 184004, presented at the SPE Middle East Oil and Gas Show and Conference, Manama, Kingdom of Bahrain, March 6-9, 2017.
3. Alsaihati, Z.A., Al-Yami, A.S., Wagle, V.B., BinAli, A., et al.: "An Overview of Polymer Resin Systems Deployed for Remedial Operations," SPE paper 188122, presented at the SPE Kingdom of Saudi Arabia Annual Technical Symposium and Exhibition, Dammam, Kingdom of Saudi Arabia, April 24-27, 2017.
4. Elyas, O., Alyami, A., Wagle, V.B. and Alhareth, N.: "Use of Polymer Resins for Surface Annulus Isolation Enhancement," SPE paper 192266, presented at the SPE Kingdom of Saudi Arabia Annual Technical Symposium and Exhibition, Dammam, Kingdom of Saudi Arabia, April 23-26, 2018.
5. Al-Yami, A.S., Al-Jubran, M., Aswad, H. and Looni, Q.: "Innovative Epoxy Resin Formulation for Downhole Casing Repair Applications," SPE paper 193328, presented at the Abu Dhabi International Petroleum Exhibition and Conference, Abu Dhabi, UAE, November 12-15, 2018.
6. Al-Yami, A.S., Wagle, V.B., Alsaihati, Z., Mukherjee, T., et al.: "Cement Compositions Including Epoxy Resin Systems for Preventing Fluid Migration," U.S. 11,168,243, November 2021.
7. Singh, P., Al-Yami, A.S., Wagle, V.B. and Safran, A.: "Introduction to an Effective Workover Method to Repair Casing Leak," SPE paper 194654, presented at the SPE Oil and Gas India Conference and Exhibition, Mumbai, India, April 9-11, 2019.
8. Ali, W., Mata, F.J., Hashmi, A.A. and Al-Yami, A.S.: "Application of Resin-Cement Blend to Prevent Pressure Build-Up in Casing-to-Casing Annulus CCA: A Novel Approach to Improve Well Integrity," SPE paper 202103, presented at the SPE/IADC Middle East Drilling Technology Conference and Exhibition, Abu Dhabi, UAE, May 25-27, 2021.

About the Authors

Wajid Ali

B.E. in Petroleum & Natural Gas Engineering,
University of Engineering and Technology

Wajid Ali is a General Solutions Engineer for Cementing at TAQA Well Services in Saudi Arabia. He has been associated with the oil field industry for 15 years. Wajid's experience includes work with leading oil field service companies while promoting and implementing new technologies.

His current research interests include optimizing cement slurry designs without compromising the wellbore integrity, and focusing on mechanical properties improvement.

Wajid has registered six technical publications in the Society of Petroleum Engineers (SPE) library related to wellbore integrity assurance and zonal isolation. He is a longtime member of SPE.

Wajid received his B.E. degree in Petroleum and Natural Gas Engineering from the University of Engineering and Technology, Lahore, Pakistan.

Faisal A. Al-Turki

B.E. in Chemical Engineering, Yanbu' Industrial College

Faisal A. Al-Turki works as a Middle East North Africa (MENA) Well Cementing Director at TAQA Well Services in Saudi Arabia. He has 18 years of oil field experience, mainly working with Saudi Aramco.

Faisal is the author of four technical publications related to wellbore integrity and zonal isolation.

He received his B.E. degree in Chemical Engineering from Yanbu' Industrial College, Yanbu', Saudi Arabia.

Athman Abbas

B.S. in Mechanical Engineering, University of Technology and Science

Athman Abbas is a Cementing Technical Manager for TAQA Well Services in Saudi Arabia, covering cementing operations for Saudi Aramco Drilling & Workover. During his 25 years of experience in the oil field, Athman has worked as a Design and Evalutation Service for Client Engineer for big drilling operators such as Shell, Oxy, BP, and Hess, and gained extensive expertise in deep-water wells, shallow gas wells, steam injection wells, high-pressure and high temperature environments, and horizontal extended reach wells.

With his previous employer, Athman was a Geo-Market Technical Manager contributing to their success in cementing work around the globe, and participated heavily in promoting and implementing new technologies that brought value to many customers, including from ultra-lightweight to extreme heavy weight cement slurries, gas tight slurries, flexible slurries, and steam injection high temperature slurries.

He received his B.S. degree in Mechanical Engineering, University of Technology and Science, Boumerdes, Algeria.

Dr. Abdullah S. Al-Yami

Ph.D. in Petroleum Engineering, Texas A&M University

Dr. Abdullah S. Al-Yami is a Senior Petroleum Engineering Consultant with the Drilling Technology Team of Saudi Aramco's Exploration and Petroleum Engineering Center – Advanced Research Center (EXPEC ARC). He has 24 years of experience with Saudi Aramco and previously worked in different positions, including as a Lab Scientist and Drilling Engineer, conducting research related to drilling engineering.

Abdullah has received several awards during his career, including Saudi Aramco's Research and Development Center (R&DC) Innovation Award and its Successful Field Application Award for his research work. He also received Saudi Aramco's EXPEC ARC Effective Publications Award. A member of the Society of Petroleum of Engineers (SPE), Abdullah was awarded the 2009 SPE Outstanding Technical Editor Award for his work on the SPE *Drilling and Completion Journal*. He also received the 2014 SPE Regional (Middle East, North Africa and South Asia) Drilling Engineering Award, and both the 2015 and 2016 CEO Saudi Aramco Excellence Award. In 2016, Abdullah received Oil & Gas Middle East Award "highly commended" recognition in the category of internal control valve (ICV) Strategy of the Year for his efforts in developing drilling products utilizing a local resources strategy. In 2017, he was awarded the Saudi Arabian Board of Engineering Award.

Abdullah is a coauthor of the textbook *Underbalanced Drilling: Limits and Extremes*; he has 127 granted U.S. patents and 152 filed patents; and has more than 100 publications to his credit, all in the area of drilling and completions.

Abdullah received his B.S. degree in Chemistry from Florida Institute of Technology, Melbourne, FL; his M.S. degree in Petroleum Engineering from King Fahd University of Petroleum and Minerals (KFUPM), Dhahran, Saudi Arabia; and his Ph.D. degree in Petroleum Engineering from Texas A&M University, College Station, TX. Abdullah is currently a Chemistry Ph.D. candidate at KFUPM majoring in Organic Chemistry and Polymer Synthesis.

Dr. Vikrant B. Wagle

Ph.D. in Surfactant and Colloidal Science, Mumbai University Institute of Chemical Technology

Dr. Vikrant B. Wagle is a Science Specialist with the Drilling Technology Team of Saudi Aramco's Exploration and Petroleum Engineering Center – Advanced Research Center (EXPEC ARC). His experience revolves around the design of novel, environmentally friendly drilling fluid additives and the development of high-pressure, high temperature tolerant drilling fluid systems.

Vikrant has 50 technical publications and 120 granted U.S. patents, and he has filed several other U.S. patent applications, all in the area of drilling fluids, cementing, and loss circulation.

He received his M.S. degree in Chemistry from the University of Mumbai, Mumbai, India, and his Ph.D. degree in Surfactant and Colloidal Science from the Mumbai University Institute of Chemical Technology, Mumbai, India.

Abdullateef A. Al-Dahmoush

M.S. in Petroleum Engineering, King Fahd University of Petroleum and Minerals

Abdullateef A. Al-Dahmoush works as Gas Drilling & Workover Operation Superintendent with the Gas Drilling Division of Saudi Aramco's Gas Drilling & Workover Department. He has 15 years of experience with Saudi Aramco and previously worked in various positions in engineering and operations.

Abdullateef received his B.S. degree in Applied Mechanical Engineering from King Fahd University of Petroleum and Minerals (KFUPM), Dhahran, Saudi Arabia, and his M.S. degree in Petroleum Engineering from KFUPM.

Fit-for-Purpose Rotary Steerable System at Bit with Continuous Survey while Drilling Improves Challenging Drilling Operations and Well Placement

Saadaldin O. Al-Husaini, Salahaldeen S. Almasmoom, David B. Stonestreet, Khalid S. Al-Malki and Jamal S. Alomoush

Abstract /

Standard surveying technologies, including measurement while drilling and rotary steerable systems (RSS), with multiple drilling bit choices, were initially used to drill 8⅜" curved and lateral sections with limited and varied results. In an effort to improve upon these inconsistent results, which negatively impacted well delivery performance, a new RSS at bit (RSSAB) and continuous survey while drilling (CSWD) tool were introduced to drill a combined vertical, curved, and lateral section in one run to deliver a smooth wellbore with higher build rates in the curve, and faster overall drilling performance. This article presents the continuous improvement seen from the onset of the first application of the RSSAB and CSWD tool, which continues to the present day.

Using specific digital modeling, the RSSAB integrated both the steering and cutting structure to achieve a more optimum well trajectory while at the same time delivering better drilling performance. The RSSAB was engineered with: (1) pistons close to the cutting structure, (2) automated trajectory control with continuous six axis inclination and azimuthal measurements, and (3) azimuthal gamma ray measurements close to the cutting structure. This new RSSAB eliminated the previous practice of reducing drilling parameters to achieve required build rates and to counter the turning tendency in the curve and lateral sections. This improvement enabled drilling with higher rates of penetration (ROP) in the curved section, plus achieving higher dogleg severity (DLS) in the curve, and also drilling a longer lateral section in one run with less tortuosity.

The CSWD tool was introduced to decrease surveying time and improve well placement accuracy. Excessive time was required when using conventional survey techniques, where surveys were taken every 95 ft during connection, and associated weight-to-weight connection time varied from 10 to 15 minutes per stand. This time was needed to free any trapped torque prior to taking the survey, recycle pumps, and wait for the survey to be transmitted and quality checked on the surface. With new CSWD capability, time was eliminated as this function provides accurate six axis surveys continuously while drilling, thereby eliminating all related survey activity steps from the operation. The increase in the number of surveys obtained while drilling also enhances well placement and the true vertical depth definition for each well drilled.

Introduction of fit-for-purpose RSSAB technology for the first time internationally, outside the U.S., and CSWD technology for the first time worldwide, has taken drilling performance to a new level, provided improvement in drilling performance, accuracy in well placement, and associated cost reduction. In a short period of time, the drilling performance improved dramatically, and the top five wells with the vertical, curved, and lateral sections drilled in one run had the highest average ROP. In addition, this newly deployed RSSAB and CSWD bottom-hole assembly (BHA) achieved:

- The field record for the longest lateral footage drilled in one day.
- The fastest time from spud to total depth (TD).
- The fastest time from spud to rig release.

Introduction

Well designs are normally enhanced to maximize efficiency gains through combining multiple well phases with an optimized number of casings and bottom-hole assembly (BHA) runs. In common cases, this would require a drilling technology capable of drilling vertical, high build rate curve and lateral intervals with superior directional control. On the continuous optimization efforts, drilling personnel strive to improve well delivery time and productivity. As a standard, the well design consists of four hole sections: 22", 16", and 12" vertical sections, as well as the 8⅜" hole size with a vertical section at the start, a 3D curve section to landing point and

an extended lateral in a low relief structural setting.

The lithology variation is one of the main challenges to drilling operations. The vertical 8⅜" section is comprised of a thick body of anhydrite with a hydrogen sulfide water-bearing limestone stringer. Going deeper, the section changes to fractured dolomitic limestone reservoirs with high porosity and permeability, which often pose a high risk of partial or total loss of circulation. The 8⅜" curve section kicks off in a zone of multiple layers of argillaceous limestone with a higher clay content that would normally lower the build rate. Subsequently, the section changes lithology to an anhydrite stringer that overlies a poor quality carbonate reservoir toward the middle of the curve.

As the well reaches the landing point, the rock properties change to overpressured mudstones with an ultra-low permeability and presence of natural fractures, Fig. 1.

The 8⅜" section consumed most of the well time (10 to 14 days) since it required two to three different BHAs for drilling. The first assembly was a motor configuration to drill the vertical interval of the section, then the curve interval was to be combined with the lateral interval in another run if the dogleg severity (DLS) requirement is below 6°/100 ft. To allow drilling the curve and lateral intervals in one run, the DLS was limited in the curve interval to below 6°/100 ft to make up for the potential drop in the buildup rate at the limestone/clay zone in the top of the curve interval. The kickoff point (KOP) was designed at the lower part of the depleted carbonate zone, which induced a risk of opening some existing fractures when starting to kickoff, sometimes causing severe loss of circulation.

In many cases, drilling a combined curve and lateral interval in one run was not possible due to the requirement of a higher DLS caused by the limestone/clay zone's low buildup rate even with controlled drilling parameters. Therefore, a dedicated high build rate assembly was required to drill the curve section, followed by a conventional rotary steerable system (RSS) to drill the lateral interval. The lateral interval was drilled with geosteering in thin brittle to ductile carbonate layers that caused a walking tendency, which reduced the drilling performance. Close trajectory control was required to reduce tortuosity and allow for the completion to reach bottom.

The drilling operations of the 8⅜" section clearly benefited from further optimization in well design, the number of BHA runs, and the drilling performance with better trajectory control, which led to a well delivery improvement and cost reduction.

This article will provide an overview of new RSS at bit (RSSAB) and continuous survey while drilling (CSWD) tool technology implementation journey with proven benefits and applications.

Technologies Overview

The RSSAB technology is designed with an actuating system that is placed with strategic precision to push against the borehole wall for propulsion[1]. This actuating system has pistons, which are located as close to the bit cutting structure as possible, which aid in better control for directional changes (planned and unplanned), helping to achieve higher build rates with

Fig. 1 *A standard well design and formation overview.*

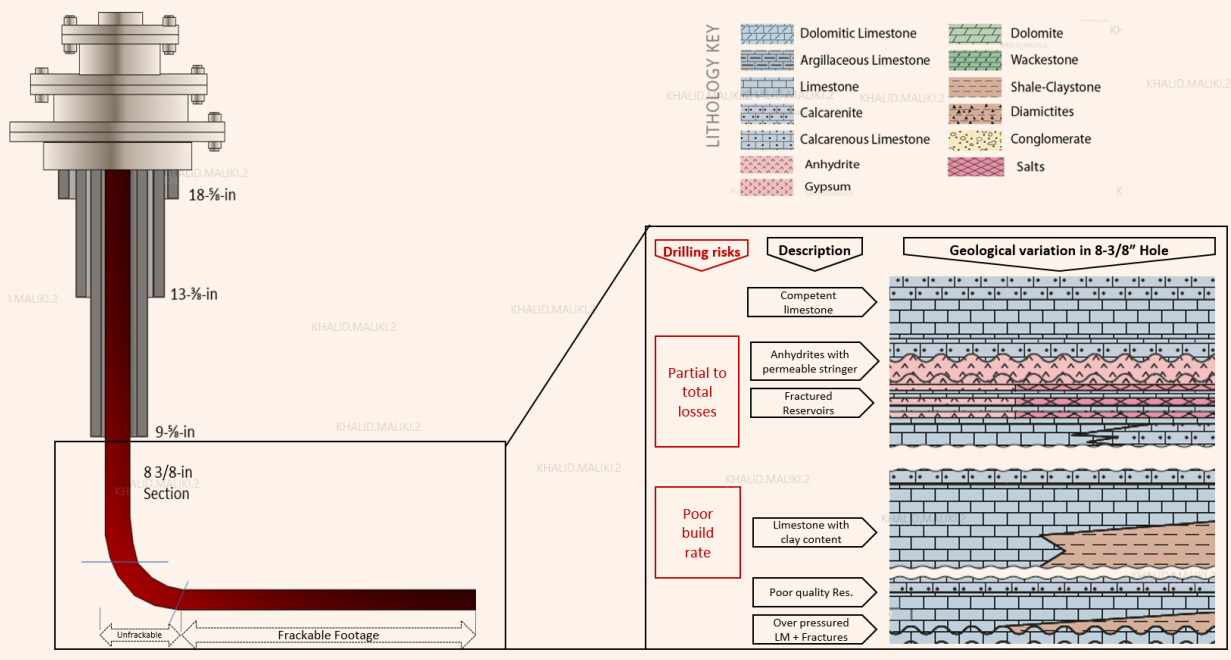

no additional hydraulic force[1].

This improvement enabled drilling with higher rates of penetration (ROP) in the curve section with higher DLS and longer lateral section in one run with less tortuosity. In addition, the RSSAB steering unit incorporates metal-to-metal hydraulic seals, which reduce erosion and increase hydraulic design capability for improved performance. It is adapted with specialized single shoulder connections to increase reliability during high DLS drilling. These connectors also enable compatibility with polycrystalline diamond compact application specific cutting structures[1]. The combination of the RSSAB system with the specially designed bits deliver combining the vertical, curve, and lateral sections with improved drilling efficiency.

The RSSAB technology itself is designed with a built-in multiaxial sub to deliver the capability to measure the comprehensive six axis continuous inclination and azimuth. Smoother wellbores with reduced tortuosity can be achieved because of the ability to automatically hold inclination and azimuth measurements[1]. An azimuthal gamma ray sub can be added to the RSSAB tool, and can be positioned close to the bit — approximately 6 ft behind the bit. The additional sub provides real-time early signs of changing lithology, allowing better real-time well placement, improved in-zone percentage, and better geosteering within the target zone sweet spot[1].

Figure 2 is a diagram showing the RSSAB technology.

The CSWD tool technology allows taking continuous, accurate, and definitive directional surveys on the bottom while drilling ahead with full parameters, and has a similar quality to the previous static surveys. In addition to the CSWD capability, the CSWD tool technology is designed with an additional three-axis real-time shock and vibration with turbine power, allowing more accurate real-time shock and vibration data transmission to the surface, as the tool is capable of a high speed telemetry up to 20 bps. In addition, geological accuracy is refined using gamma ray and electromagnetic resistivity in combination with the continuous six-axis directional and inclination sensors. These features help with the early reaction to potential drilling risks, and improve the overall drilling efficiency[2].

RSSAB and CSWD Fit-for-Purpose BHA Implementation Journey

The project evaluated different performance challenges in its 8⅜" hole size of the well, its longest section. The challenges were categorized in five areas. First, the section required multiple BHAs to drill the different vertical, high DLS curve, and long lateral intervals. Second, the vertical interval drilled through different formations with high laminated layers and utilized dedicated stand-alone BHA motors where formation tops were picked based on ROP changes.

Third, the curve interval is a 3D profile that requires high DLS with azimuthal control to land the well in an ultra-thin sweet spot, and some formation lithologies in the curve cause a drop tendency, which limit the conventional RSS building capability with azimuthal control. Therefore, this interval utilized controlled parameter drilling. Close to the landing point, several surveys were taken off the bottom to confirm the wellbore's position.

Fourth, the downhole lateral interbedding required control on drilling parameters to manage formation tendencies. Fifth, the reservoir required geosteering capabilities to allow for downhole near bit measurements to maintain in the ultra-thin sweet spot with a maximum of a 50 ft azimuth window. These challenges resulted in multiple trips, controlling of the ROP, and affected completion runs. Different strategies combined with new technologies were required to manage these inefficiencies and challenges.

Collaboration was essential to introduce and adapt the RSSAB technology (first deployment of the RSSAB in

Fig. 2 *A diagram showing the RSSAB technology[1].*

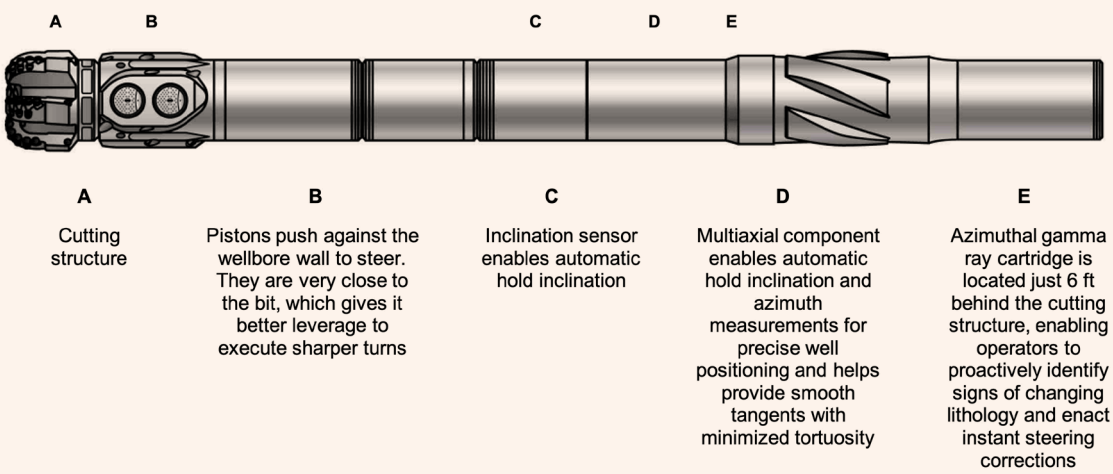

the Middle East) and CSWD technology (first worldwide deployment of the CSWD technology). The collaboration focused on BHA optimization, cutting structure design, modeling and adaptation to the environment, equipment design upgrades for downhole conditions, and well design and configuration changes.

Modeling of BHA and Cutting Structure

The BHA dynamics and stability is a major area that impacts the performance of the newly introduced RSSAB assembly. The BHA and cutting structure went through multiple iterations and modeling rounds to evaluate the different stabilization requirements, bit structure configuration and bottom-hole components. A total of three different BHA configurations, including the cutting structure, were modeled against the conventional BHA with full drilling dynamics analysis and finite element models. This helped to optimize final designs for the fit-for-purpose (RSSAB and CSWD) BHA.

In addition, modeling revealed the right BHA configuration and cutting structure that minimized the downhole dynamics of the assembly while maximizing drilling performance with the optimum drilling parameters. Figure 3 illustrates the BHA configuration journey with the final fit-for-purpose BHA. Figure 4 illustrates the RSSAB cutting structure design journey with the final cutting structure selected for the BHA.

Equipment Design Upgrades

The drilling environment includes multiple interbedding layers with compressive strengths up to 20,000 psi. This tends to induce high shock and vibration to the drilling assembly, which proved that the drilling environment is more challenging than in the U.S. To manage this geological challenge, a dedicated team from the product centers worked on enhancing the mechanical components of the technology to strengthen the piston retention mechanism and abrasion resistance. These improvements were critical to adapt the technology to the current drilling environment, Fig. 5.

The improvements are summarized by adding an anti-rotation plate to reduce the wear on the retaining rings, installing a pin cover to prevent the failed retaining rings from falling into the wellbore, and utilizing a stronger more robust material for the retaining rings.

Section Size Change and Wellhead Configurations

The RSSAB was designed for an 8½" hole section while the current well design is for an 8⅜" section. To implement the fit-for-purpose BHA, a change in hole size was required from 8⅜" to 8½".

Two engineering considerations needed to be studied and mitigated. First, tubular sizes placed in the 9⅝" casing had to be considered. A 9⅝" T-95 diverter valve with a packer is installed as part of the 9⅝" casing string and placed inside the previous 13⅜" casing. The maximum bit size to drill out this tool is 8.510", which is very close to the modified section size. Drilling out the diverter valve requires careful planning and execution to avoid damaging the bit, RSSAB and/or RSS tool.

The second challenge was the internal diameter of the 9⅝" fluted mandrel hanger of the wellhead. One of the typical internal diameters of the 9⅝" fluted mandrel hanger was 8.45", which would not allow the 8½" bit to pass through. A scope of work to enlarge the internal diameter of the 9⅝" fluted mandrel hanger to 8.55" was created after confirming that the reduced

Fig. 3 *The final fit-for-purpose BHA design improvement journey.*

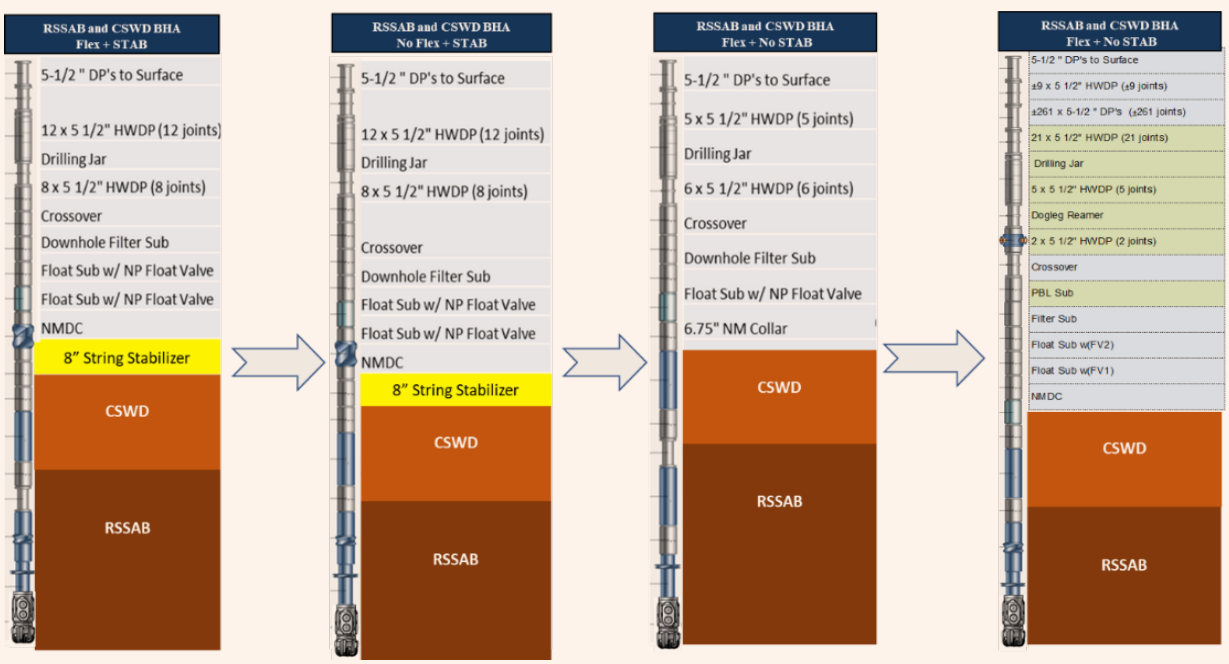

Fig. 4 *The RSSAB cutting structure design journey to Model #3 (extra blade added, more cutters added, with optimized nozzle placement).*

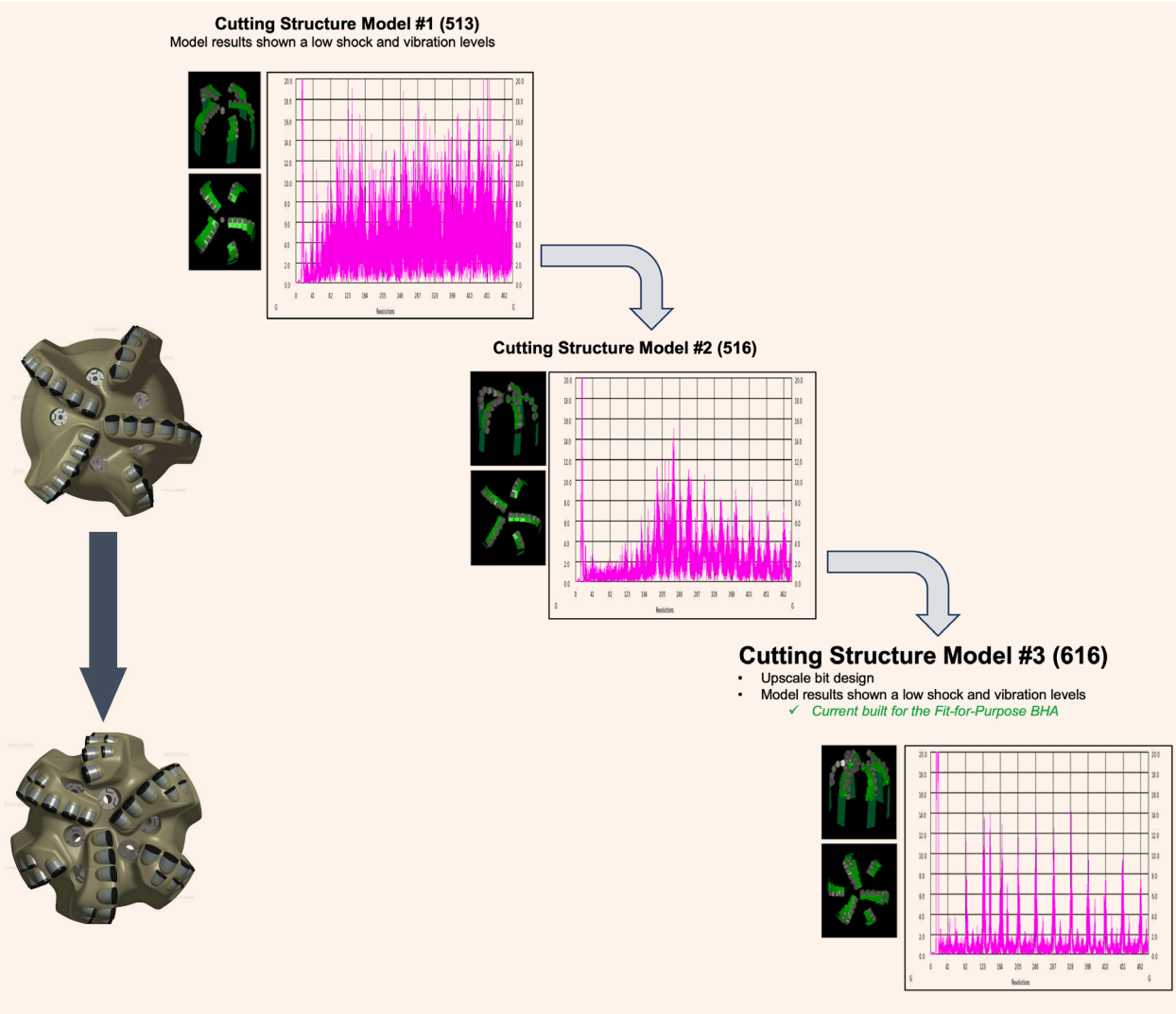

Fig. 5 *The RSSAB design upgrades done specifically to fit the geological challenges.*

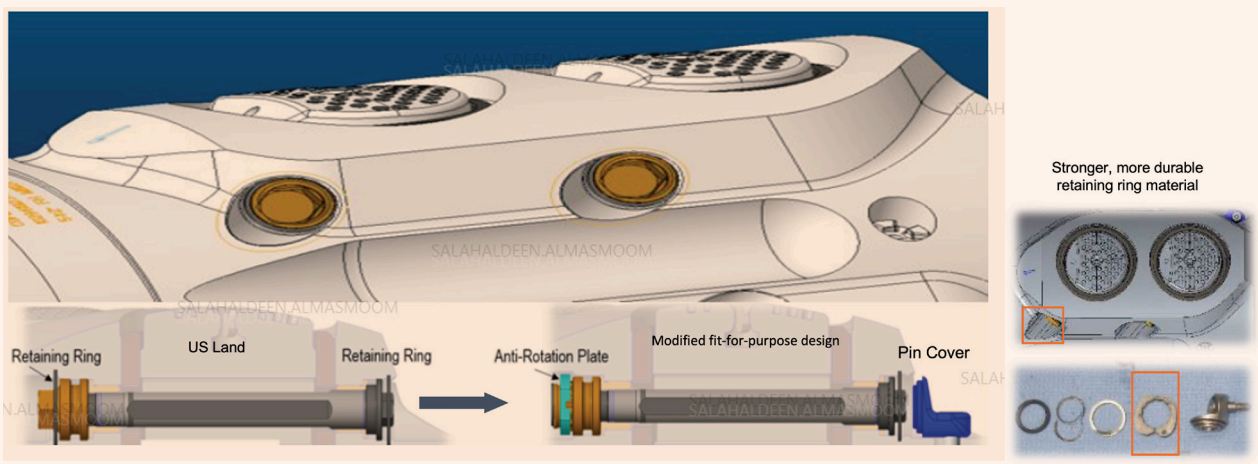

Fig. 6 *A schematic of the 9⅝" fluted mandrel hanger after modifying the internal diameter to 8.55".*

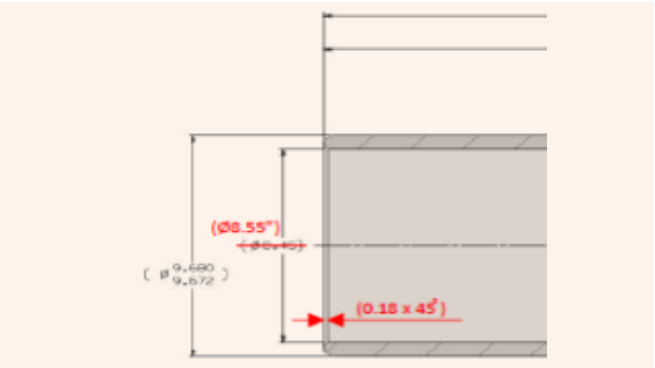

collapsed pressure rating of the thinner walled hanger body was still at an acceptable level, Fig. 6.

Fit-for-Purpose (RSSAB and CSWD) BHA Proven Benefits and Applications

The fit-for-purpose BHA managed to successfully drill a significant number of wells in the recent past with substantial improvements to drilling operations. This success provided performance improvement and cost reduction through the following initiatives:

- Well design optimization to deepen KOP.
- Maximizing the DLS in the curve section.
- Improving geosteering to drill in the deep ultra-thin targets.
- Optimizing the connection time with CSWD tool.
- Reducing tortuosity for smoother completion running.
- Characterization of specific formations with additional evaluation technologies.

The successful implementation journey of the RSSAB and CSWD tool went through three phases with a learning curve, Fig. 7.

Well Design Optimization with Deeper KOP

Before the introduction of the RSSAB and RSS technologies, the curve interval was designed to be below the 6°/100 ft DLS for the conventional RSS to be able to drill the curve and lateral, accounting for the potential drop in the buildup rate at the limestone/clay zone in the top of the curve interval. Therefore, the KOP was designed at the lower part of the depleted carbonate zone. This induced a risk of opening existing fractures when starting to slide, causing severe lost circulation. Deepening the KOP by 200 ft to 300 ft will eliminate this risk tremendously; however, the overall DLS range of the curve section would increase to ≥ 6.5°/100 ft to geosteer and land at the narrow target.

The successful implementation of the fit-for-purpose BHA (RSSAB and CSWD) allowed for deepening the KOP while achieving the required higher DLS in the curve interval, land the well earlier with a shorter vertical section, and gain more reservoir contact on the lateral interval, Fig. 8. These changes did not jeopardize well performance objectives and did not require additional BHA runs.

Improved Geosteering with Full RSSAB and CSWD BHA

Deployment of the RSSAB and CSWD technologies provided improvements in drilling performance while also improving the precision of well placement. The initial results obtained from azimuthal gamma ray real-time interpretation and CSWD trials showed that the wellbore was navigated through the ultra-thin sweet spots with optimal geometry and decision making.

The accuracy and frequency of the CSWD tool surveys have improved on-the-fly geomodeling efforts to best predict ahead of the bit as well as enhance the quality of mass planning for operations. This is critical in deep settings with dipping formations.

As a result of this tailored solution, performance and target precision was significantly improved bringing well delivery to a new level of excellence, Figs. 9 and 10.

Improved Connection Practices with Continuous Drilling Surveys

The RSSAB was combined with CSWD technology to optimize connection time. The strategic combinability of the two technologies proved to deliver further benefits on managing the nondrilling time. The elimination of

Fig. 7 *The successful implementation journey of the RSSAB and CSWD.*

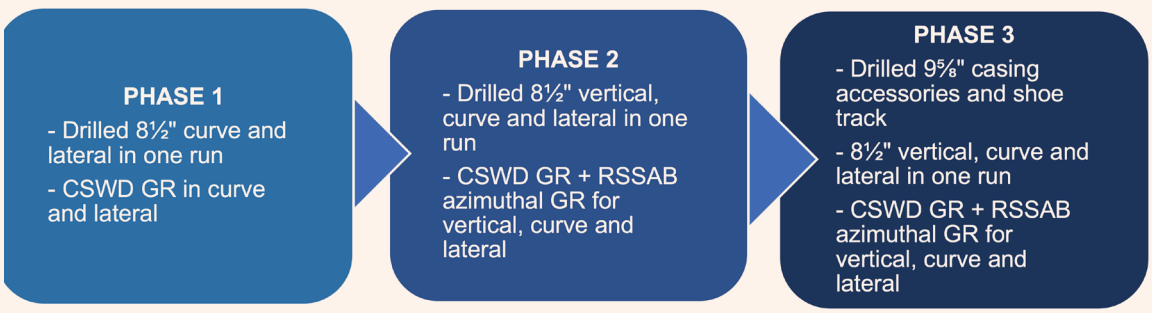

Fig. 8 *The RSSAB technology optimized well design with a deeper KOP.*

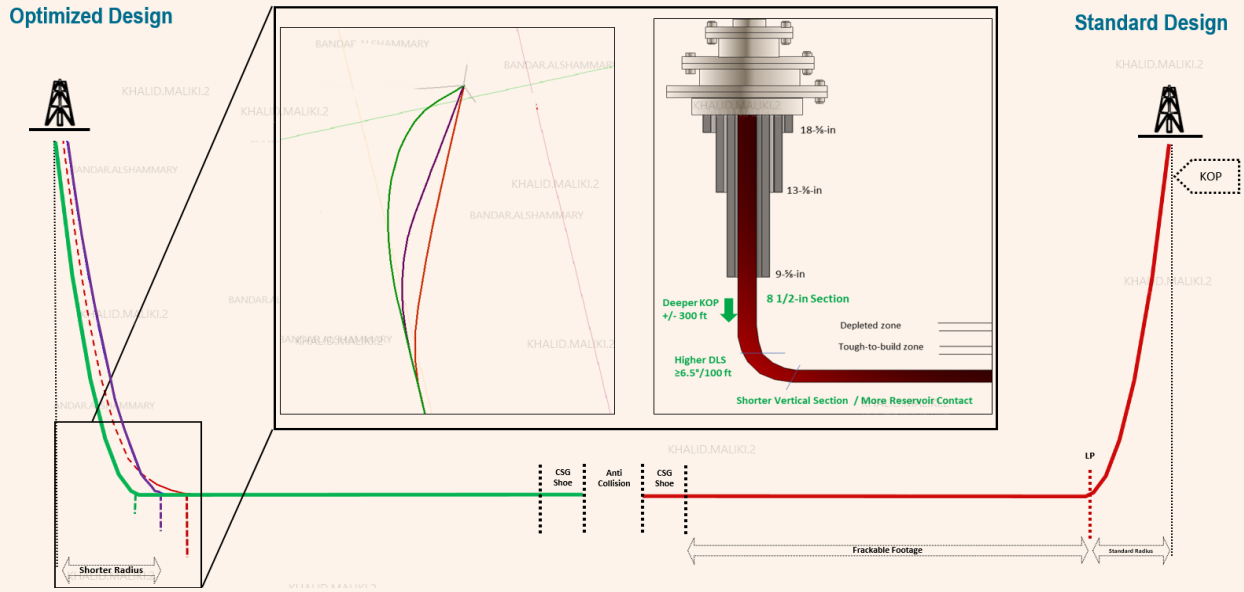

Fig. 9 *The wellbore navigation in the thin sweet spot with real-time monitoring.*

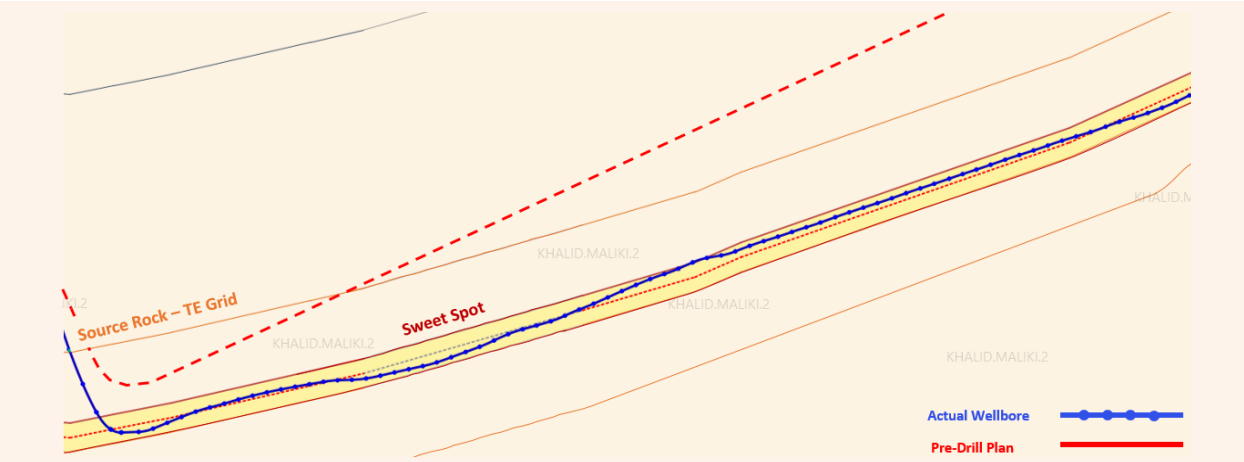

Fig. 10 *The RSSAB azimuthal gamma ray image used for an excellent well placement journey.*

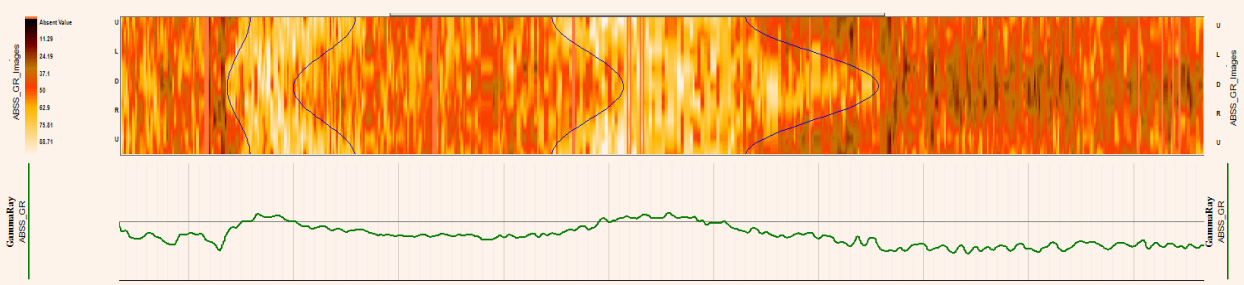

Fig. 11 *The journey of the weight-to-weight time reduction.*

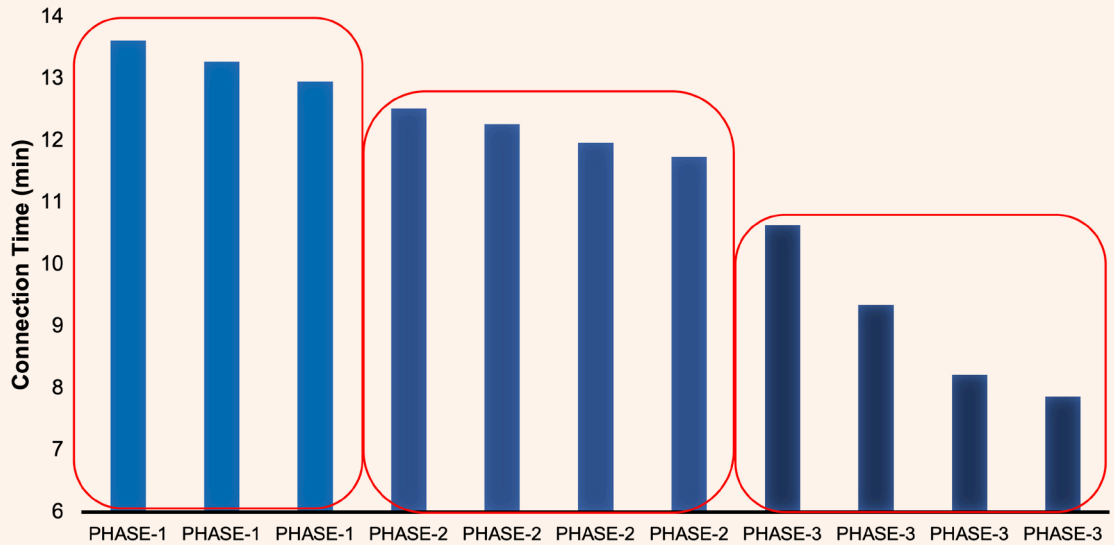

Fig. 12 *The dogleg and tortuosity comparison between the RSSAB and the conventional RSS.*

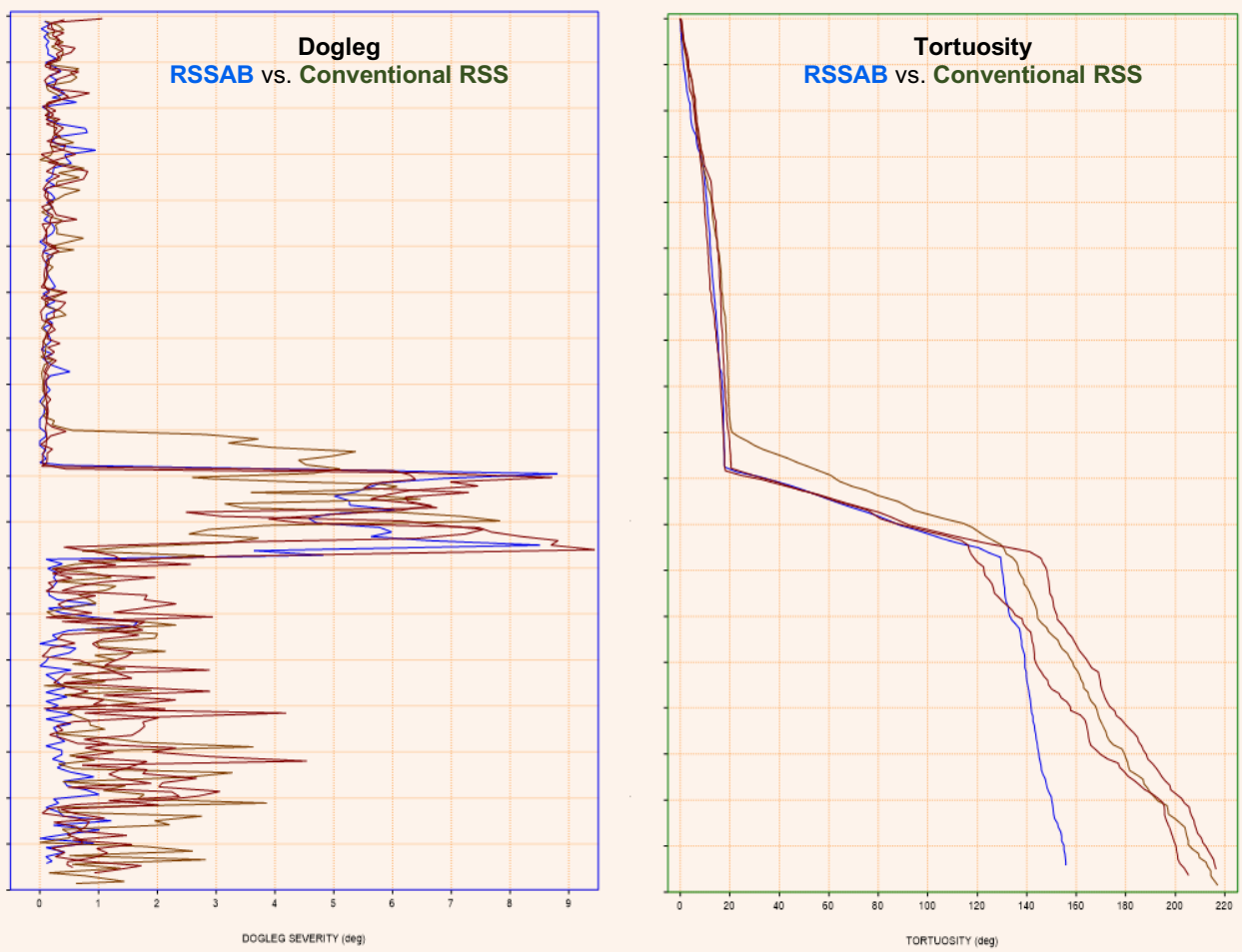

Fig. 13 *An example of the shock risk level (black dots) and lateral vibration gravity force (red dots) recorded on the CSWD tool. The shock risk levels are maintained ≤ 2, and lateral vibrations ≤ 25 Gs.*

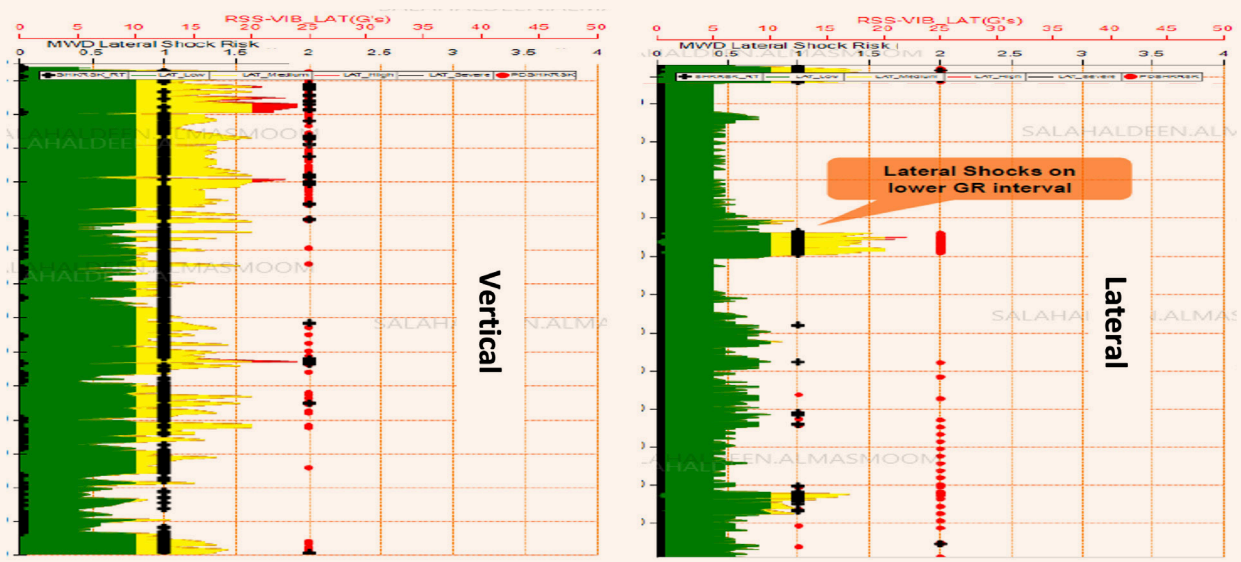

Fig. 14 *The RSSAB and CSWD combined with advanced logging while drilling technologies in one BHA for the first time worldwide.*

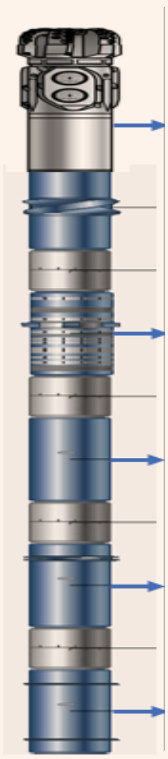

BHA Description	Cum. Length (ft)
RSSAB	13.30
Short Hop Receiver	18.55
Saver Sub	19.70
Density – Neutron – Resistivity	44.35
Saver Sub	45.56
CSWD	70.43
Saver Sub	72.04
OBM Dual Imaging	87.14
Saver Sub	88.79
Sonic Measurements	120.79

surveying time with CSWD tool allowed reducing the weight-to-weight time significantly, leading to further improvement on well delivery objectives. The CSWD tool was deployed in 16", 12", and 8½" hole sections to maximize the added value and reduce the overall well delivery time, Fig. 11.

Reduced Lateral Tortuosity

The RSSAB and CSWD technologies demonstrated a clear reduction of 20% lateral tortuosity compared to the conventional RSS assemblies, Fig. 12. Improved directional control with the RSSAB and the CSWD BHA allowed maximizing drilling parameters and drilling performance. The micro-doglegs are observed instantaneously during drilling, while the shock and vibration risk levels are kept within the acceptable range throughout the vertical, curve, and lateral intervals, Fig. 13. This helped deliver a smoother wellbore and enhance completion running to the well's TD.

Compatibility with Advanced Formation Evaluation Technologies

The RSSAB and CSWD systems showed full compatibility with advanced formation evaluation data, which is required for characterization of specific zones. Full advanced logging technologies were combined for the first time worldwide in the same fit-for-purpose BHA to deliver resistivity, porosity, sonic, and imaging data for complete reservoir mapping while achieving the planned well trajectory logging vertical, curve, and lateral intervals with one BHA, Fig. 14.

Well Delivery Improvement and Cost Reduction

The RSSAB and CSWD technologies have delivered significant results in the past several years, reducing well delivery time and associated costs by a significant amount, Fig. 15. These improvements were achieved

Fig. 15 *The RSSAB and CSWD technologies have delivered significant improvement and cost reduction.*

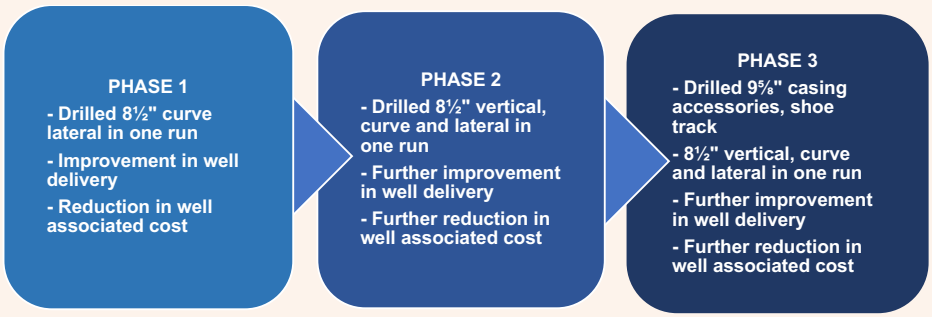

Fig. 16 *The RSSAB and CSWD technologies delivered improvement while continuously exceeding field drilling performance records.*

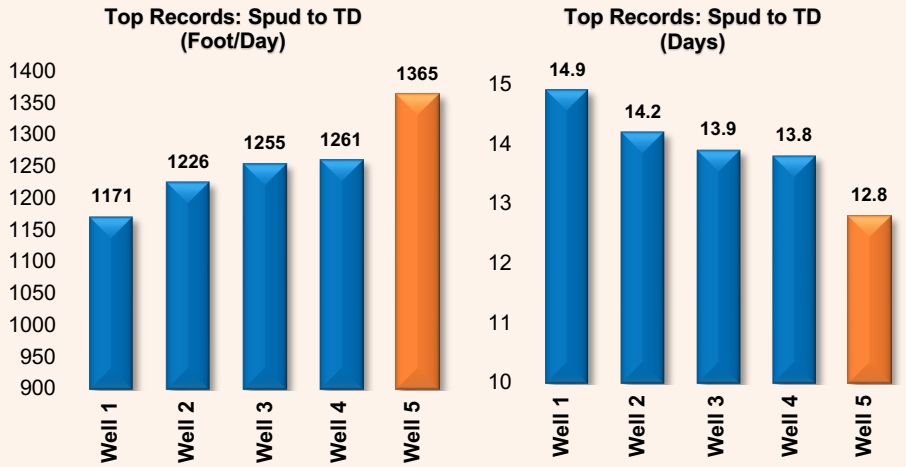

while continuously exceeding field drilling performance records, Fig. 16.

Conclusions

The new RSSAB and CSWD technologies proved to be adaptable through a complete risk analysis, BHA optimization, and drilling bit cutting structure design change. The RSSAB and CSWD technologies have improved well delivery targets. In addition, these technologies provided improved well quality by reducing tortuosity, optimizing well placement with improved geosteering inside required thin targets, and by providing advanced measurements and formation evaluation services.

The success story of aforementioned technologies opened a new performance and optimization window to extend the well's TD and further improve the well's delivery with motorized RSSAB and CSWD BHA, digital and automation implementation, and a shorter well spacing approach in future phases.

Acknowledgments

This article was presented at the International Petroleum Technology Conference, Riyadh, Kingdom of Saudi Arabia, February 21-23, 2022.

References

1. Vié, G.: "At-Bit Steerable System Enables Single-Trip Vertical, Curve and Lateral Drilling in North American Shales," *Drilling Contractor*, March 2020.
2. Lowdon, R., Breen, M., Mouyiasis, M., Edmunds, M., et al.: "Eliminating Rig Time from MWD Surveying," SPE paper 194057, presented at the SPE/IADC International Drilling Conference and Exhibition, the Hague, the Netherlands, March 5-7, 2019.

About the Authors

Saadaldin O. Al-Husaini

B.S. in Mechanical Engineering, Prince Mohammed bin Fahd University

Saadaldin O. Al-Husaini is a Senior Drilling Engineer with 8 years of professional working experience with Saudi Aramco. Throughout his career, he has worked as a Drilling Engineer in numerous areas, including the Jafurah/Rub' al-Khali Exploration and Development Division, the Northern Onshore/South Ghawar Exploration Division, and the Unconventional Drilling Ops 2 Division.

During the last 5 years, Saadaldin has been working in the Unconventional Resource Drilling Department, where he helps in the planning, designing, and execution of unconventional horizontal wells.

He received his B.S. degree in Mechanical Engineering from Prince Mohammed bin Fahd University, al-Khobar, Saudi Arabia.

Salahaldeen S. Almasmoom

M.S. in Petroleum Engineering, University of Southern California

Salahaldeen S. Almasmoom is a Senior Drilling Engineer with 10 years of professional working experience with Saudi Aramco. He is currently working in Saudi Aramco's Unconventional Resource Drilling Department, where over the last four years, Salahaldeen has been designing, planning, and executing unconventional horizontal wells. Throughout his career, he has worked as a Drilling Engineer in various areas, including in exploration and deep gas high-pressure, high temperature wells.

In addition to Salahaldeen's role as a Drilling Engineer, he has been involved with several technical teams focusing on improving drilling practices and introducing new technologies.

He is a member of the Society of Petroleum Engineers (SPE) and has contributed as an author and coauthor on several industry papers.

Salahaldeen received his B.S. degree in Petroleum Engineering from the University of Louisiana, Lafayette, LA, and his M.S. degree in Petroleum Engineering from the University of Southern California, Los Angeles, CA.

David B. Stonestreet

B.S. in Petroleum Engineering, University of Tulsa

David B. Stonestreet has been working as a Drilling Engineering Supervisor within Saudi Aramco's Unconventional Resource Drilling Department for the past eight years.

Throughout his 35 years in the oil and gas industry, David has worked for different oil and gas operating companies with operations in Texas (onshore and offshore), New Mexico, Oman, Algeria, and Saudi Arabia, primarily supervising and managing drilling, completion, and workover operations.

In 1986, David received his B.S. degree in Petroleum Engineering from the University of Tulsa, Tulsa, OK.

Khalid S. Al-Malki

B.S. in Geology, University of Durham

Khalid S. Al-Malki is an experienced Geologist, working with the Operations Planning Team of Saudi Aramco's Unconventional Resources (UR) Exploration and Characterization Department. His 16 years of experience with the company includes working in conventional exploration and development, contingent fields evaluation, reserves assessment, and geological operations. Khalid has also been involved with multidisciplinary teams in the field-scale planning for the operations of the Jafurah Basin, since the inception of the basin.

He is currently a Supervisor in the Integrated Operations Division in UR for a team that plans and executes multiple UR programs with partners. Throughout the previous stages of his career, Khalid worked on various projects and initiatives that optimized geological operations as well as associated costs.

He is an active member of the technical committees of the Society of Petroleum Engineers (SPE) and American Association of Petroleum Geologists (AAPG).

Khalid received his B.S. degree in Geology from the University of Durham, Durham, U.K.

Jamal S. Alomoush

B.S. in Earth & Environmental Sciences, Yarmouk University

Jamal S. Alomoush currently works as a Schlumberger directional drilling Business Development Manager supporting Saudi Aramco's Exploration and Unconventional Operations, where he collaborates with drilling, petrophysics, geology, reservoir and well placement teams to propose and deliver technical solutions that fit the needs of Saudi Aramco.

Jamal has more than 16 years of oil and gas industry experience, most of which are based in Saudi Arabia working for Schlumberger. His experience also includes work as a Schlumberger Surface Formation Evaluation and Drilling Optimization Engineer in various projects with Saudi Aramco.

Jamal is an active member of the Society of Petroleum Engineers (SPE). He has contributed to several industry papers, either as the author and/or coauthor.

Jamal received his B.S. degree in Earth & Environmental Sciences from Yarmouk University, Irbid, Jordan.

Condensate Banking Removal Using Slow Release of in Situ Energized Fluid

Ayman R. Al-Nakhli, Amjed M. Hassan, Abdualilah I. Albaiz and Wajdi M. Buhaezah

Abstract /

Condensate banking represents a persistent challenge during gas production from tight reservoirs. The accumulation of condensate around the wellbore can rapidly diminish gas production. When the reservoir pressure drops below the dew point, condensate starts to drop out from the gas phase, filling pores and permeable fractures, and blocking gas production. There are several strategies to mitigate condensate banking. These strategies have either demonstrated limited results or are economically not viable.

In this study, a novel method to mitigate condensate was developed using thermochemical reactants. The slow release of thermochemical reactants inside different core samples was studied. The effect of in situ generation of gas on the petrophysical properties of the rock was reported. Thermochemical treatment was applied to recover condensate on sandstone and carbonate, where the reported recoveries were approximately 70%. When a shale sample was used, the recovery was only 43%.

Advanced Equation-of-State (EoS) compositional and unconventional simulator (GEM) from the Computer Modeling Group (CMG) software was used to simulate thermochemical treatment and gas injection. The simulation study showed that thermochemical stimulation had increased the production period from 3.5 to 22.7 months, compared to gas injection.

Introduction

Natural gas gains more value day by day, which makes its production more profitable. As the production of gas increases, several challenges should be addressed to maintain cost-effective production, especially from tight reservoirs. Condensate banking is one of the most critical reasons for the decreasing production rates in gas fields around the world. When the reservoir pressure decreases below the dew point, liquid starts to drop out from gas[1]. The condensate liquid then accumulates in the pores, and decreases the permeability around the wellbore, thereby limiting gas production.

When the reservoir pressure drops below the dew point, accumulation of liquid condensate around the wellbore can form three mobility regions, Fig. 1[2]. The near wellbore area will be the first region of mobile gas and mobile condensate where both the liquid and gas phases are flowing to the wellbore. In the second region, there are also two phases of gas and liquid condensate. In this region the condensate is below the saturation point, which makes it immobile and unable to flow to the wellbore. In the faraway region, there is only a gas phase, as the reservoir pressure would be above the dew point.

Well testing can be applied to evaluate condensate banking in the reservoir, where buildup and drawdown tests can show the change in fluid type, rate variations, and fluid dynamics[3]. An analytical solution can be applied to model the three mobility regions around the wellbore, as worked out by Wilson (2004)[4]. He developed the model based on the relationship between reservoir ratios and all gas mobility and condensate saturation, using Eqn. 1, Figs. 2 and 3.

$$k = k_{min} + (k_{max} - k_{min})\left[1 - \exp\left(\frac{-1}{\alpha}\frac{r^2}{t}\right)\right] \quad (1)$$

Gas Injection

Historically, condensate banking was resolved by gas cycling, where in the condensate gas fields, the produced gas was reinjected in the well to maintain the reservoir pressure, and that will ensure it is above the dew point, thereby decreasing the possibility of liquid drops and condensate banking[5]. Nowadays, with the high economical value, it is not profitable to recycle natural gas.

Sayed and Al-Muntasheri (2016)[6] summarized different methods for condensate banking mitigation where these can be categorized as pressure maintenance methods, chemical injections, and productivity improvement. Pressure maintenance includes gas cycling and carbon dioxide (CO_2) and nitrogen (N) gas injection, while chemical solutions include wettability alternation and solvent injection. Finally, productivity improvement includes horizontal wells, hydraulic fracturing, and acidizing.

Fig. 1 *Condensate saturation below the dew point pressure flow behavior in the three known mobility regions[2].*

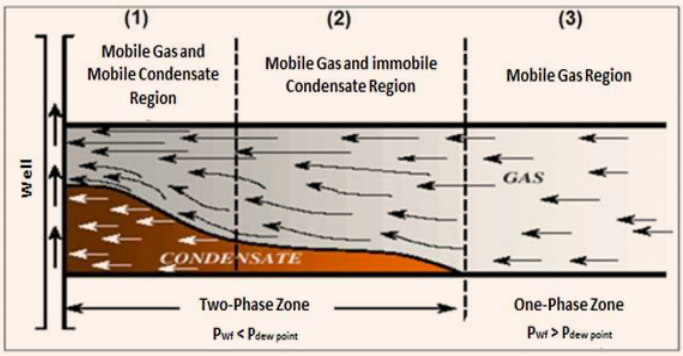

In this study, thermochemical reaction is utilized in condensate banking mitigation where this reaction produces both high temperature and pressure.

Pressure Maintenance

Maintaining reservoir pressure is one of the practices to keep production rates high. When the pressure is maintained at levels higher than dew point, the condensate accumulation decreases. In the past, it was practical to inject lean gas into the reservoir to maintain pressure. As the gas price increased, this process became less beneficial. Besides increasing the pressure, injected gas can also reevaporate the condensate, which means it can play a vital role by preventing the formation and mitigating the already formed banking[7]. The injection is not exclusive for lean gas where different gases can be used as CO_2, N, and mixture of gases.

Ahmed et al. (1998)[5] studied the effectiveness of lean gas, nitrogen gas (N_2), and CO_2 Huff-n-Puff operation on three different gas condensate systems and concluded that the process is a viable option to mitigate condensate banking in the near wellbore region. Choosing the type of gas to be injected in the reservoir depends on phase behavior of the fluid and flow characteristic of the reservoir[6].

Donohoe and Buchanan (1981)[8] did a comparison between lean gas injection and N_2 for three hypothetical fluids. They found that recovery factors of N_2 injection were comparable with lean gas injection. They also concluded that reservoirs having a condensate-to-gas ratio richer than 100 barrels/million standard cubic feet (bbl/MMscf) should be considered for N_2 injection. Introducing N_2 to the field could require building several facilities, e.g., an air separation unit and nitrogen rejection unit[9].

Huff-n-Puff injecting CO_2 in depleted gas reservoirs can be useful, where Ayub et al. (2017)[10] did a simulation study and showed that the process can mitigate condensate banking through three aspects: (1) dissolving the condensate due to low minimum miscibility pressure between condensate and CO_2, (2) condensate revaporization, and (3) increasing near well pore

Fig. 2 *The pressure curves for a typical gas condensate well[4].*

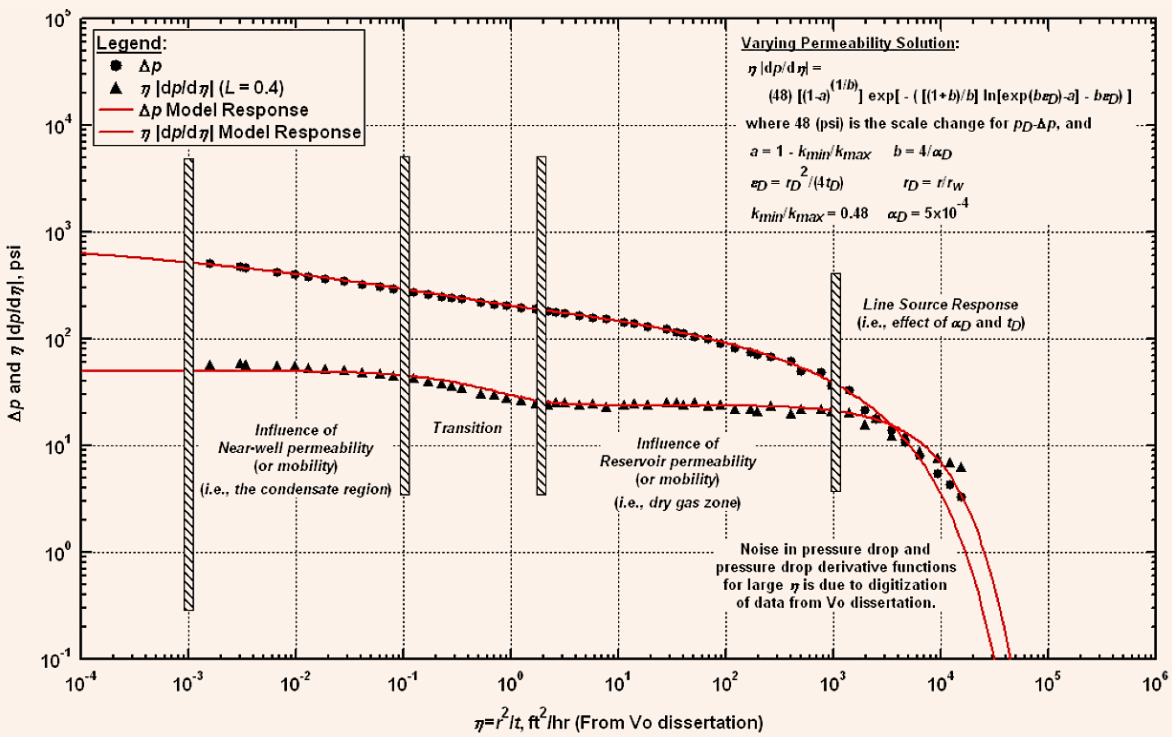

Fig. 3 *The pressure derivative curves for a gas condensate reservoir[4].*

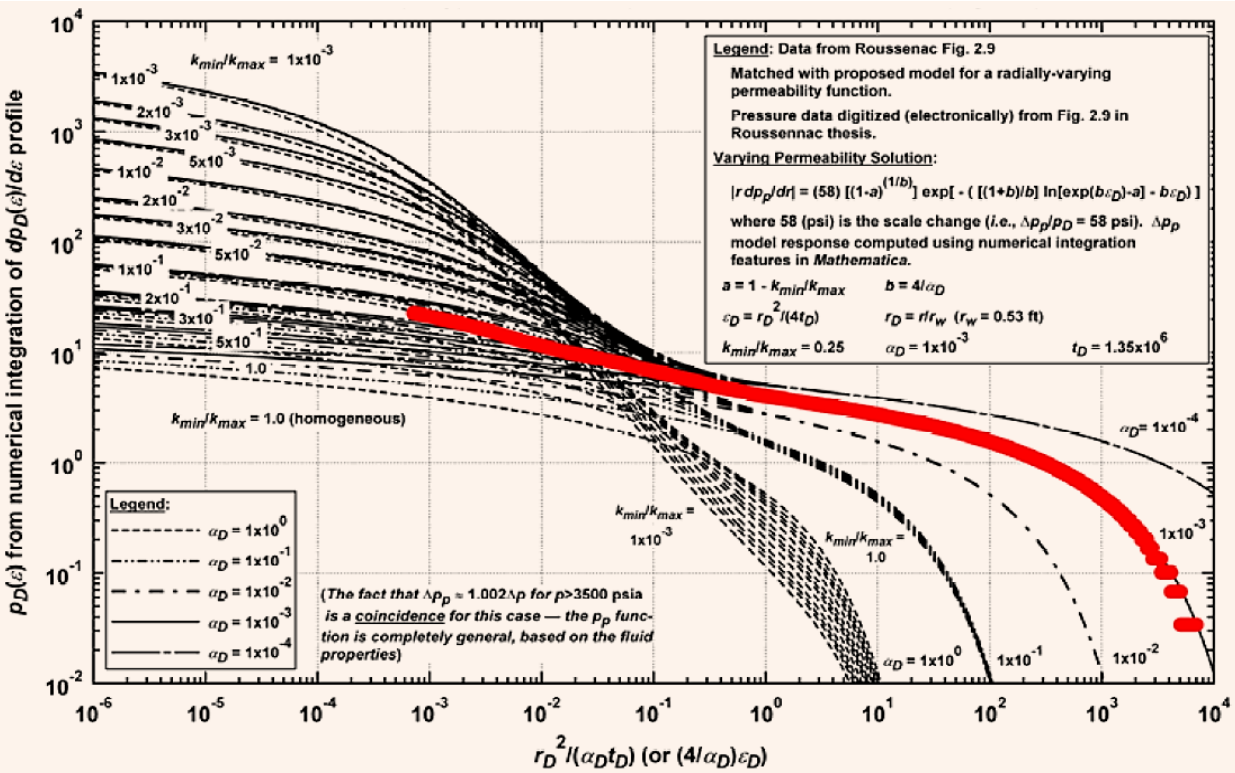

pressure. Dissolved CO_2 in water generates carbonic acid, which could be corrosive to mild steel[11-13]. Another possible damage is the precipitation of calcium bicarbonate when CO_2 is injected in the carbonate reservoir, which could plug the channels and eventually decrease production[14, 15].

Chemical Injection

Another type of injection is chemical injection. Methanol and dimethyl ether (DME) can be injected in the impacted well since they are miscible with the condensate. Al-Anazi et al. (2005)[16] discussed the effect of methanol on condensate banking where they found out that methanol injection increased production by a factor of two, before it declines again after 4 months. Liu et al. (2018)[17] used DME as a solvent to remove the liquid blockage that includes both hydrocarbons and water. The treatment showed an increase in relative permeability. This treatment is temporary when it comes to removing condensate.

Injection of a wettability alternation chemical can be applied to change rock from being liquid wet to gas wet[18]. Al-Yami et al. (2013)[2] reported a field trial of using a polymeric fluorinated surfactant to enhance gas flow and remove condensate blockage. The treatment showed an increase of gas and condensate production by 83% and 313%, respectively, which lasted for more than 2 years. One of the drawbacks of this method is that fluorochemicals and their degradation could be hazardous and harmful for humans and the environment[19-21].

Productivity Improvement

Another approach to overcome in the condensate banking challenge is horizontal drilling. Miller et al. (2010)[22] conducted a study to simulate the role of horizontal wells on reducing condensate banking. They found that the horizontal well showed less drawdown pressure and reached the dew point after 1,880 days, compared with 396 days for the vertical.

Another finding, at below dew point conditions, was that oil saturation was 0.27 for a vertical well, where it was only 0.20 for a horizontal well. Acidizing and hydraulic fracturing were applied for some time to increase permeability, remove blockage, and increase gas production.

Thermochemical Treatment Approach

A new approach was developed to mitigate condensate banking by using slow release thermochemical reactors. The new treatment can mitigate condensate by three factors. The first factor is by increasing reservoir pressure, as N_2 is generated in situ. The second factor is generation of heat and gas, which can not only evaporate condensate, but also dilute the liquid phase, therefore reduce viscosity. One of the critical factors that contribute to condensate banking is liquid loading. When there is a significant amount of

condensate and/or water in the near wellbore area and in the wellbore itself, high hydrostatic pressure will be created, which will choke the well and result in a total loss of gas production. When chemical fluids, such as solvents and acids, are pumped in the wellbore, they will also create extra choking material in the reservoir that requires lifting.

A novel treatment, based on pumping thermochemical fluid, was developed to mitigate condensate. The advantage of pumping thermochemical fluid over other solvents or acid injection is that thermochemical reactants can be designed for slow release of N_2. The release of in situ N_2 will energize the fluid in the reservoir, and greatly support flowing back liquid condensate and water not only from the well, but also from the reservoir. The new slow release recipe of the thermochemical was tested in the lab, using an autoclave system, Fig. 4.

Fluid was pumped inside the reactor at room pressure and temperature. The slow release of N_2 was monitored by the reactor gauge pressure. The reactor pressure increased from 0 psi to 15,400 psi after 10 days, Fig. 5. Then the reaction was quiet. The duration of N_2 release can be predesigned in the lab. The slow release of N_2 will allow the fluid to be pumped deep into the reservoir and slowly energize liquid condensate, which is choking the well. Not only that, but also the flow back of this reactive chemical will energize in situ wellbore fluid for effective deliquification of the wellbore.

Fig. 4 *The used autoclave system, rated up to 20,000 psi and 500 °C.*

Condensate Recovery Using Thermochemical Fluid

Three different types of rocks (sandstone, carbonate, and shale) were used to evaluate condensate removal using the new slow release system of thermochemical reactants. Table 1 shows the petrophysical properties of the three rock types used in this study. The rock samples were placed in a coreflood system and saturated with condensate. Then, several cycles of the thermochemical system were pumped to recover condensate. During each cycle, the fluid was left for socking time (to maintain the fluids in the reservoir without pumping in or out) until equilibrium was achieved. The strategy of cyclic flooding was selected to reduce treatment fluid volume by 50%, compared to single-stage flooding[23]. Around 70% of the condensate fluid was recovered from the sandstone and carbonate rocks in three cycles of injection. For shale, 43% of condensate was recovered after five cycles of injection, Fig. 6.

The slow release of in situ energized fluid within the reservoir not only helped to energize condensate, but it also creates microfracturing in tight rocks, thereby, increasing permeability and reducing capillary forces. Tight core samples were used to evaluate the effect of the slow release of the thermochemical treatment on capillary forces and productivity index. The treatment showed that capillary pressure was reduced by 56%, due to the thermochemical treatment. The productivity index was calculated during the coreflood treatment from the pressure drop, and found to be increased by 79%[23].

Field Scale Simulation

To evaluate the effect of thermochemical treatment, for condensate banking removal, an advanced Equation-of-State (EoS) compositional and unconventional simulator (GEM) from the Computer Modeling Group (CMG) software was used. Table 2 shows the initial reservoir conditions that were used in this simulation. Thermochemical treatment was compared with gas injection using the same reservoir and production conditions. A 1 km × 1 km rectangular Cartesian model, with a single well in the center, was used during the study, Fig. 7. Four different permeability layers, ranging from 10 mD to 315 mD, were used with 0.15 porosity. The reservoir temperature was set to 275 °F.

Gas Injection

During the simulation of gas injection, to remove condensate banking, the well was allowed to produce at a rate of 30 MMscfd, with downhole pressure of 7,000 psi, Fig. 8. Due to condensate accumulation, downhole

Fig. 5 *The autoclave system test shows the reactor pressure increased from 0 psi to 15,400 psi after 10 days.*

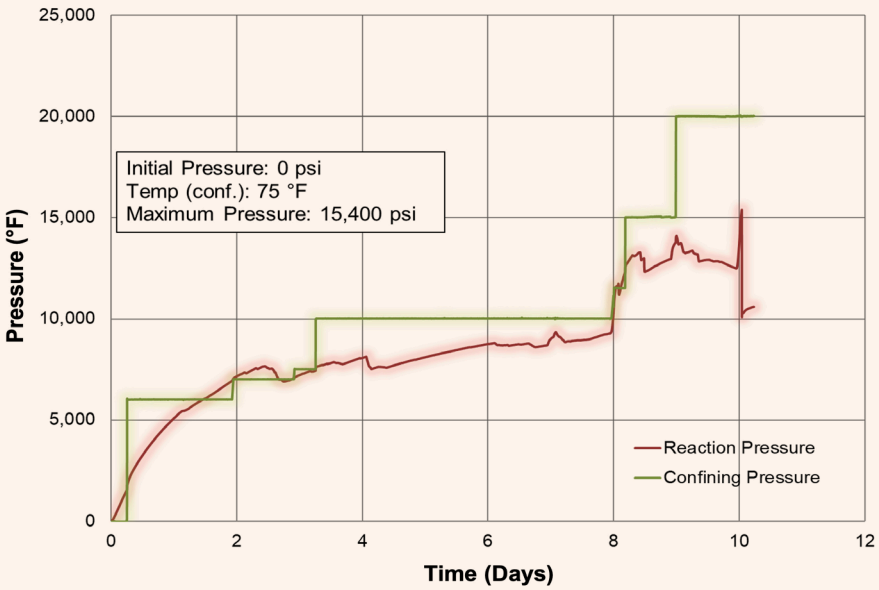

Table 1 *The petrophysical properties of the three core samples used in this study.*

Sample ID	Sample Type	Diameter (cm)	Length (cm)	Bulk Volume (ml)	Pore Volume (ml)	Porosity (%)	Absolute Permeability (mD)
SS	Sandstone	3.81	5.33	60.81	12.67	20.83	13.12
LS	Limestone	3.81	5.46	62.20	9.84	15.82	7.39
SH	Shale	3.81	5.40	61.54	1.96	3.19	0.012

Fig. 6 *The cumulative condensate recovery during thermochemical injection into sandstone (SS), limestone (LS), and shale (SH) rocks[23].*

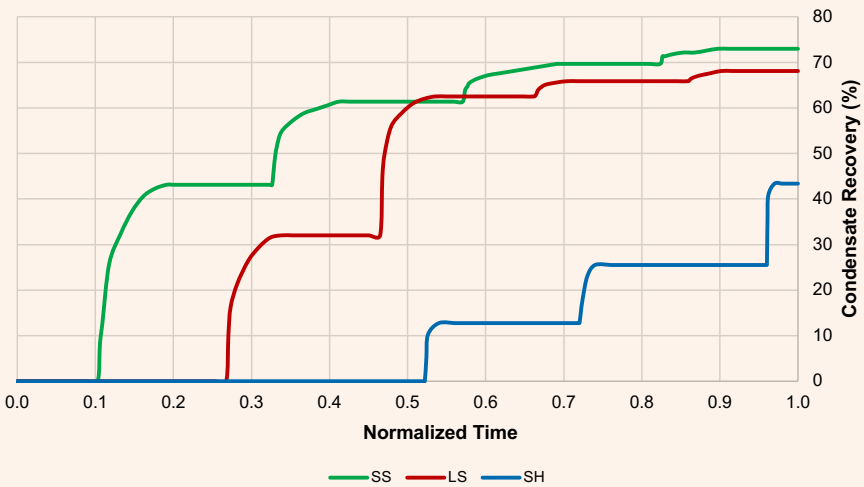

Table 2 The initial reservoir conditions used in the simulation.

Parameter	Value
Total bulk reservoir volume (ft^3)	9.00E+08
Total pore volume (ft^3)	1.17E+08
Total hydrocarbon pore volume (ft^3)	9.83E+07
Original oil in place, OOIP (stb)	1.79E+06
Original gas in place, OGIP (scf)	2.77E+10

Fig. 7 A 3D view of the rectangular model used in the simulation.

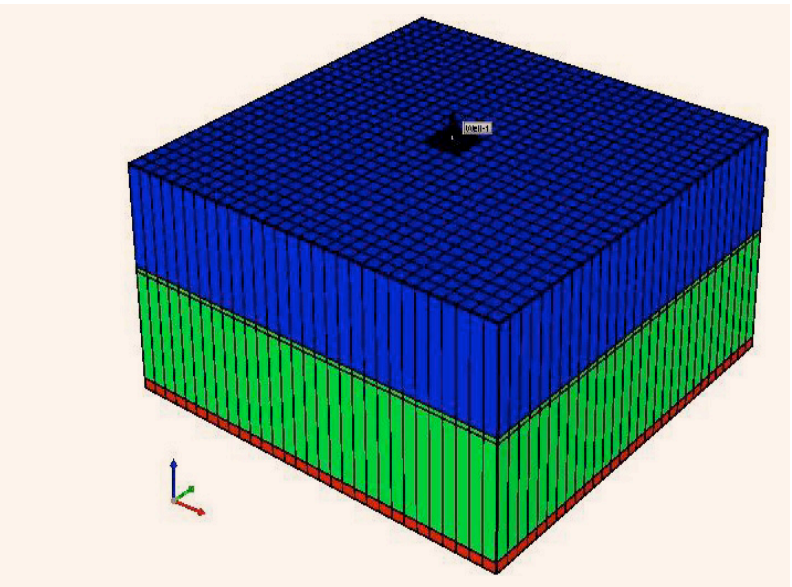

pressure was reduced to 1,500 psi, and production was stopped after 668 days. Then, three cycles of gas injection was applied, with a constant rate for one month. After the gas injection treatment, the well was opened for production at the same initial production rate. The well managed to produce for 104 days, before downhole pressure dropped to the settled lower limit of 1,500 psi, where the production was stopped.

Thermochemical Treatment

The slow release of the thermochemical treatment has three impact factors on the reservoir. In situ generated pressure will positively affect the reservoir pressure. The in situ generated N_2 will reduce condensate viscosity. The third factor is the creation of microfractures in the reservoir rock. During the simulation, and prior to thermochemical treatment, gas production was started at 30 MMscfd, with 7,000 psi downhole pressure. Downhole pressure dropped, due to condensate banking to 1,500 psi, and production was stopped after 668 days.

Then, three cycles of thermochemical treatment were applied with one week soaking time. Then, the well

Fig. 8 The profiles of gas production and the flowing downhole pressure before and after gas injection treatment.

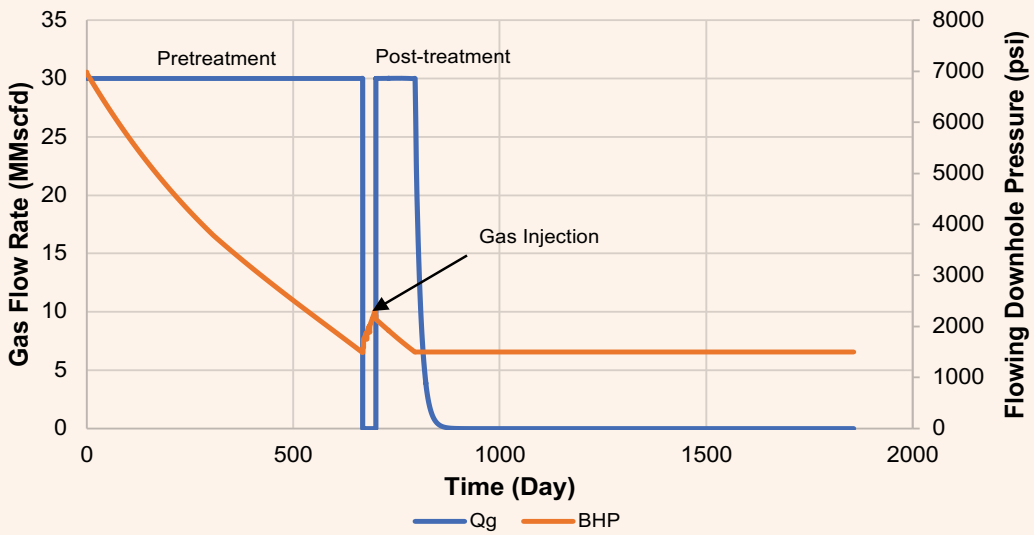

Fig. 9 *The profiles of the gas flow rate and flowing downhole pressure before and after the thermochemical treatment.*

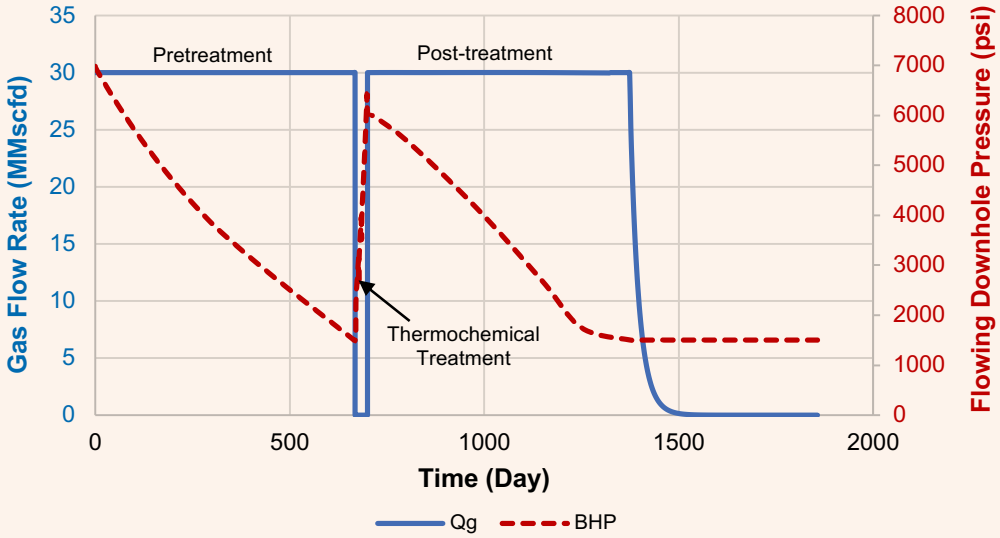

was open to production with 30 MMscfd and lasted for 680 days. This shows that thermochemical treatment was able to restore initial reservoir conditions, Fig. 9. The simulation study showed that thermochemical stimulation had increased the production period from 3.5 to 22.7 months, compared to gas injection. The production plateau was increased by a factor of 6.5, compared to gas injection.

Conclusions

In this study, the impact of the slow release of thermochemical treatment was studied. Based on the results achieved, the following conclusions can be drawn:

- A novel thermochemical treatment was developed to mitigate condensate banking in gas reservoirs.
- Laboratory testing showed that the slow release of thermochemical reactants can be achieved and delay reaction up to 10 days. The reaction delay will help to squeeze the treatment deeply in the reservoir to treat far-reaching areas.
- The thermochemical treatment provides pressure support, condensate viscosity reduction, and induced fracturing, which overall, increases condensate recovery.
- Advanced EoS GEM from CMG software was used to simulate thermochemical treatment and gas injection.
- The simulation study showed that thermochemical stimulation had increased the production period from 3.5 to 22.7 months, compared to gas injection.

Acknowledgments

This article was prepared for presentation at the Middle East Oil and Gas Show, Manama, Kingdom of Bahrain, November 28-December 1, 2021.

References

1. Al Hamad, M., Ezdeen, I. and Abdallah, W.: "Innovative Green Solution for Gas Condensate Blockage Removal," SPE paper 195143, presented at the SPE Middle East Oil and Gas Show and Conference, Manama, Kingdom of Bahrain, March 18-21, 2019.
2. Al-Yami, A.M., Gomez, F.A., AlHamed, K.I. and Al-Buali, M.H.: "A Successful Field Application of a New Chemical Treatment in a Fluid Blocked Well in Saudi Arabia," SPE paper 168086, presented at the SPE Saudi Arabia Section Technical Symposium and Exhibition, al-Khobar, Kingdom of Saudi Arabia, May 19-22, 2013.
3. Bozorgzadeh, M. and Gringarten, A.C.: "Condensate Bank Characterization from Well Test Data and Fluid PVT Properties," *SPE Reservoir Evaluation and Engineering*, Vol. 9, Issue 5, October 2006, pp. 596-611.
4. Wilson, B.W.: "Modeling of Performance Behavior in Gas Condensate Reservoirs Using a Variable Mobility Concept," MS thesis, Texas A&M University, December 2003, 79 p.
5. Ahmed, T., Evans, J., Kwan, R. and Vivian, T.: "Wellbore Liquid Blockage in Gas Condensate Reservoirs," SPE paper 51050, presented at the SPE Eastern Regional Meeting, Pittsburgh, Pennsylvania, November 9-11, 1998.
6. Sayed, M.A. and Al-Muntasheri, G.A.: "Mitigation of the Effects of Condensate Banking: A Critical Review," *SPE Production & Operations*, Vol. 31, Issue 2, May 2016, pp. 85-102.
7. Aziz, R.M.: "A 1982 Critique on Gas Cycling Operations on Gas Condensate Reservoirs," SPE paper 11477, presented at the Middle East Oil Technical Conference and Exhibition, Manama, Kingdom of Bahrain, March 14-17, 1983.
8. Donohoe, C.W. and Buchanan Jr., R.D.: "Economic Evaluation of Cycling Gas Condensate Reservoirs with Nitrogen," *Journal of Petroleum Technology*, Vol. 33, Issue 2, February 1981, pp. 263-270.

9. Abdulwahab, H. and Belhaj, H.: "Managing the Breakthrough of Injected Nitrogen at a Gas Condensate Reservoir in Abu Dhabi," SPE paper 137330, presented at the Abu Dhabi International Petroleum Exhibition and Conference, Abu Dhabi, UAE, November 1-4, 2010.

10. Ayub, M., Ramadan, M., Bataweel, M.A. and Al-Mulhem, A.A.: "Removal of Gas Condensate by CO_2 Huff-n-Puff Injection: A Simulation Study," SPE paper 188572, presented at the Abu Dhabi International Petroleum Exhibition and Conference, Abu Dhabi, UAE, November 13-16, 2017.

11. Russick, E.M., Poulter, G.A., Adkins, C.L.J. and Sorensen, N.R.: "Corrosive Effects of Supercritical Carbon Dioxide and Cosolvents on Metals," *The Journal of Supercritical Fluids*, Vol. 9, Issue 1, March 1996, pp. 43-50.

12. George, K.S. and Nešić S.: "Investigation of Carbon Dioxide Corrosion of Mild Steel in the Presence of Acetic Acid — Part 1: Basic Mechanisms," *CORROSION*, Vol. 63, Issue 2, February 2007, pp. 178-186.

13. McGrail, B.P., Schaef, H.T., Glezakou, V-A., Dang, L.X., et al.: "Water Reactivity in the Liquid and Supercritical CO_2 Phase: Has Half the Story Been Neglected?" *Energy Procedia*, Vol. 1, Issue 1, February 2009, pp. 3415-3419.

14. Izgec, O., Demiral, B., Bertin, H.J. and Akin, S.: "CO_2 Injection in Carbonates," SPE paper 93773, presented at the SPE Western Regional Meeting, Irvine, California, March 30-April 1, 2005.

15. Pruess, K., Xu, T., Apps, J. and Garcia, J.: "Numerical Modeling of Aquifer Disposal of CO_2," *SPE Journal*, Vol. 8, Issue 1, March 2003, pp. 49-60.

16. Al-Anazi, H.A., Walker, J.G., Pope, G.A., Sharma, M.M., et al.: "A Successful Methanol Treatment in a Gas/Condensate Reservoir: Field Application," *SPE Production & Facilities*, Vol. 20, Issue 1, February 2005, pp. 60-69.

17. Liu, W., Ganjdanesh, R., Varavei, A., Yu, W., et al.: "Numerical Modeling and Optimization of Condensate Banking Treatment in the Hydraulic Fractured Shale Gas Condensate Reservoir," URTEC paper 2902081, presented at the SPE/AAPG/SEG Unconventional Resources Technology Conference, Houston, Texas, July 23-25, 2018.

18. Sayed, M. and Al-Muntasheri, G.: "A Safer Generation of Wettability Alteration Chemical Treatments," SPE paper 184566, presented at the SPE International Conference on Oil Field Chemistry, Montgomery, Texas, April 3-5, 2017.

19. Key, B.D., Howell, R.D. and Criddle, C.S.: "Fluorinated Organics in the Biosphere," *Environmental Science & Technology*, Vol. 31, Issue 9, August 1997, pp. 2445-2454.

20. Ellis, D.A., Martin, J.W., de Silva, A.O., Mabury, S.A., et al.: "Degradation of Fluorotelomer Alcohols: A Likely Atmospheric Source of Perfluorinated Carboxylic Acids," *Environmental Science & Technology*, Vol. 38, Issue 12, May 2004, pp. 3316-3321.

21. Strazza, C., del Borghi, A. and Gallo, M.: "Development of Specific Rules for the Application of Life Cycle Assessment to Carbon Capture and Storage," *Energies*, Vol. 6, Issue 3, March 2013, pp. 1250-1265.

22. Miller, N., Nasrabadi, H. and Zhu, D.: "Application of Horizontal Wells to Reduce Condensate Blockage in Gas Condensate Reservoirs," SPE paper 130996, presented at the International Oil and Gas Conference and Exhibition in China, Beijing, China, June 8-10, 2010.

23. Al-Nakhli, A.R., Hassan, A., Mahmoud, M. and Al-Majed, A.: "Removal of Condensate Banking from Different Formations Using Thermochemical Treatment," SPE paper 197847, presented at the Abu Dhabi International Petroleum Exhibition and Conference, Abu Dhabi, UAE, November 11-14, 2019.

About the Authors

Ayman R. Al-Nakhli

M.S. in Entrepreneurship for New Business Development, Open University Malaysia

Ayman R. Al-Nakhli is a Petroleum Scientist in Saudi Aramco's Exploration and Petroleum Engineering Center – Advanced Research Center (EXPEC ARC), where he leads the research program on thermochemicals and develops technologies related to conventional and unconventional reservoirs such as pulse fracturing, stimulation, diverting agents, and heavy oil.

Ayman has developed and field deployed several novel technologies, with four of them being commercialized with international service companies. He received the World Oil Award for Best Production Chemical in 2015.

Ayman has filed more than 20 patents, published 35 journal papers, and 40 conference papers.

He received his B.S. degree in Industrial Chemistry from King Fahd University of Petroleum and Minerals (KFUPM), Dhahran, Saudi Arabia, and an M.S. degree in Entrepreneurship for New Business Development from Open University Malaysia, Bahrain.

Amjed M. Hassan

M.S. in Petroleum Engineering, King Fahd University of Petroleum and Minerals

Amjed M. Hassan is a Ph.D. Researcher at King Fahd University of Petroleum and Minerals (KFUPM), and a lecturer at the University of Khartoum, Sudan. His research interests are varied and cover condensate removal processes, enhanced oil recovery methods, well testing, and artificial intelligence applications in the petroleum industry.

Amjed has participated in many workshops, conferences, and regional contests. He has received several awards, the most recent include the Society of Petrophysicists and Well Log Analysts (SPWLA) prize for the best research in petrophysics, and the Schlumberger award for the best academic performance in petroleum engineering.

Amjed is the author of 15 of scientific articles and Society of Petroleum Engineers (SPE) papers.

He received his M.S. degree in Petroleum Engineering from KFUPM.

Abdualilah I. Albaiz

B.S. in Chemistry Science, King Fahd University of Petroleum and Minerals

Abdualilah I. Albaiz is a Petroleum Scientist working with the Production Technology Team of Saudi Aramco's Exploration and Petroleum Engineering Center – Advanced Research Center (EXPEC ARC). Abdualilah is part of several research projects that utilizes thermochemicals in stimulation and production enhancement.

In 2020, he received his B.S. degree in Chemistry Science from King Fahd University of Petroleum and Minerals (KFUPM), Dhahran, Saudi Arabia.

Wajdi M. Buheazah

A.S. in Chemistry, Jubail Industrial College

Wajdi M. Buheazah is a Lab Technician working with the Production Technology Team of Saudi Aramco's Exploration and Petroleum Engineering Center – Advanced Research Center (EXPEC ARC). His work focuses on smart fluids. Prior to joining Saudi Aramco in 2019, Wajdi worked for several service companies, including Schlumberger.

In 2012, Wajdi received his A.S. degree in Chemistry from the Jubail Industrial Collage, Jubail, Saudi Arabia.

A Novel System for Large Depth of Investigation Pulsed Neutron Measurements and Enhanced Reservoir Saturation Evaluation

Yahia A. Elaher and Dr. Gregory J. Schmid

Abstract /

Despite its value and importance to oil field development and reservoir management, carbon/oxygen (C/O) logs are commonly associated with significant challenges; that are either related to the wellbore logging environment and/or the physics of the measurement. A shallow depth of investigation (DOI) is considered the greatest challenge related to the nature of the pulsed neutron measurement. It can imply a high degree of uncertainty on the measurement and consequently the calculated water saturation, affecting the true assessment of the reservoir fluids' saturations, especially in challenging logging environments.

In this article we introduce and prove an innovative approach to increase the DOI of the pulsed neutron measurement. Currently, all pulsed neutron logging tools use an electric pulsed neutron generator (PNG), or "particle accelerator" or minitron, to probe downhole formations with 14 MeV neutrons and record the returning gamma ray signal at a shallow DOI, which is in the range of 7" for C/O measurement and 12" for sigma measurement.

In this new approach, we introduce the idea of increasing DOI of the measured gamma rays through increasing the energy level of the neutrons emitted by a PNG. To prove the concept, a computer modeling and simulation study was conducted using Monte Carlo N-Particle (MCNP) for a pulsed neutron logging tool to determine DOI for neutron energies higher than 14 MeV.

The study involved five different combinations of borehole and formation fluids. Each involved a "block" of 24 MCNP calculations. The 24 calculations inside each block represented the 24 possible combinations of three neutron energies (14 MeV, 20 MeV, and 40 MeV), two gamma ray spectral types (inelastic, capture), and four detectors. Data simulation shows that the DOI rises substantially with energy for all tested detectors, where the enhancement in DOI with the increase in neutron energy is more prolific in case of the inelastic measurement compared to the capture measurement. And of course, the deeper the detector — further from the source — the better the DOI, although this can compromise the precision of the measurement. Yet with the recent technology advancements, mainly in PNG (producing more neutron population) and gamma ray detector technology (higher and faster count rates), this shall enhance the precision of the measurement and enable us to acquire both accurate and precise measurements with deeper detectors.

This patented, innovative approach shall significantly reduce and possibly eliminate one of the main reasons behind the uncertainty of reservoir saturation monitoring using pulsed neutron logs, which is a shallow DOI of the measurement. Having a PNG that can produce neutrons at higher energy levels compared to the current industry standard should allow a deeper, more accurate, and a better representative evaluation of the reservoir.

Introduction

Reservoir surveillance is of critical importance for integrated reservoir management. Accurate oil saturation monitoring is needed for operational decision making and planning. Where the process involves running an open hole resistivity log for the calculation of the initial formation fluid saturation, later on, a well is completed to commence with the surveillance plan, which either will rely on using resistivity logs as well (in case no water injection scheme is followed) or pulsed neutron logs.

The later may involve carbon/oxygen (C/O) logs (used in case of fresh, mixed, or unknown formation water salinity exists) or sigma logs (used in case of high or known formation water salinity). Both types of measurements are generated due to the downhole nuclear interactions between neutrons and the formation, plus the wellbore and near wellbore logging environment. These nuclear events causing the production of inelastic gamma rays (used in C/O log interpretation) and capture gamma rays (used in sigma log interpretation) generally occurs in a time window of microseconds, roughly up to 30 μs for the inelastic gamma ray, and up to 1

ms for the capture gamma ray.

Accordingly, the radial distance into the reservoir (or the depth of investigation (DOI) of the measurement) at which these events take place is quite shallow. This implies a higher degree of uncertainty on the measurement, and consequently, the calculated water saturation, affecting the true assessment of the reservoir fluids' saturations — especially in case of challenging logging environments. Eventually, this shall compromise reservoir management plans, particularly in the case of mature oil fields where these logs can be the only means of determining the remaining oil saturation required to design the suitable oil recovery scheme.

In pursuit of solving this issue, this article discuss a unique approach and a study that proves that pulsed neutron measurements can be attained at a deeper DOI, and therefore provide a more reliable and representative assessment of the true formation fluids' saturations. This can be accomplished through the development of a new pulsed neutron generator (PNG) that can produce neutrons at a higher energy level, compared to the current industry standard of producing neutrons at 14 MeV.

The conducted study — which involved a specific tool design along with a relevant tool characterization — showed an almost 3" increase in DOI at a simulated energy level of 40 MeV compared to the current industry standard of 14 MeV.

Pulsed Neutron Logging

Current pulsed neutron logging tools uses an electric PNG or "particle accelerator" or minitron; to probe downhole formations with 14 MeV neutrons and record the returning gamma ray signal. PNG is different from a chemical neutron source or "chemical isotope" since it does not produce neutrons unless it is powered on, and so it is more user-friendly in terms of health, safety, and environment concerns. The PNG is also generally a preferred alternative to chemical neutron sources because the pulsing mode of operation for neutron generators allows for time dependent neutron and gamma ray measurements to be made, which is quite useful in formation evaluation applications. Finally, PNG produces high energy neutrons required for measuring inelastic gamma rays (C/O measurement).

The PNG outputs high-energy neutrons at approximately 14 MeV. The neutrons will interact with the elements in the wellbore and formation, causing the generation of different types of gamma rays. These gamma rays are then measured by detectors in the same logging tool, then further analyzed to ultimately produce the formation fluids' saturation used for reservoir monitoring.

Figure 1 illustrates the neutron interactions in a downhole logging environment, where it undergoes three main interactions:

1. **Inelastic scattering:** This takes place while the neutron is highly energetic at an energy of higher than 8 MeV. The neutron collides with a nucleus, leaving the nucleus in a higher energy excited state. The excited nucleus will return almost instantaneously to its ground state by emitting gamma rays, which are called inelastic gamma rays. This type of gamma ray is the one used for C/O logging application to measure and assess formation water saturation independent of formation water salinity values.
2. **Elastic scattering:** This is the dominant mechanism by which a neutron loses energy. An elastic collision is one in which the neutron collides with the nucleus of an atom, but does not excite the nucleus. The only energy transferred to the nucleus

Fig. 1 *The neutron interactions and different types of measured gamma rays in a downhole logging environment.*

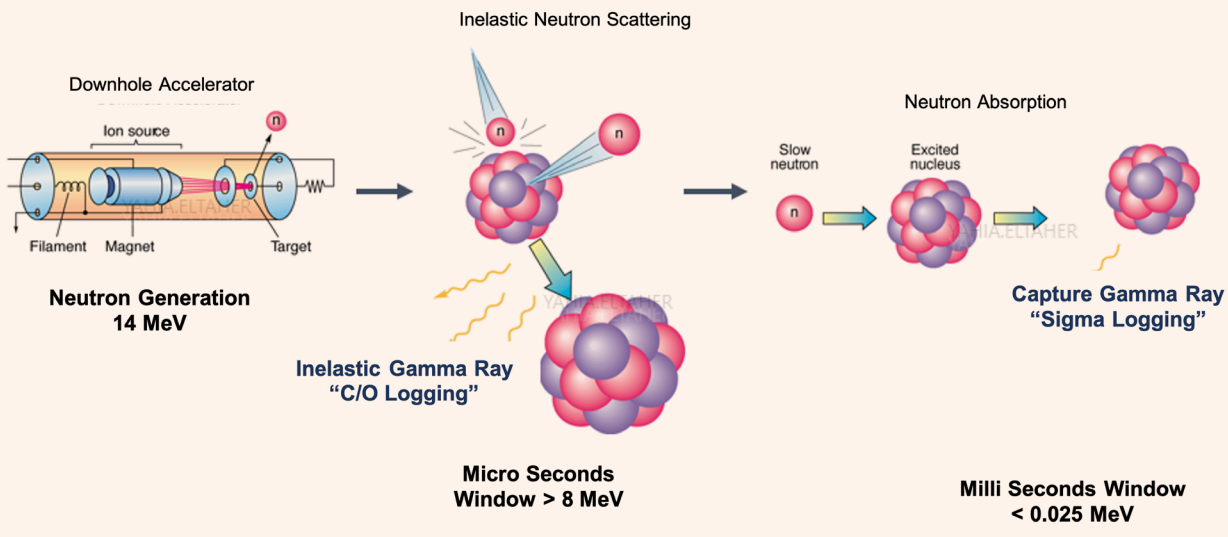

is kinetic energy and gamma rays released in this case.

3. **Thermal capture:** Once neutrons have lost sufficient energy through scattering, the slowed down neutrons with an energy of lower than 0.025 MeV can interact directly with the nucleus of the absorbing material in a process called neutron capture, and release of captured gamma rays, which is used for sigma logging application, to assess formation water saturation in the case of high formation water salinity only.

The main differences between both types of neutron sources:

Chemical Source

A radioactive isotope chemical source, always on, with a lifetime dependent on the isotope's radioactive decay half-life time. There are two commonly used chemical sources: The Am-241/Be (americium-beryllium) source, and the Cf-252 (californium) source. Both types of chemical sources produces lower energy distribution of neutrons (with an average of ≈ 4.5 MeV for Am-241/Be and ≈ 2.5 MeV for Cf-252), and so are not capable of having inelastic gamma ray such as the C/O measurement. For example, the Am-241/Be source would produce neutrons through the bombardment of beryllium with an alpha particle emitted from the unstable radioactive isotope Am-241, as shown in Eqn. 1:

$$ {}^{4}Be + {}^{2}He \rightarrow {}^{6}C + {}^{1}_{0}n \quad (1) $$

Electrical Source (PNG)

A PNG produces mono-energetic high energy neutrons (14 MeV) with no half-life time, but dependent on temperature and pulse duty — operationally active time. PNG produces neutrons through particle collision of an accelerated ionized deuterium with a tritium atom, as shown in Eqn. 2:

$$ {}^{2}_{1}H + {}^{3}_{1}H \rightarrow {}^{4}_{2}He + {}^{1}_{0}n \quad (2) $$

A Novel Study

There have been some recent advances in the logging industry, which introduced novel means to improve the population of the produced neutrons[1, 2]. This improvement has already been materialized in one of the latest pulsed neutron logging tools, which produces neutrons at 3.5×10^8 n/s, almost three times higher than the neutron output of $\approx 1 \times 10^8$ n/s by its predecessors. This new generation of PNGs shows an improvement in terms of the statistics of the measurement, i.e., better signal to noise ratio; however, there is no change with regards to the energy of the produced neutrons — the neutron energy remains at 14 MeV.

In this study, we introduce the idea of increasing the DOI of the measured gamma rays through increasing the energy level of the neutrons emitted by a PNG. Consequently, this shall provide a deeper measurement, which will be more representative of the true formation fluids' saturations, with less influence from the near wellbore environmental factors. To prove the concept behind this idea, we conducted a computer modeling and simulation study using Monte Carlo N-Particle (MCNP) — which is a code that can be used for neutron, photon, electron, or coupled neutron/photon/electron transport — for a pulsed neutron logging tool to determine the DOI for neutron energies higher than 14 MeV. This study is meant to verify and quantify this effect.

Fig. 2 An illustrated geometry for MCNP calculations.

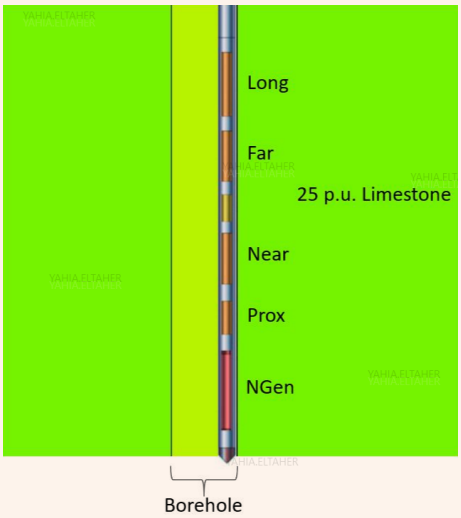

A logging tool was placed inside an open hole borehole traversing a 25 p.u. limestone formation. Figure 2 shows the neutron generator is where the neutrons are produced, and the Prox, Near, Far, and Long detectors are where the neutron induced gamma rays are detected. These four detectors are set in order of distance from the neutron generator, so that the Prox is the closest and Long is the furthest detector.

Structure of the MCNP Calculations

There are five different combinations of borehole and formation fluids that were considered. Each combination involved a "block" of 24 MCNP calculations. The 24 calculations inside each block represented the 24 possible combinations of three neutron energies (14

Table 1 The five blocks of MCNP calculations.

Block #	Borehole Fluid (O/W)	Formation Fluid (O/W)
1	50/50	50/50
2	100/0	30/70
3	100/0	90/10
4	0/100	30/70
5	0/100	90/10

Table 2 *The 24 MCNP calculations inside each block.*

Calculation #	Neutron Energy (MeV)	Spectrum	Detector
1	14	Inelastic	Prox
2	14	Inelastic	Near
3	14	Inelastic	Far
4	14	Inelastic	Long
5	14	Capture	Prox
6	14	Capture	Near
7	14	Capture	Far
8	14	Capture	Long
9	20	Inelastic	Prox
10	20	Inelastic	Near
11	20	Inelastic	Far
12	20	Inelastic	Long
13	20	Capture	Prox
14	20	Capture	Near
15	20	Capture	Far
16	20	Capture	Long
17	40	Inelastic	Prox
18	40	Inelastic	Near
19	40	Inelastic	Far
20	40	Inelastic	Long
21	40	Capture	Prox
22	40	Capture	Near
23	40	Capture	Far
24	40	Capture	Long

MeV, 20 MeV, and 40 MeV), two gamma ray spectral types (inelastic and capture) and four detectors (Prox, Near, Far, and Long).

The five blocks were differentiated based on the oil-water ratios (O/W) of the borehole and formation fluids. For the purpose of this study, oil is defined to be CH2 with a density of 0.8 g/cc, and water is defined as 70 kppm saltwater with a density of 1.05 g/cc. The five blocks are defined in Table 1, and the 24 calculations inside each block are listed in Table 2. The total number of calculations performed for this study is 120.

Workflow to Calculate DOI

The MCNP calculations were run on a computer cluster, where the simulation model incorporates information and characterization data that is relevant to a specific tool design in this case. As mentioned earlier, all pulsed neutron tools use the same physics for neutron generation and gamma ray detection. Differences mainly occur in the material of the gamma ray detectors, the detectors' spacing and tool electronics.

By default, the Prox and Near calculations involved 50 million histories, while the Far and Long calculation involved 150 million and 300 million histories, respectively. For better counting statistics, the Far detector was sometimes re-run with 600 million histories while the Long detector was sometimes re-run

Fig. 3 *The gamma ray origin points for the Near detector counts (formation only, 2D projection).*

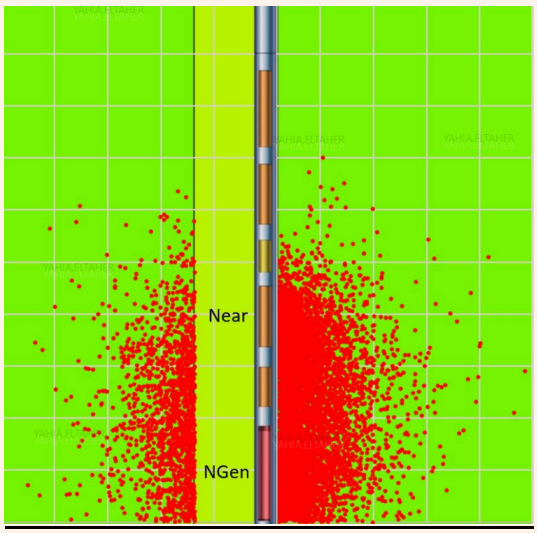

with 900 million histories or more. The calculations were all run in a certain mode (PTRAC) that allows the origin point of each detected gamma ray to be identified. Figure 3 shows an example from a Near detector inelastic calculation.

For the formation gamma rays, the radial distance of each origin point from the center of the borehole was calculated. By subtracting off the radius of the borehole, the radial distance into the formation, or "depth," was determined for each point. The depth points were then histogrammed over many events so as to establish a depth profile, Fig. 4. By performing a running integration over the depth profile, the fraction of total points lying within each depth was determined (righthand side of Fig. 4). By definition, the depth that contained 95% of the total points was said to be the DOI.

DOI Base Case

Block l of Table l was chosen as the base case to which all the other blocks will be compared to. The base case is plotted in Fig. 5.

Fig. 4 *The depth profile (left) and DOI determination (right) (Near detector, Block 1, calculation #2).*

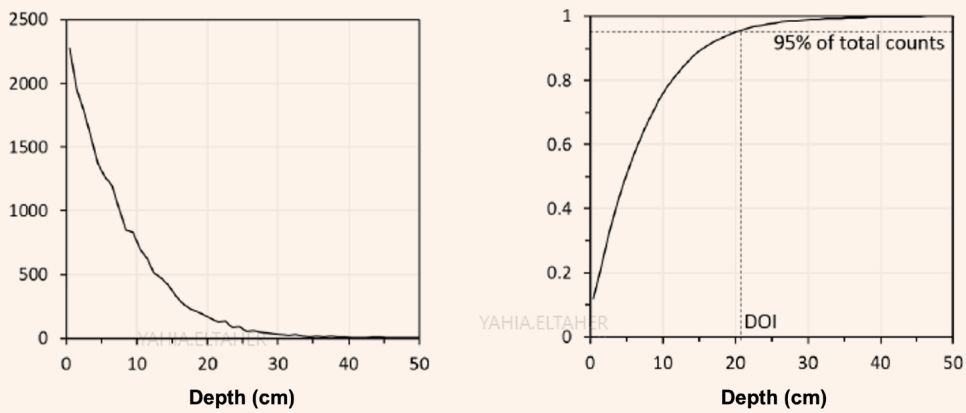

Fig. 5 *The inelastic (left) and capture (right) DOI for the Block 1 set of Table 1.*

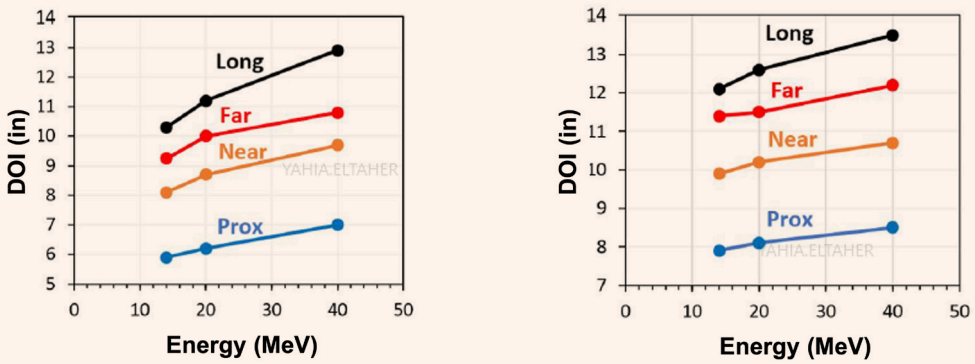

Fig. 6 *The inelastic and capture DOI for Blocks 2 to 5 of Table 1. The calculations, shown by the solid lines, are overlaid on the base case of Block 1 shown by the light dashed lines. In some cases, the effects of finite statistical precision is evident on the trends of the curves.*

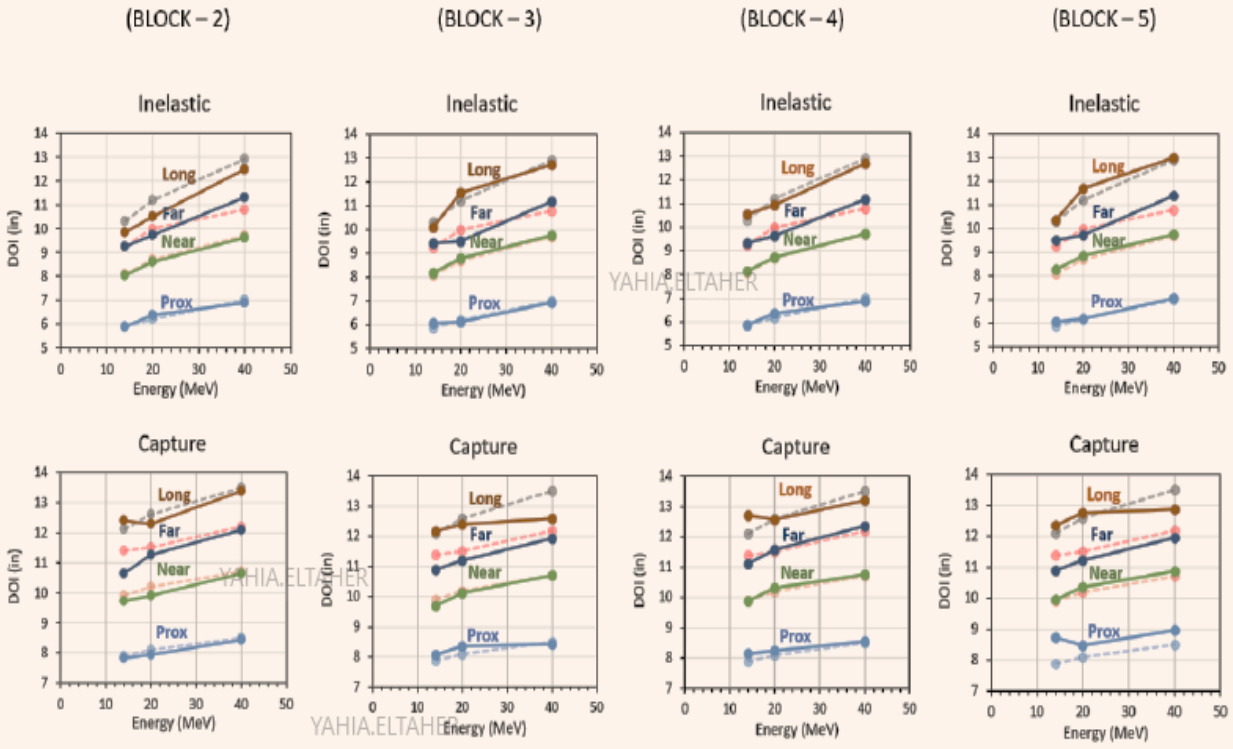

A preliminary conclusion is immediately apparent, i.e., the DOI increases with neutron energy for all detectors for both inelastic (C/O) and capture (sigma) measurements. The biggest improvement is for the inelastic Long detector measurement, which sees almost 3" deeper into the formation at 40 MeV.

Remaining Calculations

All remaining calculations, blocks 2 to 5 of Table 1, were run, and are plotted in Fig. 6. All calculations show the same observation of an increased DOI function in the neutron energy level, with respect to both the inelastic and the capture measurements. Although, some calculations experienced a statistical variation error such as that in block 3 for the Far detector inelastic measurement, and almost all the five blocks' calculation for the Long detector capture measurement.

The source of uncertainty is partly related to the nature of the measurement with an increased statistical variation moving away from the source, also the type of the detector being used for this specific tool, which might involve fewer counting statistics. The uncertainty estimate is 0.1" to 0.2" at 14 MeV (for all detectors); however, this is not valid above 14 MeV in the case of the Long detector where above 14 MeV the Long detector was apparently showing higher uncertainty.

Uncertainty in the Long detector is somewhere around 0.3" in scenarios without high chlorine, and 0.6" in scenarios with high chlorine. One possible explanation for the greater uncertainty is that there are some nuclear reactions, which are negligible below 14 MeV, but become prominent above 14 MeV, which cannot be handled by MCNP simulation. So, it is possible that these higher energy simulations — > 14 MeV — may require even more histories to recover the correct answer.

In Fig. 6, the average calculations are overlaid on top of the base case for comparison. Results shows that the changes in DOI associated with different borehole and formation fluids were within the statistical precision of the measurements, and therefore fairly small. It can be inferred that the type of formation fluid might have a more significant impact on the DOI of the measurement.

In Fig. 7, data from all experiments (all five blocks) for each detector is averaged, after eliminating imprecise data points to minimize statistical fluctuation. The clear conclusion from Figs. 5 to 7 is that by the time 40 MeV is reached, a significant improvement in DOI is achieved.

Figure 8 illustrates the average increase of DOI (after discarding statistical calculations) in percentage vs. the increase in neutron energy level, for each detector. It is observed that the enhancement in the DOI is more prominent in the case of the Long detector inelastic measurement compared to the same measurement from detectors closest to the source. The increase in the DOI is more uniform among all detectors in the

Fig. 7 *The average of the DOI curves, using data from all experiments (all five blocks) for each detector.*

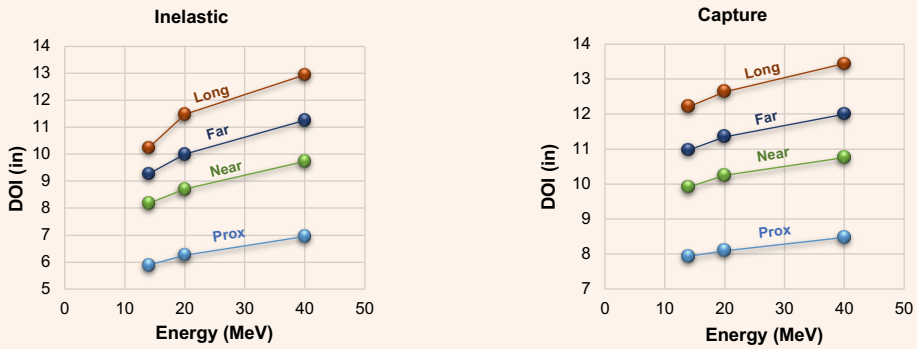

Fig. 8 *The average increase of the DOI curves in percentage vs. the increase in neutron energy level, for each detector.*

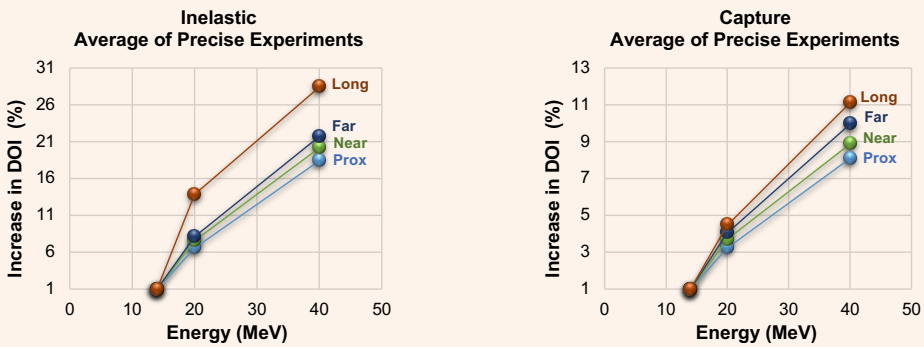

Table 3 *The DOI in inches for the inelastic measurements.*

Detector	Energy	Block 1	Block 2	Block 3	Block 4	Block 5	Ave	Max
Prox	14	5.9	5.9	6.06	5.87	6.06	5.89	6.06
	20	6.2	6.38	6.14	6.38	6.18	6.26	6.38
	40	7	6.89	6.93	6.89	7.05	6.95	7.05
	14	8.1	8.03	8.19	8.15	8.27	8.18	8.27
Near	20	8.7	8.62	8.78	8.74	8.86	8.71	8.86
	40	9.7	9.61	9.76	9.72	9.76	9.74	9.76
	14	9.25	9.25	9.41	9.33	9.53	9.28	9.53
Far	20	10	9.72	9.5	9.65	9.72	9.81	10
	40	10.8	11.3	11.18	11.18	11.38	11.26	11.38
	14	10.3	9.84	10.08	10.55	10.35	10.24	10.55
Long	20	11.2	10.51	11.54	10.95	11.69	11.48	11.69
	40	12.9	12.48	12.72	12.68	12.99	12.95	12.99

Table 4 *The DOI in inches for the capture measurements.*

Detector	Energy	Block 1	Block 2	Block 3	Block 4	Block 5	Ave	Max
Prox	14	7.9	7.84	8.07	8.15	8.74	7.94	8.15
	20	8.1	7.95	8.35	8.23	8.47	8.09	8.35
	40	8.5	8.43	8.43	8.54	8.98	8.48	8.98
	14	9.9	9.72	9.69	9.88	9.96	9.91	9.96
Near	20	10.2	9.9	10.12	10.31	10.35	10.25	10.35
	40	10.7	10.63	10.71	10.75	10.87	10.76	10.87
	14	11.4	10.63	10.91	11.1	10.91	10.97	11.1
Far	20	11.5	11.26	11.2	11.58	11.22	11.35	11.58
	40	12.2	12.09	11.93	12.36	11.97	12.00	12.36
	14	12.1	12.4	12.17	12.72	12.36	12.21	12.36
Long	20	12.6	12.28	12.4	12.56	12.76	12.64	12.76
	40	13.5	13.39	12.6	13.2	12.87	13.36	13.5

case of the capture measurement.

To help quantify this finding, the average of all calculations at 14 MeV, 20 MeV, and 40 MeV for all four detectors from each block are listed in Tables 3 and 4, for inelastic and capture measurements, respectively. It has to be noted that these figures are not absolute, and should not be taken as a general reference, due to the reasons mentioned earlier, in addition to the selected workflow to conduct the study; where its main objective was proof of concept. Note that some calculations were not considered in the data averaging column, or the maximum value column, due to their high statistical variation.

Logging Environment Effect on Pulsed Neutron Measurement

The pulsed neutron logging tools currently being used in oil fields' reservoir surveillance are limited with its shallow DOI into the formation. Consequently, downhole measurements are highly affected by the wellbore and near wellbore environmental factors, such as the wellbore washouts (or hole enlargement), poor cement condition behind the production casing, drilling mud filtrate invasion into the formation, and wellbore fluid re-invasion[3]. The examples discussed next will illustrate the impact of such factors on the pulsed neutron measurements, and accordingly, the calculated formation fluids' saturations derived from these logs.

Figure 9 shows that the impact of wellbore washout or enlargement (as shown with orange shading on track 4) on the C/O raw data (dashed blue line); where the brown shading on the same track shows the decrease in the C/O ratio across the washed out zones in a wellbore filled with water (track 3), with extreme effect just below the casing shoe (top highlighted zone) where the washout is the largest.

Cement quality is not only critically important in well control, but also has a direct effect on pulsed neutron reservoir saturation monitoring[3]. Figure 10 shows the effect of cement quality on saturation monitoring using C/O logs. In this case, the C/O log data processing shows a false apparent increase in water volume (track 3) across the intervals where the cement quality is poor due to fluid channeling, as shown by the cement bond log variable density log image (track 4) and ultrasonic cement bond map (track 5)[3].

During drilling; the drilling mud filtrate invades into the near wellbore formation. The amount of the filtrate invaded and the depth of the invasion depend on how well the mud properties — such as solid particle size distribution — match the formation rock properties — such as pore throat size distribution — and the overbalance pressure applied during drilling.

The example in Fig. 11 demonstrates the effect of drilling mud filtrate invasion, as evidenced by the separation of the original open hole resistivity logs with different DOIs (track 4). One year after the well was cased hole completed, part of this invaded filtrate was still detectable by the shallow pulsed neutron log, especially the shallower C/O log (track 5)[3].

The examples here show the significant impact of unfavorable downhole logging conditions on the pulsed neutron measurement and the accuracy of saturation monitoring using these logs. This consequently,

Fig. 9 *The effect of wellbore washout on the C/O log measurement.*

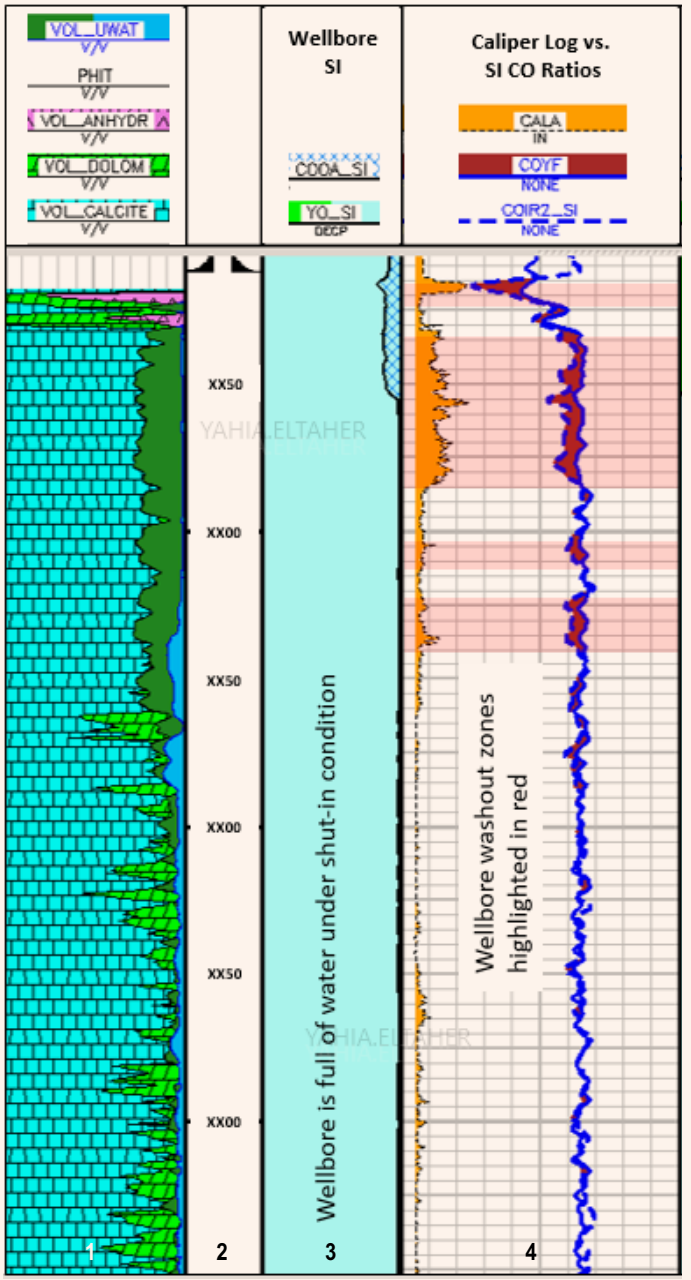

compromises reservoir management decisions for oil field development and management. Therefore, the application of the discussed new approach shall help eliminate the high uncertainty associated with the physical limitation of these nuclear measurements due its shallow DOI.

Conclusions

The main challenge facing reservoir surveillance using pulsed neutron logs when compared to the relatively deep saturation profiling from resistivity logs (up to 120" deep) is its shallow DOI, which is generally in the range of 7" for C/O measurement and 12" for sigma measurement. This limitation places a high uncertainty on the saturation calculation from such logs, especially in situations where data is affected by wellbore or near wellbore environmental factors, as illustrated earlier. Therefore, the need for a deeper pulsed neutron measurement is crucial for accurate and more reliable reservoir saturation monitoring. This has been proven achievable through the development of a new PNG that can produce neutrons at a higher energy level.

The conducted MCNP simulation study was run to determine the DOI for a pulsed neutron logging tool at high neutron energies — > 14 MeV. The results, averaged over a variety of different borehole and formation fluids, shows that the DOI rises substantially with energy for all tested detectors. For example, in the case of the Long detector inelastic measurement, the increase over the 14 MeV value is almost 3" at 40 MeV, which is equivalent to 28.5% using the average of most precise calculations, and 29% using the maximum value only.

In the case of the Long detector capture measurement, the increase over the 14 MeV value is almost 1.5" at 40 MeV, which is equivalent to almost 11% using the average of most precise calculations, and 11.6% using the maximum value only.

Accordingly, it can be inferred that the enhancement in DOI with the increase in neutron energy is more prolific in the case of the inelastic measurement compared to the capture measurement. The deeper the detector (further from the source) the better the DOI, although this can compromise the precision of the measurement. Yet with the recent technology advancements mainly in PNG (producing more neutron population) and gamma ray detector technology (of higher and faster count rates), this should enhance the precision of the measurement and enable us to acquire both accurate and precise measurements at deeper detectors.

One observation to note is that block #5 calculations are generally showing the best results in terms of improvement in DOI with the increase in neutron energy level. This infers that water in the wellbore and oil in the formation are more favorable compared to other scenarios. On the contrary, oil in the wellbore and water in the formation is observed to be the least favorable condition, as per block #2 calculations, where the least improvement in DOI is encountered.

Acknowledgments

This article was presented at the International Petroleum Technology Conference, Riyadh, Kingdom of Saudi Arabia, February 21-23, 2022.

Fig. 10 *The effect of poor cement quality on apparent water saturation calculated from the C/O measurements.*

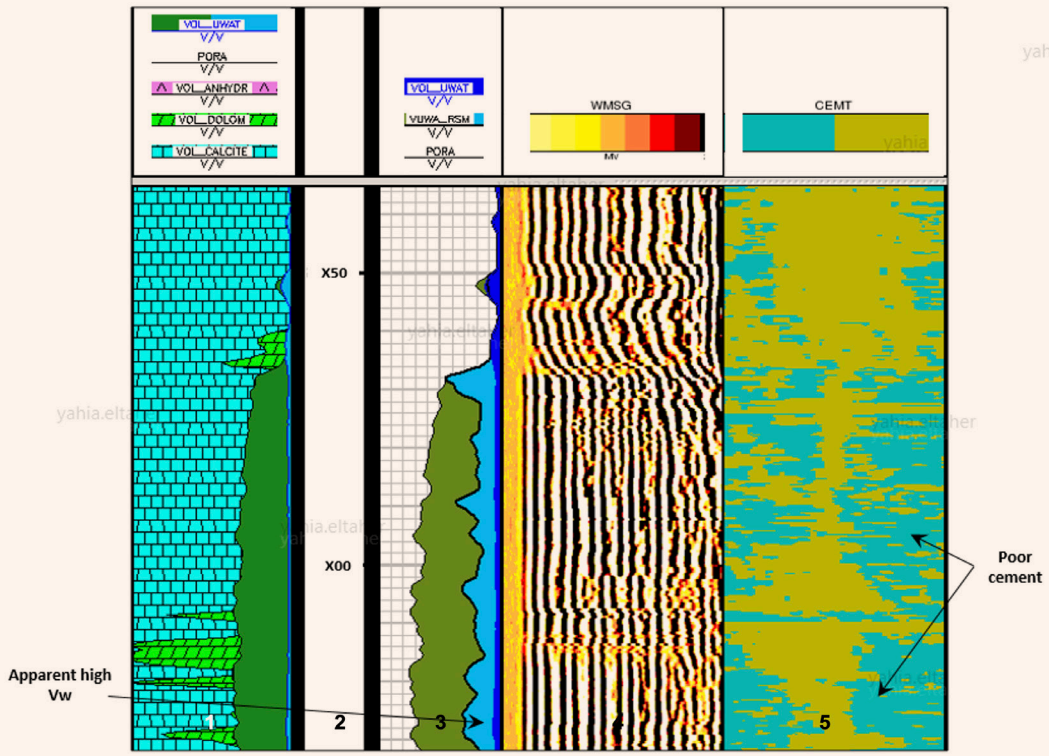

Fig. 11 *The effect of drilling mud filtrate invasion on C/O and capture (sigma) log measurements. Tracks 4 and 5 display C/O and sigma log results (dark blue is water volume derived from deep open hole resistivity log, light blue is water volume from pulsed neutron log, and green is oil).*

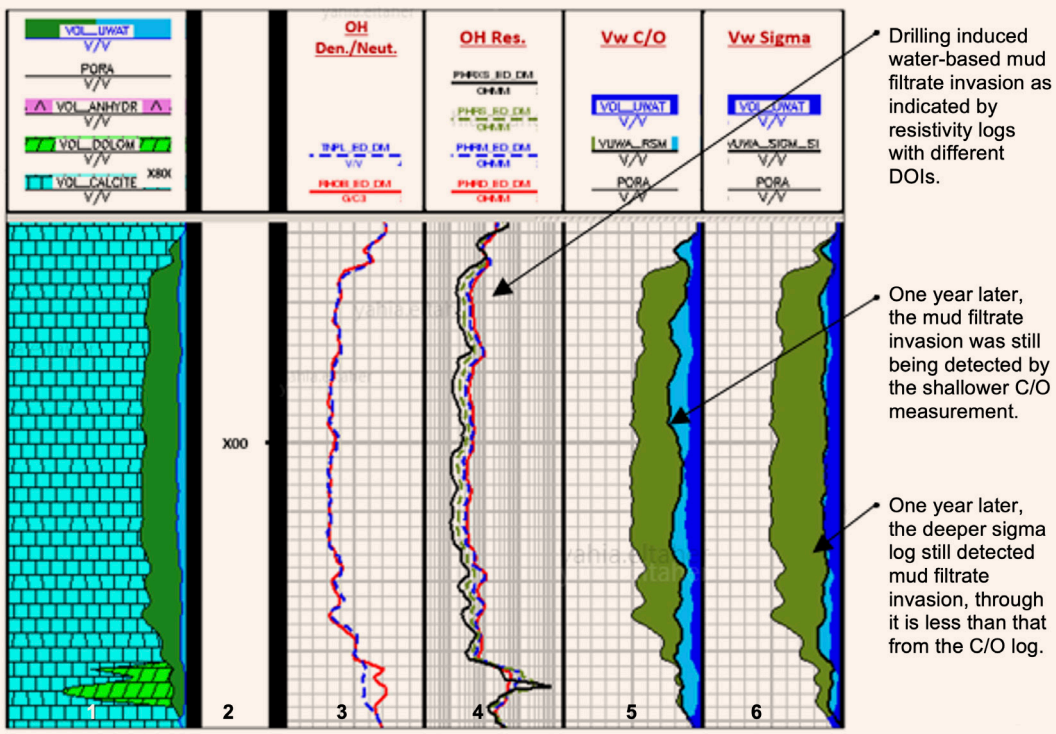

References

1. Rose, D., Zhou, T., Beekman, S., Quinlan, T., et al.: "An Innovative Slim Pulsed Neutron Logging Tool," paper presented at the SPWLA 56th Annual Logging Symposium, Long Beach, California, July 18-22, 2015.
2. Navarro, J. and Guo, W.: "High-Efficiency, High-Yield Pulsed Neutron Generators for the Well Logging Industry," SPE paper 181345, presented at the SPE Annual Technical Conference and Exhibition, Dubai, UAE, September 26-28, 2016.
3. Eltaher, Y., Ma, S.M. and AlNasser, M.: "Critical Factors Affecting Pulsed Neutron Saturation Monitoring in Carbonate Reservoirs," SPE paper 192216, presented at the SPE Kingdom of Saudi Arabia Annual Technical Symposium and Exhibition, Dammam, Kingdom of Saudi Arabia, April 23-26, 2018.

About the Authors

Yahia A. Eltaher

B.S. in Geology and Chemistry, Cairo University

Yahia A. Eltaher is a Petrophysicist working in Saudi Aramco's Reservoir Description Division of the Northern Area Petrophysics Unit, focusing on reservoir surveillance. He has more than 16 years of experience in logging and formation evaluation. Yahia started his career as an Operation Petrophysicist with the Gulf of Suez Petroleum Co. in Egypt. He then joined Halliburton for eight years, working in various locations throughout the Middle East. During this period, Yahia provided support and consultation, regionally and globally, with regards to pulsed neutron logging, production logging, and well integrity.

He has authored and published several technical papers and filed two patents with regards to reservoir saturation monitoring.

Yahia received his B.S. degree in Geology and Chemistry from Cairo University, Giza, Egypt.

Dr. Greg J. Schmid

Ph.D. in Physics, Duke University

Dr. Greg J. Schmid is a Staff Physicist at Weatherford who supports the pulsed neutron logging tools. Prior to joining Weatherford, he worked as a Scientist for Sandia National Laboratories, Schlumberger, and the University of California.

In 1989, Greg received his B.S. degree in Physics from Rensselaer Polytechnic Institute, Troy, NY, and in 1995, he received his Ph.D. in Physics from Duke University, Durham, NC.

Greg is the author of 61 publications and holds two granted patents.

A Novel Foamed Acid System Stabilized by Composite Material for Fracturing Applications

Dr. Abeer A. Alarawi, Dr. Bader G. Alharbi and Ahmed S. Busaleh

Abstract /

Carbonate reservoirs hold 60% of the world's oil and 40% of the gas. Therefore, developing high-impact and innovative technologies for well stimulation, such as foamed acid fracturing fluids, is essential for restoring well productivity and enhancing commercial productivity for carbonate reservoirs. Acid fracturing treatment is associated with reactivity control, fluid loss control, and conductivity generation challenges. For overcoming some drawbacks associated with conventional acid fracturing, foamed acid fluid is applied to enhance retardation, reduce water consumption, improve acid diversion, remove water or emulsion blocks, and improve conductivity generation. In this study, a unique foamed acid system stabilized by composite material was studied to develop fracturing fluid at 275 °F to 350 °F. In addition, the foam stability, rheology, and morphology characteristics were investigated using several characterization tools at 275 °F to 350 °F.

The composite material, comprised of a nanosheet and a surfactant, were added to either a pure acid or acid system that contains several additives for developing stable surfactant/nanosheet-based foamed acid fluid. To evaluate foam rheological properties and the thermal stability at dynamic conditions, foam loop rheometer experiments were conducted at 275 °F to 350 °F, 1,050 psi, and 70% nitrogen (N) quality. A high-resolution optical microscope was also utilized to observe foam texture morphology and further assess foam stability. In addition, the foam decaying time was observed by determining the foam half-life time — foam volume altering as a function of time.

The static and dynamic results illustrated that foamed acid fluid stability and thermal adaptability were improved after adding composite material at 275 °F to 350 °F. The viscosity of foamed acid increased by double and its viscosity was higher than 45 centipoise (cP) at a shear rate of 300 S^{-1} and 350 °F. In addition, the foam structure of the surfactant/nanosheet-based foamed acid displayed a small hexagonal bubble size, which positively affected the stability of foam to reach up to three hours at 300 °F. In contrast, the stability of pure foamed acid was one hour.

This result is attributed to the adsorption of composite material at the liquid-gas interface layer that enhances the mechanical strength of the foam layer (lamellae film) and provides a more robust barrier between the gas bubbles and liquid phase, resulting in delaying the coalescence of the bubbles. The developed surfactant/nanosheet-based foamed acid possesses several advantages over the conventional acid fracturing fluids: long stability, adequate viscosity (obtained without adding gelling agent), low water consumption, and high efficiency at 275 °F to 350 °F.

Introduction

Hydrocarbons are one of the most important energy sources for human civilization, and are expected to continue to be the primary source of energy in the coming eras. Therefore, numerous techniques and technology have been developed to boost hydrocarbon commercial productivity, such as hydraulic fracturing. Based on that, acid fracturing treatment is the viable and economically friendly technique to fracture the formation without damage. It is associated with challenges like reactivity control, fluid loss control, and conductivity generation. The alternative method to overcome these drawbacks is utilizing foamed acid fluids[1, 2]. In general, several researchers have studied foamed fracturing fluids properties and concluded that it is a promising approach to reduce water consumption, clay expansion and well blocking, fluids leakoff, and related formation damage issues[3].

In detail, foams are a mixture comprised of liquid and gas phases, where the liquid phase performs as a moving phase and gas as a diffused phase. Therefore, their rheological properties rely on many factors, including gas type, surfactant, stabilizing additive, foam quality, temperature, pressure, bubble texture, shear rate, and viscosity[4].

Based on the literature, the first reported foam fluid for fracturing application was in Youngstown, Ohio, in 1975. The foam contained only a mixture of acid, water, and nitrogen (N) and displayed better fracturing

performance than the traditional hydraulic fracturing fluids. Later, other foamed fluids were created by mixing liquid carbon dioxide (CO_2) and nitrogen gases (N_2), and used successfully for a large-scale hydrofracturing operation in the Devonian shale well in Jackson County, West Virginia[5].

Harris et al. (1987)[6] reported the result of foam fluid stability experiment at high temperature, 300 °F. He used a recirculating loop viscometer to demonstrate the rheological behavior of N_2-based foamed fluid stabilized by guar gum additive. He found that foam stability relies on the surfactant concentration, not the gelling agent[6]. In another study published, Harris et al. (1993)[7] investigated the effect of adding additives like gel stabilizer, polymer, and high pH crosslinked fluid on the foam rheology at high temperatures, 300 °F. In this study, borate ions play a role in enhancing foam viscosity where it forms a complex crosslink pair with the guar stabilizing additive. Increasing the crosslinker concentration led to an improved foam stability at high temperatures — up to 250 °F at a pH of 10.

Barati and Liang (2014)[8] reported that high pH is required to bond the borate ions and form a crosslink with the gelling agent. Verma et al. (2017)[9] studied bentonite clay as a gelling agent to improve foam rheology at low concentrations of anionic surfactant. They studied many foams' characteristics such as apparent viscosity, viscoelasticity, and thermal stability. They attributed foam thermal stability enhancement to the adsorption of polymer molecules of surfactant onto the guar/bentonite clay particle's surface that results in better stabilization of foam bubbles[9]. Wang et al. (2017)[10] reported the experimental results of high-pressure and high temperature foam stability. They observed that the performance of CO_2-based foam was greatly affected by the surfactant type and its hydrophilic lipophilic balance value, i.e., cationic or nonionic surfactants.

Nanoparticles have also been widely studied to improve foam's stability for fracturing application at high temperatures[11]. In one example, silicon dioxide (SiO_2) nanoparticles were applied in several experiments to enhance foam stability at high temperatures[12], which had been used to improve the stability and thermal adaptability in the presence of an anionic surfactant sodium dodecyl benzenesulfonate (SDBS) at high temperature — 90 °C. They also found that the proppant carrying capacity of SiO_2/SDBS foams was slightly larger than the SDBS foam and gel/SDBS foams[11]. Emrani and Nasr-El-Din (2017)[13], conducted several experiments to find the optimal surfactant concentration for CO_2-based foam stability at high temperature (212 °F) and pressure (800 psi)[13]. They found that the temperature and pressure displayed differing effects on foam stability when an anionic surfactant was utilized. Nanoparticles enhanced the foams' stability of the nonionic surfactant, surfactant with guar gum, and viscoelastic surfactant[13].

These studies point out that the foam's thermal stability can improve by applying the synergetic between nanoparticles and surfactant. This sort of material combination can cause bifunctional effect where nanoparticles resist foam decaying at high temperatures and surfactant possesses high adsorption ability at the gas-liquid phase interface[11]. As a result, it led to increase the mechanical strength of the foam's lamellae, slowing the foam's drainage rate and decreasing bubble coalescence[14].

Along with nanoparticles, nanosheet materials have also been applied as foam stabilizer additives for fracturing applications. Nanosheets are a relatively new material, which has been widely studied for its unique properties and significance to extensive applications, including energy materials, biosensors, catalysis, and biomedicine[15]. Bulk nanosheet material crystallizes in stacks of strongly bonded layers with weak Van der Waals force, allowing exfoliation into individual, atomically thin layers[16]. In addition, nanosheet has a rich active surface, amphiphile, and size depending on characteristics that perfectly create very stable emulsions with organic solvents[17].

In this study, the composite material comprised of surfactant and nanosheets was applied to improve thermal stability and rheological property of foamed acid fracturing fluid at high temperature conditions, 275 °F to 350 °F.

Materials

Commercially available surfactants were utilized to prepare foamed acid fracturing fluids. The critical micelle concentration of the surfactant was nearly 1 wt% to 2 wt% at 25 °C. The nanosheet material was used in a powder form. The nanosheet, with a purity of > 99.8 wt%, has a nearly spherical shape. For the foamed acid system, 5% hydrochloric (HCl) acid was mixed with other additives such as a corrosion inhibitor and iron stabilizer. N_2 was used with a purity of 99.9 wt%. All the dispersions were mixed using deionized water.

Method

Preparation of Nanosheet/Surfactant Dispersions

The nanosheet/surfactant dispersion was prepared by mixing 3 vol/vol% of nanosheet and 5 vol/vol% of surfactant in 100 ml of deionized water. The dispersion was stirred for 24 hours at high revolutions per minute to ensure homogeneity.

Preparation and Characterization of Foamed Acid Fluids

Foamed acid fluids were statically examined by measuring the foam's half-life time. In addition, the influence of temperature, additives, and surfactant/nanosheet composite on foamability, and stability were also studied. The surfactant/nanosheet-based foamed acid was prepared by the warning blander method where 100 ml of surfactant/nanosheet dispersion was mixed with 5% HCl acid or a 5% HCl acid system for 15 minutes at a high shear rate using a Torrington Connecticut, 06790 blender.

Then, the prepared foamed acid solution was transferred to a sealed cylinder to record foam decaying time (half-life time measurements) at 77 °F to 200 °F

using an atmospheric oven pressure. In addition, foam dynamic viscosity, micromorphology, and thermal stability were evaluated using a foam loop rheometer and microscope instrument. A foam loop rheometer was utilized to investigate the effect of dynamic conditions on the foam's stability and rheological properties. Several tests were conducted at share rates of 300 S^{-1}, 275 °F to 350 °F, 1,500 psi, and 70% N_2 quality using a high-pressure, high temperature foam rheometer system (Chandler Engineering, Model: 8500-3K), Fig. 1.

The working mechanism of the instrument is as follows: a Coriolis flow meter provides mass flow measurement of the sample. The differential pressure between the tube's two ends is measured using differential pressure transducers — high and low ranges. The shear rate and stress of the fluid flow through the pipe were calculated using Eqns. 1 and 2. The N_2 quality was calculated from obtained liquid and gas mixture mass measurements. A high-resolution optical microscope was used to observe the morphological structure of foams during dynamic testing assessed with a view cell and light bulb assembly, Fig. 2.

$$\text{Shear Rate } (\gamma), s^{-1} = \frac{8 \times Velocity}{Tube\ ID} \quad (1)$$

$$\text{Shear Stress } (\tau), {}^{lb_f}/_{ft^2} = \frac{Tube\ ID \times Differntial\ Pressure}{4 \times Tube\ Length} \quad (2)$$

Results and Discussion

Static Foam Stability

In hydraulic fracturing, long foam stability is important for efficient fracturing performance to withstand

Fig. 2 *The class oven includes a flow loop, Coriolis flow meter, view cell, and light bulb assembly.*

Fig. 1 *A schematic of the high-pressure, high temperature foam rheometer system (Chandler Engineering, Model: 8500-3K).*

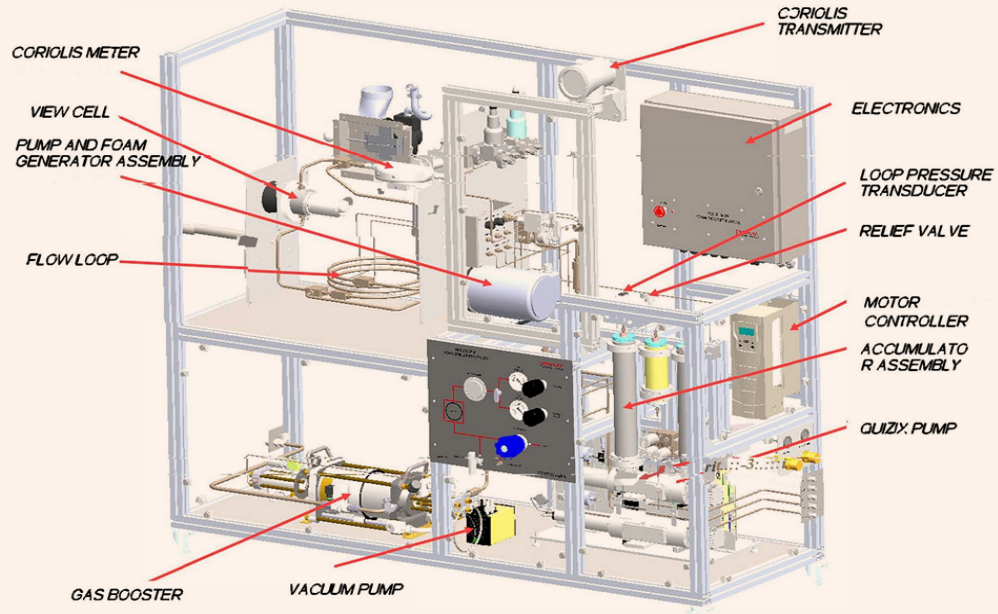

the pumping process and temperature increase with an increasing well depth. During the foamed fluid pumping operation, the temperature of foamed fluid increases gradually with depth, which might deteriorate the foam stability. Therefore, the injection process time and well temperature are essential parameters to effective foamed acid designing. Accordingly, a foam half-life time of 5% HCl acid and 5% HCl acid system fluids — stabilized by surfactant/nanosheet composite or surfactant — were examined at a wide range of temperatures, 77 °F to 200 °F, Fig. 3.

Figures 4 and 5 show the images of static foam stability (half-life time) tests at 200 °F of 5% HCl acid and 5% HCl acid system foams stabilized by surfactant/nanosheet composite, and only surfactant.

For 5% HCl acid foams, the half-life time of surfactant/nanosheet-based foamed was longer (360 minutes) than that of the surfactant-based foam (480 minutes)

Fig. 3 *Foam half-life time of 5% HCl acid and 5% HCl acid system foamed fluids stabilized by surfactant/nanosheet composite or surfactant at 77 °F to 200 °F.*

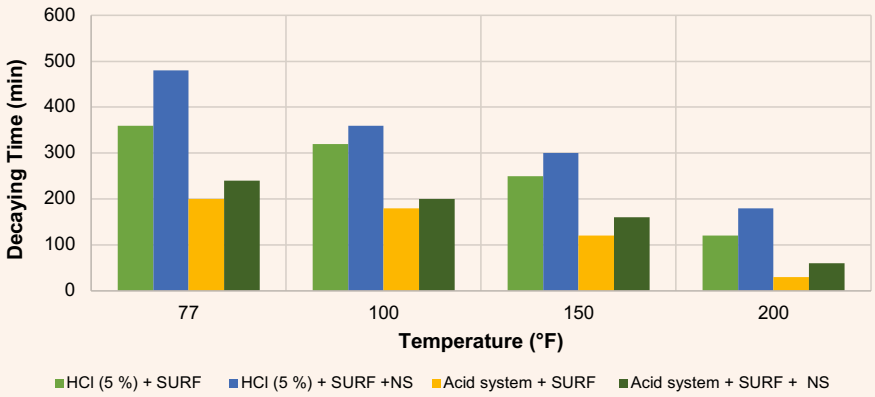

Fig. 4 *The static foam stability (half-life time) tests at 200 °F of 5% HCl acid foamed fluids stabilized by surfactant/nanosheet composite and surfactant.*

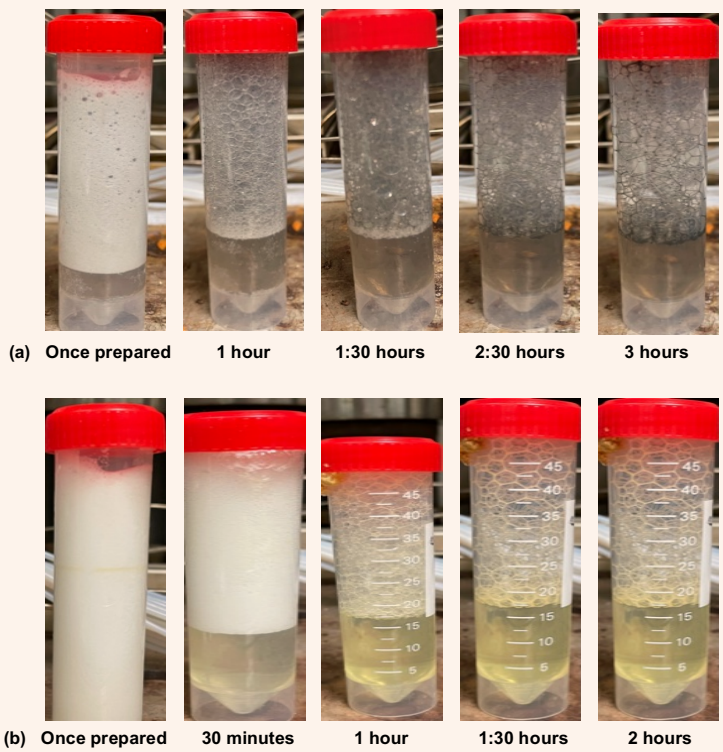

Fig. 5 *The static foam stability (half-life time) tests at 200 °F of 5% HCl acid system foamed fluids stabilized by either surfactant/nanosheet composite or only surfactant.*

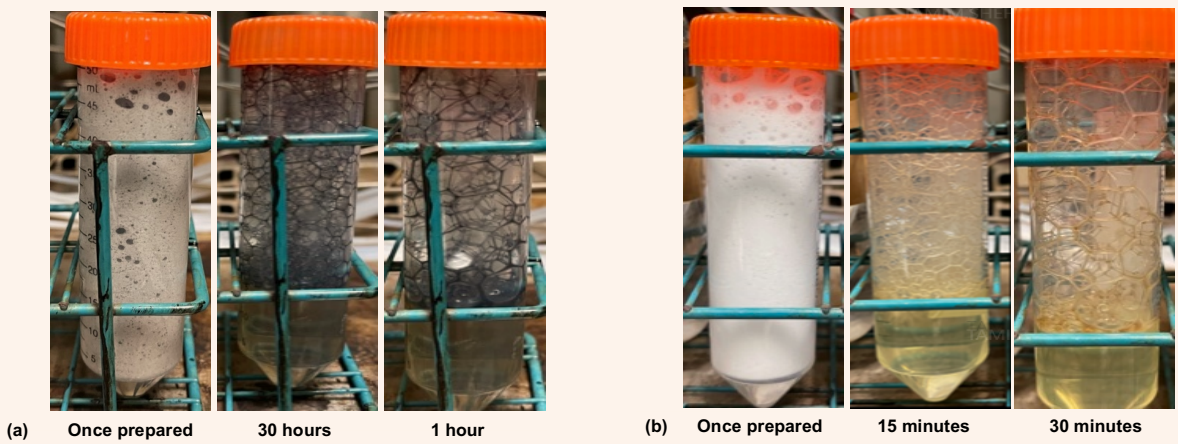

at 77 °F. The half-life time at 150 °F was reduced to 250 and 300 minutes for surfactant and surfactant/nanosheet-based foams, respectively. The thermal stabilities at 200 °F of the surfactant/nanosheet and surfactant-based foams were 180 and 120 minutes, respectively. In contrast, the foamed 5% HCl acid system stabilized by either surfactant/nanosheet or only surfactant demonstrated less half-life time than the 5% HCl acid foams, due to the effect of the additives in the acid system.

The thermal stabilities at 200 °F of the surfactant/nanosheet and surfactant foams were 60 and 30 minutes, respectively. As the drainage progressed, the surfactant-based foam's average thickness deteriorated with time faster than the surfactant/nanosheet composite-based foam, which is a disadvantage to foam stability, especially in a long-time fracturing operation with a low flow rate. The surfactant/nanosheet composite exhibited a significant enhancement in the foamed acid thermal stability compared to the foams that were stabilized with only surfactant — by a 20% to 50% improvement in foam half-life time.

Foam Rheological Characteristics

Foamed fluid viscosity is an essential property to the fracturing process performance, including proppant suspension and filtration, due to the unique structure of foamed fluids (contains microstructure-size bubbles). The viscosity of foamed fluid significantly relies on the bubble's property, scale, volume fraction, stability, and alerting over time[11].

Figure 6 demonstrates the altering of foam viscosity with time of several foamed acid fluids stabilized by either surfactant or surfactant/nanosheet composite at fixed share rates of 300 S^{-1}, 70% N_2 quality, 1,500 psi, and a wide range of temperatures, 275 °F to 350 °F.

Fig. 6 *The altering foam's viscosity with a time curve of foamed fluids stabilized by surfactant and surfactant/nanosheet composite at 300 S^{-1}, 70% N_2 quality, 1,500 psi, and a wide range of temperatures, 275 °F to 350 °F.*

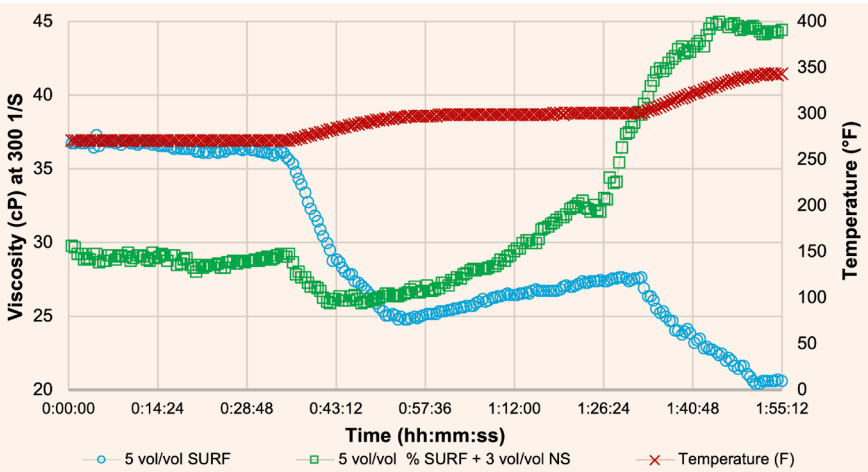

For the surfactant-based foam, 5 vol/vol%, the viscosity reached 37 cP at 275 °F, and then decreased with time to 26 cP to 22 cP at temperatures of 300 °F to 350 °F, respectively. The decrease in viscosity can be attributed to the increase in liquid drainage, and the coalescence of the bubbles with an increasing temperature that negatively affects foam quality and stability.

For the surfactant/nanosheet composite-based foam, 5.0 vol/vol% surfactant, and 3.0 vol/vol% nanosheet, the viscosity exhibited a slightly low value — 28 cP at 275 °F — followed by a rapid increase to 45 cP at 350 °F. At a temperature of 350 °F, the surfactant/nanosheet composite-based foam's viscosity was two times that of the surfactant-based foam, reflecting the positive impact of the nanosheet on reducing foam rupture and improving foam stability at high temperature, due to the strong adhering ability of surfactant/nanosheet particles to the bubble surface, which enhanced foam resisting toward deformation. The viscosity of the foamed 5% HCl acid fluid stabilized by either surfactant, 5 vol/vol%, or surfactant/nanosheet composite, 5.0 vol/vol% surfactant and 3.0 vol/vol% nanosheet, at 300 S^{-1}, 70% N_2 quality, 1,500 psi, and 300 °F, Fig. 7.

The average viscosity of foamed acid fluid stabilized by only surfactant was 25 cP during the testing time. For the foamed acid stabilized by the surfactant/nanosheet composite, the initial average viscosity was around 18 cP, and then increased to 30 cP after passing 45 minutes of testing time. At a temperature of 300 °F, the surfactant/nanosheet composite effectively prevented foam film rupture and improved thermal stability that enriched the foamed acid characteristics for an efficient fracturing operation.

Foam Film Microstructure

The dynamic foam stability was also investigated from the perspective of altering the foam's microstructure with time. Figure 8 shows the foam film microstructure of 5% HCl acid stabilized by a surfactant/nanosheet composite and surfactant at 300 °F. At the beginning of the experiment, the surfactant-based foamed acid bubbles' size was small and the bubbles' population was enormous. After passing 30 minutes of testing time, the bubbles of the foamed film started to expand and take a hexagonal shape. The population was reduced due to the bubbles coalescing, forced by the Young-Laplace phenomena (the merging between big and small bubbles driven by the pressure difference).

In contrast, the 5% HCl acid foamed acid bubbles stabilized by a surfactant/nanosheet reserved their hexagonal shape and population for approximately three hours. This result reflects robust foam morphology, demonstrating that a surfactant/nanosheet composite strengthens the foam film and prevents bubbles from collapse and drainage. The perfect foam film microstructure of surfactant/nanosheet-based foamed acid is associated with the strong adsorption ability, high specific surface area, and temperature resistance of the nanosheet at high temperatures.

These properties help the nanosheet particles to bond with surfactant molecules and then accumulate at the surface of the bubble. This particle model creates a supportive layer between foam and liquid phase, preventing foam from coalescing, drainage, and deformation.

Conclusions

The composite of the surfactant and nanosheet successfully enhanced the stability and rheological characteristics of 5% HCl acid and 5% HCl acid system foamed fluids; this is a significant result for a foamed acid pumped from a surface at an average temperature to a high temperature reservoir. The foamed acid fluids were statically and dynamically investigated utilizing

Fig. 7 *The altering foam viscosity with a time curve of foamed 5% HCl acid fluids stabilized by surfactant or surfactant/nanosheet at 300 S^{-1}, 70% N_2 quality, 1,500 psi, and 300 °F.*

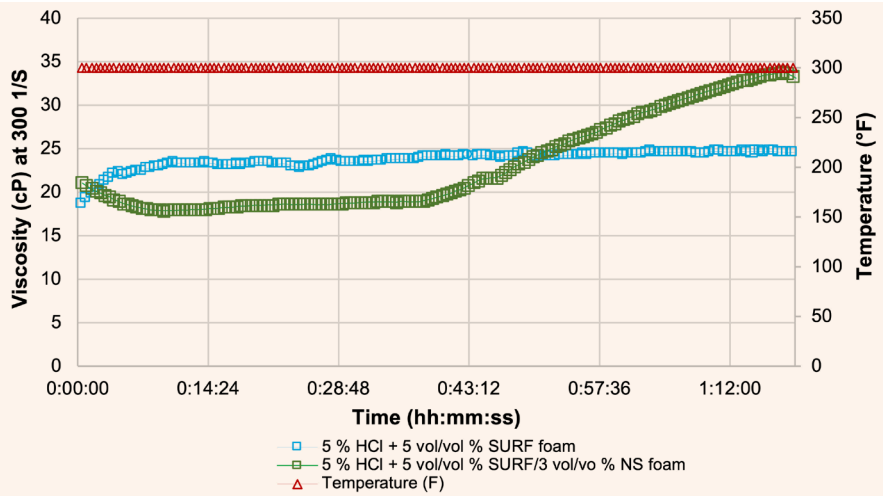

Fig. 8 *The foam film morphologies of 5% HCl acid foamed fluids that are stabilized by (a) surfactant, and (b) surfactant/nanosheet at 300 °F.*

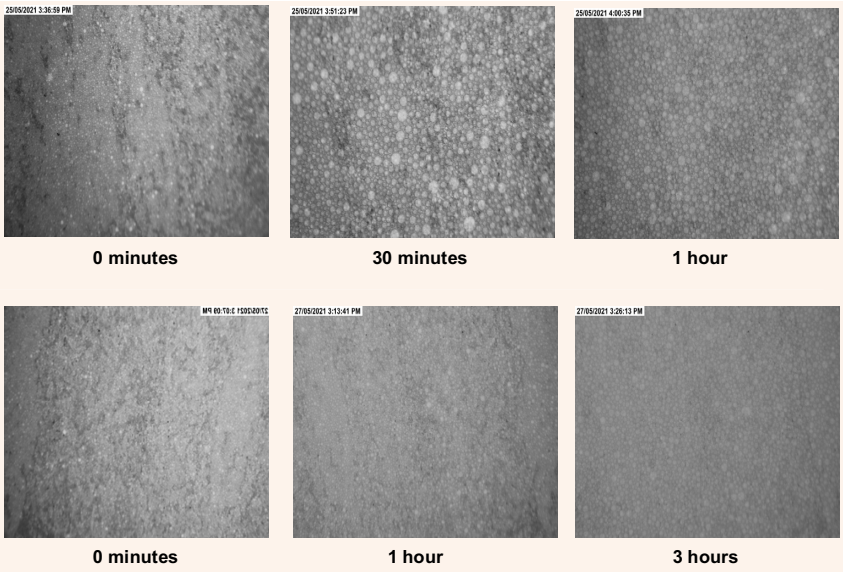

several characterizing techniques. Based on the results of this study, the following conclusions were drawn:

- The surfactant/nanosheet composite improved the foamed acid stability by nearly 20% to 50%, compared to the foamed acid stabilized by the surfactant only.
- The effect of temperature on the foam deformation was reduced for foamed acid fluids stabilized by the surfactant/nanosheet composite at 275 °F to 350 °F.
- The surfactant/nanosheet foamed acid demonstrated viscosity values double that of foamed acid fluids stabilized with only surfactant at 275 °F to 350 °F, 300 S^{-1}, 1,500 psi, and 70% N_2 quality.
- The foamed acid microstructure of the surfactant/nanosheet composite possesses a robust texture and huge population compared to the surfactant-based foamed acid at 300 °F.
- The surfactant/nanosheet foamed acid bubbles reserved their hexagonal shape for three hours, while the surfactant foam bubbles expanded and had a semi-hexagonal shape after one hour of measuring time.

Acknowledgments

This article was presented at the International Petroleum Technology Conference, Riyadh, Kingdom of Saudi Arabia, February 21-23, 2022.

References

1. Zou, C., Zhao, Q., Zhang, G. and Xiong, B.: "Energy Revolution: From a Fossil Energy Era to a New Energy Era," *Natural Gas Industry B*, Vol. 3, Issue 1, January 2016, pp. 1-11.
2. Abas, N., Kalair, A. and Khan, N.: "Review of Fossil Fuels and Future Energy Technologies," *Futures*, Vol. 69, May 2015, pp. 31-49.
3. Ahmed, S., Hanamertani, A.S. and Hashmet, M.R.: "CO_2 Foam as an Improved Fracturing Fluid System for Unconventional Reservoir," *Exploitation of Unconventional Oil and Gas Resources — Hydraulic Fracturing and Other Recovery and Assessment Techniques*, April 2019.
4. Akhtar, T.F., Ahmed, R., Elgaddafi, R., Shah, S., et al.: "Rheological Behavior of Aqueous Foams at High Pressure," *Journal of Petroleum Science and Engineering*, Vol. 162, March 2018, pp. 214-224.
5. Wanniarachchi, W.A.M., Ranjith, P.G., Perera, M.S.A., Lashin, A., et al.: "Current Opinions on Foam-Based Hydro-Fracturing in Deep Geological Reservoirs," *Geomechanics and Geophysics for Geo-Energy and Geo-Resources*, Vol. 1, Issues 3-4, November 2015, pp. 121-134.
6. Harris, P.C. and Reidenbach, V.G.: "High Temperature Rheological Study of Foam Fracturing Fluids," *Journal of Petroleum Technology*, Vol. 39, Issue 5, May 1987, pp. 613-619.
7. Harris, P.C.: "Chemistry and Rheology of Borate Crosslinked Fluids at Temperatures to 300 °F," *Journal of Petroleum Technology*, Vol. 45, Issue 3, March 1993, pp. 264-269.
8. Barati, R. and Liang, J-T.: "A Review of Fracturing Fluid Systems Used for Hydraulic Fracturing of Oil and Gas Wells," *Journal of Applied Polymer Science*, Vol. 131, Issue 16, August 2014.
9. Verma, A., Chauhan, G. and Ojha, K.: "Synergistic Effects of Polymer and Bentonite Clay on Rheology and Thermal Stability of Foam Fluid Developed for Hydraulic Fracturing," *Asia-Pacific Journal of Chemical Engineering*, Vol. 12, Issue 6, November/December 2017, pp. 872-883.
10. Wang, Y., Zhang, Y., Liu, Y., Zhang, L., et al.: "The Stability Study of CO_2 Foams at High Pressure and High Temperature," *Journal of Petroleum Science and Engineering*, Vol. 154, June 2017, pp. 234-243.
11. Lv, Q., Li, Z., Li, B., Li, S., et al.: "Study of Nanoparticle

Surfactant Stabilized Foam as a Fracturing Fluid," *Industrial & Engineering Chemistry Research*, Vol. 54, Issue 38, 2015, pp. 9468-9477.

12. Latif, W.M.S.M., Sharbini, S.N., Wan Sulaiman, W.R. and Idris, A.K.: "Utilization of Silicon Dioxide Nanoparticles in Foam Enhanced Oil Recovery — A Comprehensive Review," *IOP Conference Series: Materials Science and Engineering*, Vol. 469, Issue 1, January 2019.
13. Emrani, A.S. and Nasr-El-Din, H.A.: "Stabilizing CO_2 Foam by Use of Nanoparticles," *SPE Journal*, Vol. 22, Issue 2, April 2017, pp. 494-504.
14. Zhao, G., Wang, X., Dai, C., Sun, N., et al.: "Investigation of a Novel Enhanced Stabilized Foam: Nano-Graphite Stabilized Foam," *Journal of Molecular Liquids*, Vol. 343, December 2021.
15. Kang, M-H., Lee, D., Sung, J., Kim, J., et al.: "Comprehensive Nanoscience and Nanotechnology," Chapter 4 in *Comprehensive Nanoscience and Nanotechnology*, Vol. 2, (eds.) Andrews, D.L., Lipson, R.H. and Nann, T., 2nd edition, Elsevier BV, 2019.
16. Wang, Q.H., Kalantar-Zadeh, K., Kis, A., Coleman, J.N., et al.: "Electronics and Optoelectronics of Two-Dimensional Transition Metal Dichalcogenides," *Nature Nanotechnology*, Vol. 7, Issue 11, November 2012, pp. 699-712.
17. Mejia, A.F., Diaz, A., Pullela, S., Chang, Y-W., et al.: "Pickering Emulsions Stabilized by Amphiphilic Nano-Sheets," *Soft Matter*, Vol. 8, Issue 40, August 2012, pp. 10245-10253.

About the Authors

Dr. Abeer A. Alarawi

Ph.D. in Material Science and Engineering, King Abdullah University of Science and Technology

Dr. Abeer A. Alarawi is a Petroleum Scientist working in the Production Technology Division of Saudi Aramco's Exploration and Petroleum Engineering Center – Advanced Research Center (EXPEC ARC). Her work focuses specifically on advanced materials, foamed fracturing fluids, and water shutoff. Abeer is currently involved in several research projects related to the study of rocks-fluid interaction.

She has authored and coauthored more than six technical articles. Abeer has five submitted invention disclosures.

In 2008, she received her B.S. degree in Physics from Taibah University, Medina, Saudi Arabia. Abeer then received her M.S. degree in 2014 and her Ph.D. degree in 2018, both in Material Science and Engineering from King Abdullah University of Science and Technology (KAUST), Thuwal, Saudi Arabia.

Dr. Bader G. Alharbi

Ph.D. in Petroleum Engineering, Heriot-Watt University

Dr. Bader G. Alharbi joined Saudi Aramco in 2006 as a Petroleum Engineer. Bader is currently working in the Production Technology Division of Saudi Aramco's Exploration and Petroleum Engineering Center – Advanced Research Center (EXPEC ARC), where he is a focus area champion of smart fluid. Bader's research interests include well stimulation and scale mitigation.

He has authored and coauthored more than 21 technical papers. Bader has two granted patents and more than 10 submitted invention disclosures.

He received his B.S. degree in Chemical Engineering, and his M.S. degree in Petroleum Engineering, both from King Fahd University of Petroleum and Minerals (KFUPM), Dhahran, Saudi Arabia. Bader received his Ph.D. degree in Petroleum Engineering from Heriot-Watt University, Edinburgh, Scotland, U.K.

Ahmed S. Busaleh

A.S. in Industrial Chemistry Technology, Jubail Industrial College

Ahmed S. Busaleh joined Saudi Aramco in 2014 as a Lab Technician. He is currently working in the Production Technology Division of Saudi Aramco's Exploration and Petroleum Engineering Center – Advanced Research Center (EXPEC ARC).

Ahmed has contributed to several in-house projects, including water shutoff, propped fracturing, and foamed fracturing fluids. He has also participated in several patent applications and publications as a coauthor.

In 2012, Ahmed received his A.S. degree in Industrial Chemistry Technology, from Jubail Industrial College, Jubail, Saudi Arabia.

Advanced Coating to Mitigate PDC Cutter Thermal Degradation in PDC Bit Manufacturing

Dr. Jianhui Xu, Dr. Guodong Zhan, Timothy E. Moellendick and Dr. Wenhui Jiang

Abstract /

Polycrystalline diamond compact (PDC) cutters on drill bits are the primary cutting elements to shear and scrape the formations during the drilling process. In the PDC drill bit manufacturing, PDC cutters are attached onto a drill bit with silver-copper-zinc alloys by using a brazing process. PDC cutters face the challenge of thermal degradation during this brazing process.

This article studies the development of an advanced coating on a PDC cutter to mitigate its thermal degradation in the brazing process. The advanced coating is applied by a physical vapor deposition process on the PDC cutter. The coated cutter surface is checked by scanning electron microscope (SEM) for the coating integrity. Both the coated and uncoated cutters are brazed and de-brazed to mimic the heating cycle of drill bit manufacturing. They are then tested in a vertical turret lathe to shear a rotating granite rock. The volume losses from the wear scars of the cutters after specific passes are compared among those of the coated and uncoated PDC cutters.

The SEM results show that the coating has maintained good integrity on the PDC cutter surfaces. The coating is continuous, dense without porosity, or microcracks. No obvious oxidation is observed after a high temperature heat treatment at 740 °C, which was used to mimic the overheating brazing process — commonly encountered during bit manufacturing. Then, the vertical turret lathe test results show that the coating on the PDC cutters improves the wear resistance by 50% when compared with that of uncoated cutters, following the brazing and de-brazing simulation.

This work presents a solution to the thermal degradation of the PDC cutters after the brazing process by using an advanced coating process. With the improved wear resistance due to the coating protection, the life of a drill bit and its rate of penetration during the drilling process can be significantly improved. It is expected to save a lot of drilling time and cost for the drilling operation in the exploration and production sector.

Introduction

The drill bit is a primary tool to drill the formation when exploiting the hydrocarbon resources underground. As one of main types of drill bits, the polycrystalline diamond compact (PDC) drill bit currently dominates the majority of drilling footages in various formations and downhole conditions[1]. This dominance is mainly due to the tireless developments in: (1) new materials and process, (2) new designs, and (3) optimizations of drilling parameters.

As is well-known, the PDC cutters on the drill bits are the main cutting elements to shear and scrape the formations during drilling[1]. The sharp edges of the PDC cutters are engaged into the formation with certain weight, depth and speed, to enable such shearing and scraping functions. The PDC cutters, therefore, face the challenges of wear, vibration, and thermal impacts. Therefore, the hardness, toughness and thermal resistance of the PDC cutters are the main properties that people always want to improve.

The PDC cutters are made of diamond table and tungsten carbide substrate, and typically bonded to each other by hot pressing with high-pressure and high temperature[2]. In the PDC drill bit manufacturing, PDC cutters are attached onto a drill bit with silver-copper-zinc alloys by a brazing process[3]. The silver-copper-zinc based alloys are used due to their low melting point, good flowability in a molten state, and great proximity to the tungsten carbide substrate of the PDC cutters for bonding strength.

Table 1 lists several commonly used brazing materials for bonding PDC cutters to drill bits and their properties, as recommended by the American Welding Society. Depending on the brazing material selection, the brazing temperature can range from 680 °C to 740 °C to melt the brazing material and make its flowability sufficient to bond the PDC cutter. On the other hand, PDC cutters are typically made by using graphite or diamond powder as a raw material, and then processed with high-pressure and high temperature using a hot press, commonly with the help of a metallic catalyst, such as cobalt (Co), nickel (Ni), or iron (Fe), among which Co is the most commonly used element[2, 4].

Consequently, the conversion of graphite to diamond is reversible when the temperature, atmosphere, and

Table 1 *Commonly used brazing materials for PDC cutter bonding to drill bits. (Ag: silver, Cu: copper, Sn: tin, Zn: zinc, Mn: manganese, Ni: nickel).*

AWS Spec.	Solid Temp. (°C)	Liquid Temp. (°C)	Brazing Temp. (°C)	Composition (wt%)					Bonding Strength
				Ag	Cu	Sn	Zn	Other	
BAG 7	620	650	680 - 760	56	22	5	17	—	Weakest
BAG 22	680	700	730 - 810	49	16	—	23	7.5 Mn, 4.5 Ni	Strongest
BAG 24	660	705	735 - 815	50	20	—	28	2 Ni	Medium

the existence of a catalyst are able to trigger the kinetics of the phase transformation in which diamond is transformed back to graphite. Besides this phase transformation, it also possibly engages the chemical reaction of diamond with oxygen or an oxidizing element to make carbon monoxide or carbon dioxide at an even lower temperature.

Table 2 lists the degradation temperatures for these scenarios. The temperature, as low as 600 °C, can start to witness the degradation when there is no inert atmospheric protection of the unleached cutter, which contain a high percentage of Co. The leached cutter, with a very limited amount of Co, might delay the degradation temperature up to 700 °C to 800 °C. Although, if the cutter is fully protected by the inert atmosphere, this degradation temperature can be further pushed up to about 960 °C. Therefore, the inert atmospheric protection is critical during the brazing process to improve the resistance to these thermal degradations. We typically rely on the flux, which can be in either a paste or powder state, to provide such atmospheric protection after it is heated up. Subsequently, the flux application often cannot be done continuously, due to the high complexity. Due to the manual process, it is very easy for braziers who work in the challenging environment to lose control of the flux and the processing temperature.

The temperature of the oxyacetylene torch can be easily overshot locally or universally to over 750 °C. When such a scenario happens, considering the overlap (about 50 °C) of the brazing temperature and the temperature to trigger the transformation of the leached cutter, it seems that the thermal degradation of the PDC cutter is unavoidable. This is especially true when the unleached cutter with high a Co content in the diamond table is used, as the transformation can be more severe.

In addition to the temperature concern, the process is time-consuming. For example, it takes more than 1 hour for 2 to 3 braziers to work together to braze the PDC cutters on an 8½" PDC bit, after it is preheated in an oven. The long process is going to make the thermal degradation even worse. Overall, in the existing PDC bit manufacturing process, PDC cutters generally face the challenge of thermal degradation, especially during the brazing process.

A study was conducted to mimic the brazing process of PDC cutters by heat treatment at 700 °C for 10 minutes with and without protective gas. The wear resistance of these cutters using protective gas during the heat treatment shows an obvious improvement up to 16% in the tests by cutting the rocks, Table 3, by comparing the 59% reduction vs. the 43% reduction of the cutters heat treated in both air and protective gas (nitrogen). As a reference, the abrasive ratio in the table is defined as the volume loss of the rock divided by the volume loss of the cutter. The higher the abrasive ratio is obtained, the better wear resistance the cutter has. Therefore, it is essential to provide the protective condition for the PDC cutters during the preheating and the brazing processes at high temperatures.

This article studies the development of an advanced coating on PDC cutters to mitigate its thermal degradation in the brazing process. The advanced coating is applied by a physical vapor deposition process on the PDC cutter. The coated cutter surface is examined by a scanning electron microscope (SEM) for the coating integrity. A wear test using a vertical turret lathe

Table 2 *Thermal degradation temperatures in different atmosphere temperatures and the existence or nonexistence of Co.*

Degradation and Transformation	Environment	Co	Temperature (°C)
C (diamond) → C (graphite)	Vacuum or Inert Gas	Nonexisting	~1,500
		Existing	~960
C (diamond) + O_2 → CO + CO_2	Air	Nonexisting	700 - 800
		Existing	600 - 750

Table 3 Wear resistance of PDC cutters before and after heat treatment at 700 °C at 10 minutes with and without protective gas.

		Abrasive Ratio (× 10^6)		
No.	Heat Treatment	Before Heat Treatment	After Heat Treatment	Reduction of Abrasive Ratio (%)
1	700 °C/10 min (Air)	2.37670	0.96847	59.25
2	700 °C/10 min (Air)	2.91760	1.21518	58.35
3	700 °C/10 min (N_2)	1.77359	1.00572	43.29
4	700 °C/10 min (N_2)	2.25750	1.30664	42.12

to shear a rotating granite rock shows the significant improvement of wear resistances of both the leached and unleached PDC cutters by applying such a coating on at least the portion of the diamond table.

With the improved wear resistance due to the coating protection, the life of a drill bit and its rate of penetration during the drilling process can be significantly improved. It is expected to save a lot of drilling time and cost for drilling operations in the exploration and production sector.

Experiment

We have selected PDC cutters that are 16 mm in diameter and 13 mm in height for our study. The grade is proper to a universal application with a conventionally flat front surface with 0.4 mm × 45° chamfer on the diamond table. Figure 1 shows the selected PDC cutters with four different coatings used. All of the coatings are physical vapor depositions with proprietary chemical compositions and processes. After the initial trial, we determined to use coating 4 for further tests, based on the best integrity of the coating, as determined later by SEM.

The thermal treatment is conducted in an electric resistance furnace on the PDC cutters with and without the optimized coating 4. The furnace was heated and held at a temperature of 740 °C. The cutters were then put into the furnace for 10 minutes to mimic the brazing temperature in air without protective gas. These cutters were then put into a vertical turret lath to cut rotating granite rock to examine their wear resistance.

Figure 2 is a schematic of the vertical turret lathe testing setup. The vertical turret lathe testing parameters are:

- Constant linear cutting speed: 4 m/s.
- Feed rate: 0.6 mm/revolution.
- Cutting depth: 2 mm.

A higher temperature, up to 800 °C, was further chosen to process the PDC cutters with and without

Fig. 2 A schematic of the vertical turret lathe testing setup.

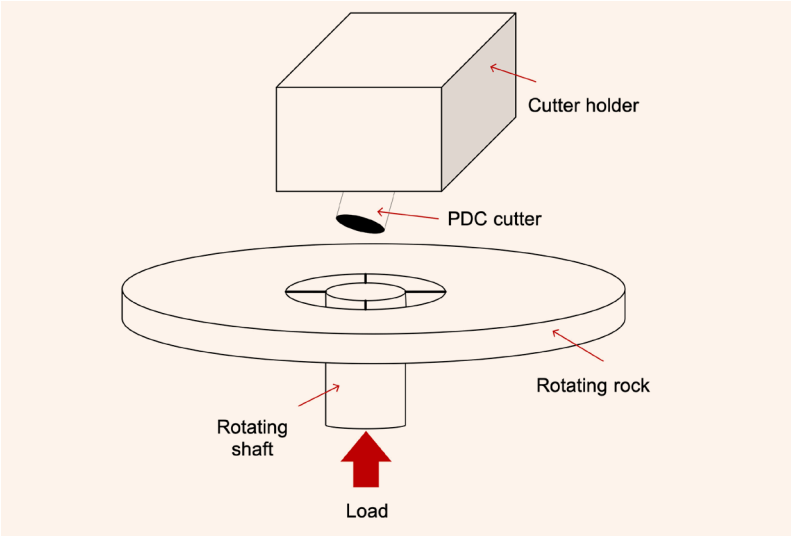

Fig. 1 Coating types tested for the study: (a) uncoated; (b) Coating 1; (c) Coating 2; (d) Coating 3; and (e) Coating 4.

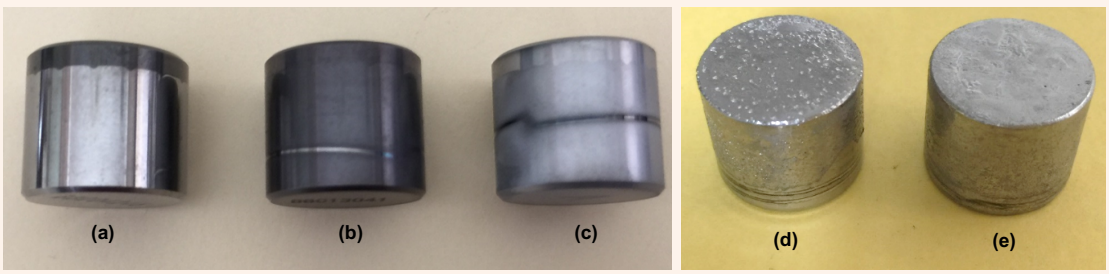

the coating to mimic the extreme conditions of overheating during the brazing process. The processed cutters were examined by SEM for surface oxidation or damage.

In the vertical turret lathe test, while mild parameters with only 0.5 mm cutting depth are commonly used, our testing parameters are very aggressive by using a 2 mm cutting depth to differentiate the PDC cutters in various conditions within several hours with dozens of passes, instead of several days with over hundreds of passes. After the vertical turret lathe tests, the worn surfaces of the cutters — after various passes — were captured while recording the volume losses of the granite rocks, which are used to gauge the wear resistance of the PDC cutters.

As an example of calculating the volume loss of the granite in this aggressive test, 15 passes can remove about 8,062 cm^3 of the granite rock.

Results and Discussion

As shown in Fig. 3, the PDC cutters were heat treated in the electric resistance furnace at 740 °C for 10 minutes. The uncoated cutters show severe oxidation since the furnace does not have protective gas. The surfaces on the tungsten carbide substrates with Co show the grey oxidation color, Fig. 3a, and the coated PDC cutters do not show any oxidation color, Fig. 3b.

With the same set up to heat up to a higher temperature at 800 °C, the PDC cutters are then put into the furnace and held for 10 minutes. The oxidation on the uncoated PDC cutters is more prominent. We conducted SEM to identify the oxidation layers on the surfaces of the PDC cutters. In Fig. 4a, the uncoated PDC cutter shows the oxidation layer on the surface of the diamond table. The bright contrasts in the image are from the electric discharge while capturing SEM images due to the dielectric property of the oxidation layer. Figure 4b is a typical morphology of a diamond table without oxidation after it is protected by the coating. Also, in Fig. 4b, one can see that the coating is continuous without any missed spots, showing that it is dense and does not have any porosity to expose the diamond body.

Figure 5 shows the wear scars of the unleached PDC cutters with and without coatings after vertical turret lathe wear tests, and after the PDC cutters experienced the heat treatment in air at 740 °C for 10 minutes to mimic the commonly used brazing temperature. One thing which attracts attention is that all of the cutters are worn fairly fast. The main reason is the testing parameters are very aggressive to differentiate the PDC cutters within a short time.

Fig. 3 *The PDC cutters after heat treatment at 740 °C in air for 10 minutes: (a) Uncoated PDC cutters, and (b) Coated PDC cutters.*

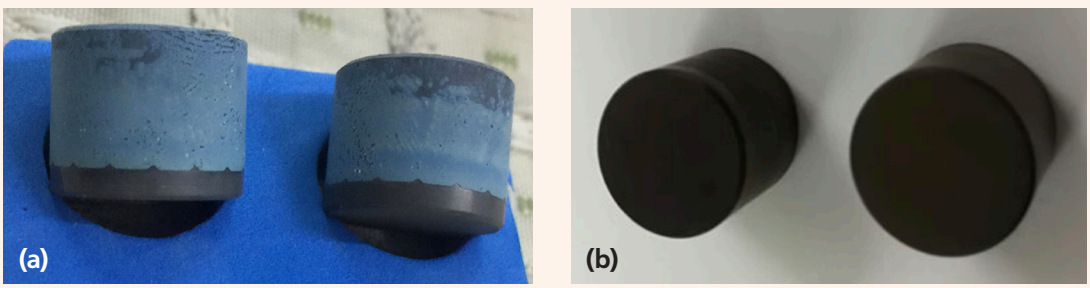

Fig. 4 *The SEM images of the PDC cutters after heat treatment in air at 800 °C for 10 minutes: (a) Uncoated PDC cutters, and (b) Coated PDC cutters.*

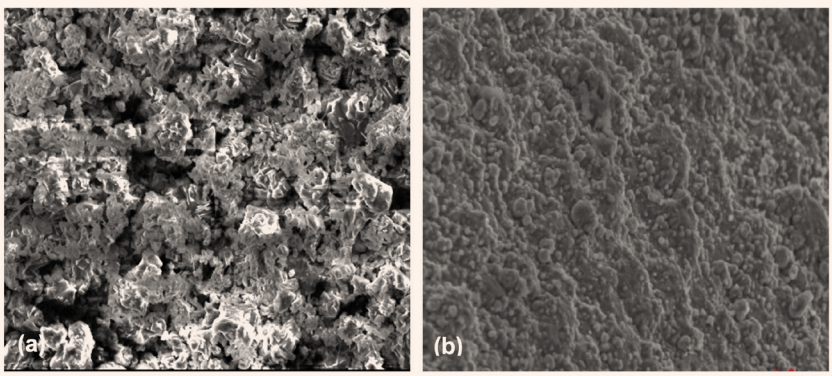

Fig. 5 *The vertical turret lathe wear scars of unleached PDC cutters after heat treatment in air at 740 °C for 10 minutes: (a) Uncoated PDC cutters after a number of passes, and (b) Coated PDC cutters after a number of passes.*

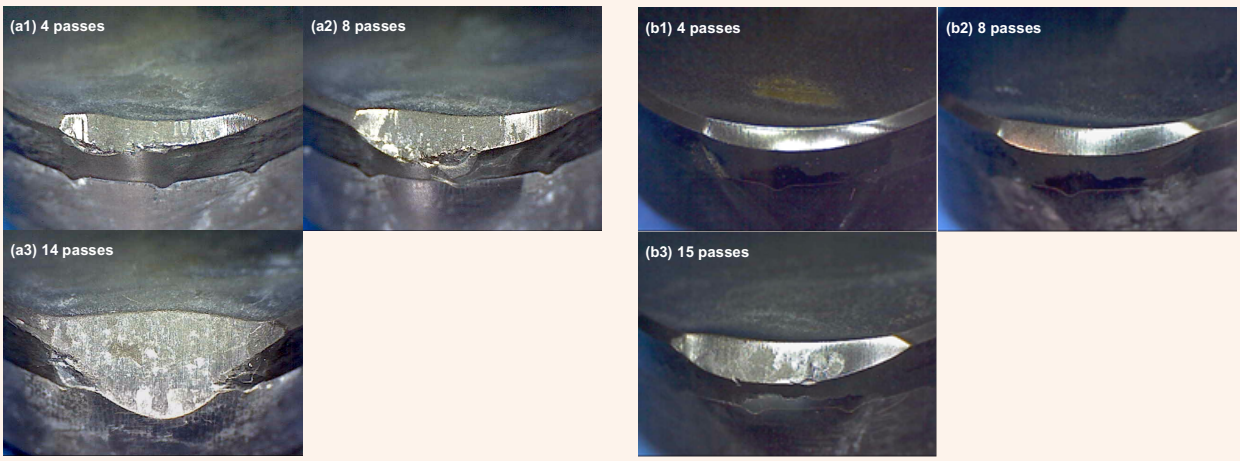

The wear scars of the uncoated cutters show some small chippings on the edges even after only four passes. It implies that the PDC cutters without coating protection during the heat treatment process have been embrittled significantly. The severe wear is then observed after 14 passes. On the other hand, the minimal to moderate degree of wear is observed on the coated cutter after 15 passes.

The improvement by coating is obvious, based on the set of images of the wear scars. From the images, we can easily say that the coating increases the wear resistance by over 50%. The improvement should be due to the protection of the coating from direct contact with the oxidizing environment during the heat treatment process, so that the thermal degradation, including phase transformation or chemical reaction, was mitigated significantly.

While the unleached PDC cutters were first tested, it is also critical to test the coating effect on the thermal damage for the leached PDC cutters because they are more commonly used on the PDC bits these days. The Co percentage in the diamond table close to the

Fig. 6 *The vertical turret lathe wear scars of the leached PDC cutters after heat treatment in air at 740 °C for 10 minutes: (a) Uncoated PDC cutters after a number of passes, and (b) Coated PDC cutters after a number of passes.*

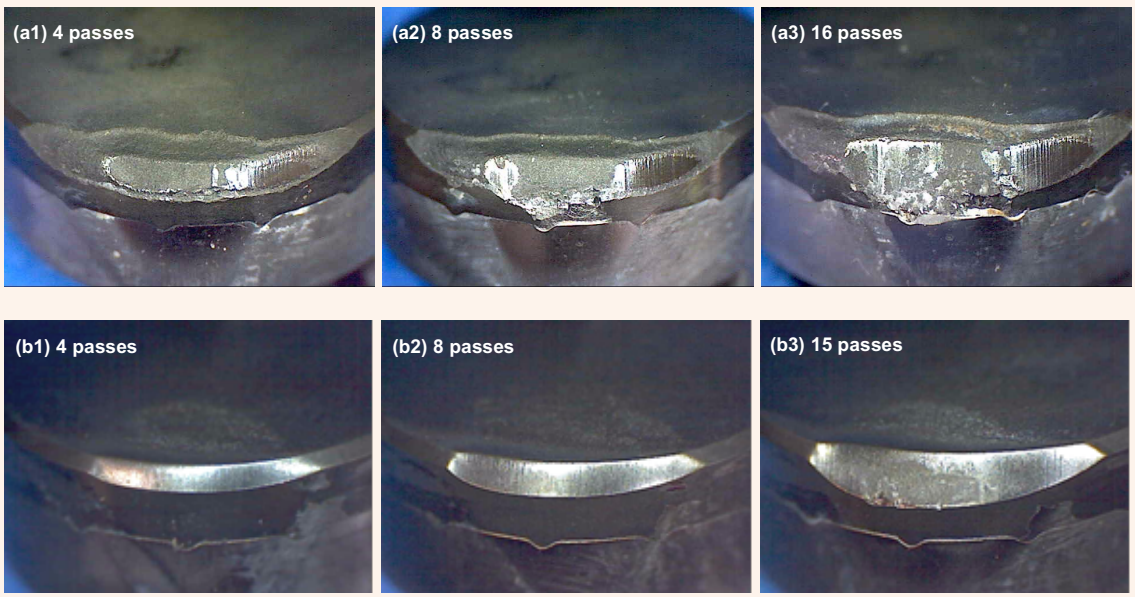

outside surface typically dropped from 5 wt% to 10 wt% and to 1 wt% to 2 wt% after the leaching process. The affected layer of leaching is typically about 0.5 mm to 1.2 mm. The typical leaching process uses acid (such as hydrofluoric, nitric, sulfuric, or hydrogen peroxide, or their combinations) to dissolve the Co from the network structure of diamond D-D bonds[5].

With a reduced Co percentage, the PDC cutter is expected to increase the wear resistance, and reduce the thermal stress within the diamond table during the drilling process when the diamond table shears the formation. This is due to a reduced mismatch of thermal expansion in the different phases of the diamond table.

Figure 6 shows the wear scars after a number of passes in the vertical turret lathe wear tests. When comparing the unleached PDC cutters, the wear scars in the leached PDC cutters are smaller at the same testing passes, such as four or eight passes. This reflects the benefit of the leaching process. When comparing the uncoated and leached PDC cutters, the coated and leached PDC cutters also show the improvement of the wear resistance. From the images, one can see that there is no obvious chipping on the coated cutter, an indication that the PDC cutter keeps its integrity during heat treatment because of the coating protection.

The images show that wear resistance of the coated PDC cutter is increased above 50%. This is a significant improvement. To improve the material development of the PDC cutter, it typically takes 10 years to improve 50% wear resistance in the history. This coating alone is able to provide an equivalent of 10-year development effort of the new diamond materials.

Conclusions

The surface coating on the PDC cutter, at least to cover the diamond table, can provide the protection from thermal degradation during the PDC cutter's brazing process. The coating is to isolate the diamond material from the oxidizing atmosphere and keeps the integrity of the diamond's D-D bonding. The surface oxidation examination by SEM confirms the protection. The vertical turret lathe wear test verifies the significant improvement of wear resistance by applying the coating on the PDC cutter. The wear ratio on the coated unleached PDC cutter and leached PDC cutters can improve above 50%, when compared with their corresponding counterparts without coating.

One of the tests in the future will concern the impact resistance by applying drop tower methodology, which is to check the toughness of the coated PDC cutter after the brazing process. Combining the wear resistance, the toughness of the PDC cutter is another crucial characteristic when a design engineer selects the PDC cutters in their design of PDC drill bit. Furthermore, the coated PDC cutters will be implemented on the PDC drill bit and a full-scale field test will be conducted.

Acknowledgments

This article was presented at the International Petroleum Technology Conference, Riyadh, Kingdom of Saudi Arabia, February 21-23, 2022.

References

1. Scott, D.: "A Bit of History: Overcoming Early Setbacks, PDC Bits now Drill 90% Plus of Worldwide Footage," *Drilling Contractor*, July/August 2015, pp. 1-7.
2. Wentorf Jr., R.H. and Rocco, W.A.: "Diamond Tools for Machining," U.S. Patent 3,745,623, 1973.
3. Knemeyer, F.S. and Daniels, W.H.: "Method for Fabricating a Rotary Drill Bit and Composite Compact Cutters Therefore," U.S. Patent 4,156,329, 1979.
4. De Lai Anthony, J.: "Diamond Compact Abrasive," U.S. Patent 3,141,746, 1964.
5. Setlur, D.R., Hughes, M.D., Francis, M.J., Sreshta, H.A., et al.: "Polycrystalline Diamond Cutting Element," U.S. Patent 8,919,463, 2014.

About the Authors

Dr. Jianhui Xu

Ph.D. in Materials Science and Engineering, University of Kentucky

Dr. Jianhui Xu is a Materials Engineer with the Drilling Technology Division at Saudi Aramco's Exploration and Petroleum Engineering Center – Advanced Research Center (EXPEC ARC). He joined Saudi Aramco in 2019. Prior to that, Jianhui worked at Schlumberger as a Materials Engineer for 6 years and at the CNPC USA Corporation as a Senior Materials Engineer/ Group Lead for another 6 years.

His research interests are smart materials, nano-technologies, hard materials, degradable materials, coating materials, and process. Jianhui is an expert in the material and process solutions for applications to work in specialty and hostile environments within the oil and gas industry, including drilling tools and completion tools.

He has published 25 scientific publications and holds 20 patents and applications. Jianhui has been serving as a reviewer for several internationally prestigious journals, including *Materials Science and Engineering* and *Philosophical Magazine Letters*. He is an active member of The Minerals, Metals and Materials Society (TMS) and the Society of Petroleum Engineers (SPE).

In 2008, Jianhui received his Ph.D. degree in Materials Science and Engineering from the University of Kentucky, Lexington, KY.

Dr. Guodong "David" Zhan

Ph.D. in Metallurgical Engineering, Huazhong University of Science and Technology

Dr. Guodong "David" Zhan is a Science Specialist and the Team Leader of the Advanced Drilling Tools team in the Drilling Technology Division at Saudi Aramco's Exploration and Petroleum Engineering Center – Advanced Research Center (EXPEC ARC). David is a world-renowned materials scientist and expert in advanced drilling tools/technology. He has over 29 years of experience in industrial R&D and managerial positions, including positions as Chief Engineer and R&D Manager at top oil/gas and semiconductor global companies, such as Schlumberger, NOV, and Applied Materials.

Additionally, David has held academic positions at the University of London and the University of Colorado at Boulder, and staff scientist positions at the Japan National Institute for Materials Science and the Shanghai Institute of Ceramics, Chinese Academy of Sciences.

He is an active member of the Society of Petroleum Engineers (SPE) where he serves on several conferences such as the SPE International Petroleum Technology Conference and the Asia Pacific Drilling Technology Conference/ International Association of Drilling Contractors as co-chair and technical committee member. David is also serving as an editorial board member and reviewer for a number of international scientific journals published by The Minerals, Metals and Materials Society and the Material Research Society.

He has won several prestigious international industry and academic awards, e.g., the World Oil Award and the E&P Hart Energy Award.

David has published 96 peer-reviewed articles in journals such as *Nature Materials* and *Nature Scientific Reports*, 105 conference proceedings, and has more than 120 filed/published/granted U.S. patents, with an H-index of 37.

In 1994, he received his Ph.D. in Metallurgical Engineering from Huazhong University of Science and Technology, Wuhan, China, and completed a postdoctoral fellowship in Nanomaterials and Nanotechnology at the University of California at Davis.

Timothy E. Moellendick

B.S. in Petroleum Engineering, Marietta College

Timothy E. Moellendick is the Chief Technologist for the Drilling Technology Division at Saudi Aramco's Exploration and Petroleum Engineering Center – Advanced Research Center (EXPEC ARC). Timothy is considered the industry expert in casing and liner drilling applications and engineering.

In his previous role as Director of Technology for Schlumberger, he was responsible for growing the technical and operational knowledge base used to develop, plan, and execute this technology worldwide. Timothy has also held drilling operations and engineering positions, including Senior Drilling Engineer, Drilling Manager for North America, Senior Field Engineer/Directional Driller and Operations Coordinator for the Gulf Coast of Mexico.

With more than 25 years of oil and gas industry experience, he leads a team of world-class researchers in developing the next generation of drilling technology required by Saudi Aramco's Drilling and Workover stakeholders.

In 1996, Timothy received his B.S. degree in Petroleum Engineering from Marietta College, Marietta, OH.

Dr. Wenhui Jiang

Ph.D. in Materials Science and Engineering, Institute of Metal Research

Dr. Wenhui Jiang is a Consulting Materials/ Metallurgical Engineer (and CEO) at WHJ Materials Solutions, LLC, Houston, TX. He has been working on materials and metallurgy for drilling and remedial tools, and completion components for 15 years.

Wenhui has more than 90 publications in peer-reviewed journals, and over 10 patents and patent applications.

He received his Ph.D. degree in Materials Science and Engineering from the Institute of Metal Research, Chinese Academy of Sciences, Shenyang, China.

From 100 Patents Granted in 77 Years to the Top Performer in the Industry — the Story Behind Our Rapid Growth in Patents

Michael J. Ives

Over the past 20 years, we strongly invested in innovation as part of our corporate culture to ensure our operations' long-term sustainability and efficiency. As a result, our patent portfolio has continued to expand.

Up to 2011, we had only been granted 100 U.S. patents over a period of 78 years. Fast forward, in 2021 alone, we were awarded 864, Fig. 1 — ranking us first in the oil and gas industry, and in the top 50 list of all companies and universities that received U.S. patents in 2021 (based on Patent 300® List).

This achievement marks an important milestone in Aramco's quest to become a technology leader. It shows Aramco's innovation, with approximately 66% of the 864 U.S. patents granted in 2021 originating from new ideas.

The story of our company's rapid growth of patents underpins our drive to achieve leadership in technology and innovation. That drive has been there from the company's beginning — and now, the patents inevitably follow as a result of our focus on innovation. Through our growing portfolio of patents, we reinforce our commitment to innovation and to maintain our competitive advantage, helping to drive value and efficiency across all operations.

Figure 2 compares the 2021 U.S. granted patents among international oil companies and shows Saudi Aramco having a leading position with 864 granted patents. ExxonMobil follows with 313, followed by Shell with 95.

Figure 3 shows the top technology domain distribution of the granted U.S. patents in 2021 for Saudi Aramco with upstream technology domains of production and drilling leading.

Why patents matter

Innovation is vital for maintaining a competitive market position in our growing business portfolio and continually improving our performance. Given global challenges and the importance of low carbon economies, innovation and collaboration will need to be accelerated and elevated even further.

Fig. 1 *Saudi Aramco's filed and granted U.S. patents from 2016 to 2021.*

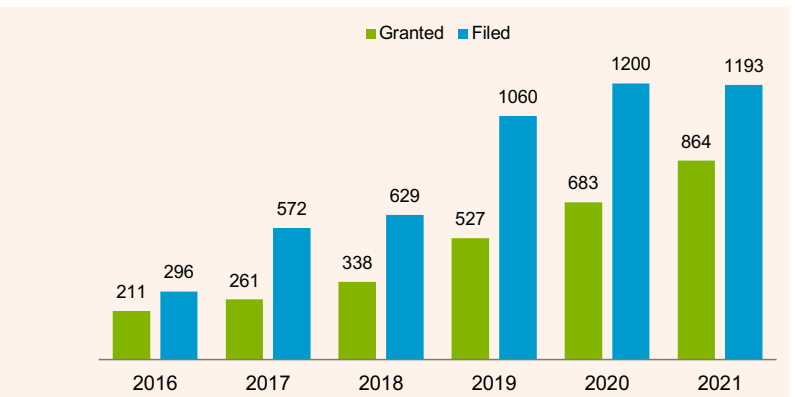

While patents are a leading indicator of innovation, the ultimate goal is to create value through the development of solutions that help to address a particular need. Such results are often only possible with significant upfront investments, and patents make it possible to recoup these costs and potentially generate additional revenue through commercialization.

How we drove patent growth

In 2012, we began to expand our research operations outside of our headquarters in Dhahran, Saudi Arabia. We focused on setting up a network of research and technology centers worldwide in proximity to global talent hubs. This boost in research capabilities also accelerated the stream of patents, particularly in high priority areas, such as low carbon solutions and products across multiple key industries.

We have also set up a wide range of co-development programs with leading academic organizations and research institutions, such as the Rice University Carbon Hub in the U.S., Tsinghua University in China, the Korea Advanced Institute of Science and Technology (KAIST) in South Korea, and Saudi Arabia's King Abdullah University of Science and Technology (KAUST). These collaborations are focused on potential high-impact solutions across the energy value chain.

Fig. 2 *A comparison of the U.S. granted patents in 2021 between the leading international oil companies.*

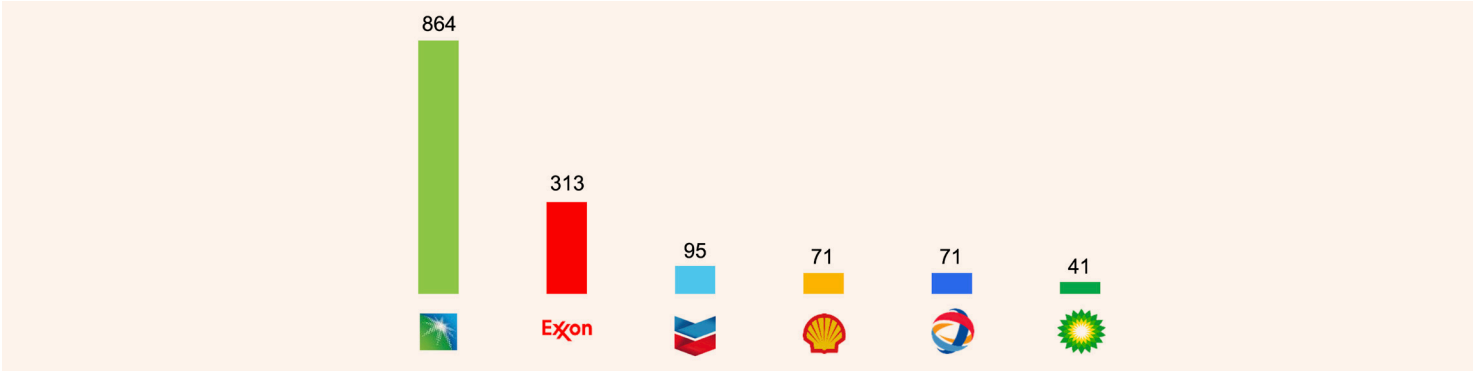

Fig. 3 *Saudi Aramco's 2021 granted patents by technology domain.*

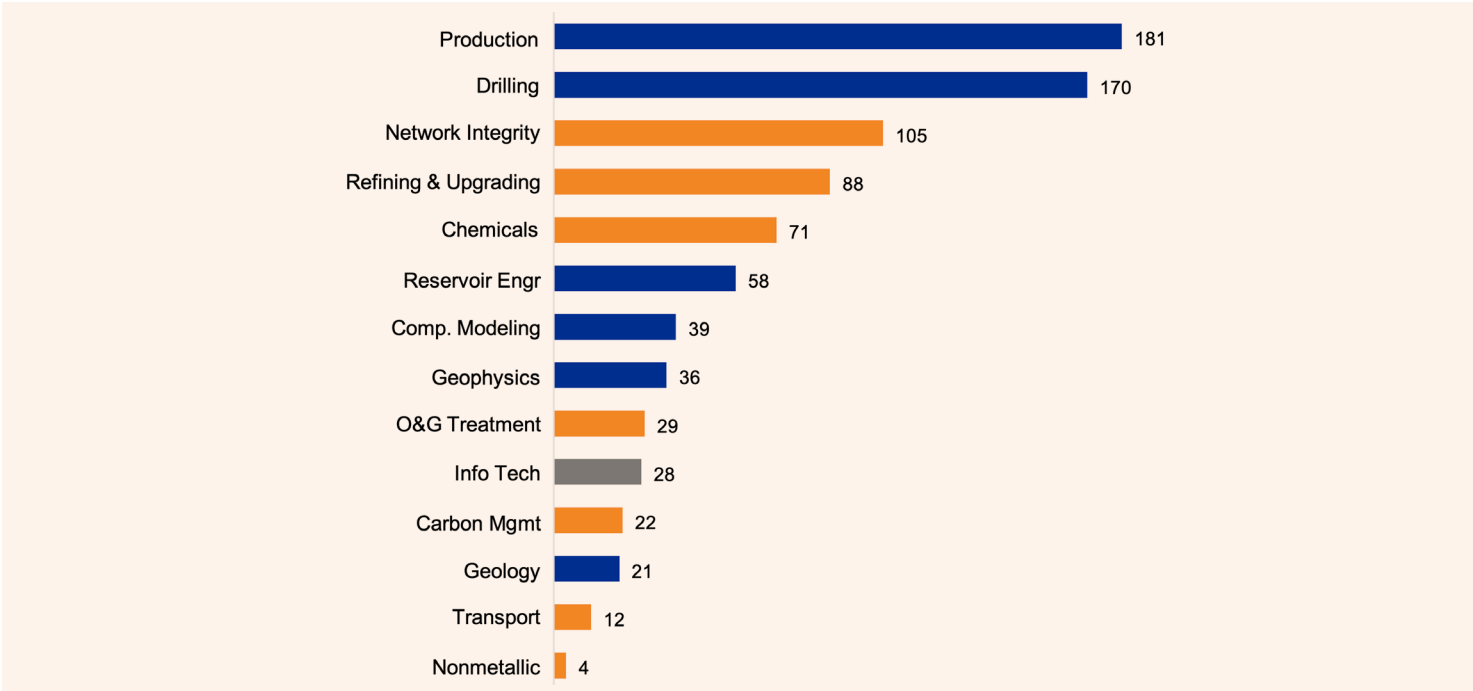

We help customers and partners address some of their most pressing challenges, particularly those related to carbon management and environmental performance.

Putting patents to work

While many of the patented solutions are still being developed for our operations and products, we are increasingly helping develop and advance solutions beyond our core business. This role and contribution are possible given the company's deep insights into most areas of the energy value chain, coupled with growing experience with developing leading technology and scaling it. A dedicated team is helping to orchestrate collaboration with partners, getting solutions ready for market introduction, and commercializing patented solutions and industry breakthroughs.

The patents of the future

There is a new emphasis on solutions related to the Fourth Industrial Revolution and its opportunities, such as artificial intelligence and machine learning. These new generation technologies will enable further advancement of our systems and products and their performance, including in the area of low carbon technologies and support of environmental stewardship solutions.

For the complete list of the 2021 granted patents, please visit our publications website at *www.saudiaramco.com/jot*.

Notes

Notes

Have an article you would like to publish? Here are our guidelines.

These guidelines are designed to simplify and help standardize submissions. They need not be followed rigorously. If you have any questions, please call us.

Length

Average of 2,500-4,000 words, plus illustrations/photos and captions. Maximum length should be 5,000 words. Articles in excess will be shortened.

What to send

Send text in Microsoft Word format via email. Illustrations/photos should be clear and sharp. Editable files are requested for graphs, i.e., editable in Excel.

Procedure

Notification of acceptance is usually within three weeks after the submission deadline. The article will be edited for style and clarity and returned to the author for review. All articles are subject to the company's normal review. No paper can be published without a signature at the manager level or above.

Format

No single article need include all of the following parts. The type of article and subject covered will determine which parts to include.

Working Title
Lorem Ipsum here.

Abstract
Usually 150-300 words to summarize the main points.

Introduction
Different from the abstract in that it sets the stage for the content of the article, rather than telling the reader what it is about.

Main body
May incorporate subtitles, artwork, photos, etc.

Conclusion/Summary
Assessment of results or restatement of points in introduction.

Endnotes/References/Bibliography
Use only when essential. Use author/date citation method in the main body. Numbered footnotes or endnotes will be converted. Include complete publication information. Standard is *The Associated Press Stylebook*, 52nd ed. and *Wesbter's New World College Dictionary*, 5th ed.

Acknowledgments
Use to thank those who helped make the article possible.

Illustration/Tables/Photos and explanatory text

If the files are large, these can be submitted separately, due to email size limits. Initial submission may include copies of originals; however, publication will require the originals. When possible, submit original images. Color is preferable.

File Format

Illustration files with .EPS extensions work best. Other acceptable extensions are .TIFF/.JPEG/.PICT.

Permission(s) to reprint, if appropriate

Previously published articles are acceptable but can be published only with written permission from the copyright holder.

Author(s)/Contibutor(s)

Please include a brief biographical statement.

Submission/Acceptance Procedures

Papers are submitted on a competitive basis and are evaluated by an editorial review board comprised of various department managers and subject matter experts. Following initial selection, authors whose papers have been accepted for publication will be notified by email.

Papers submitted for a particular issue but not accepted for that issue may be carried forward as submissions for subsequent issues, unless the author specifically requests in writing that there be no further consideration.

Submit articles to:

Editor
The Saudi Aramco Journal of Technology
C-10B, Room AN-1080
North Admin Building #175
Dhahran 31311, Saudi Arabia
Tel: +966-013-876-0498
Email: *william.bradshaw.1@aramco.com.sa*

Submission deadlines

Issue	Paper submission deadline	Release date
Winter 2022	August 4, 2022	December 30, 2022
Spring 2023	November 7, 2022	March 31, 2023
Summer 2023	February 1, 2023	June 30, 2023
Fall 2023	May 9, 2023	September 30, 2023

There is more.

Gas Injection Optimization under Uncertainty in Subsurface Reservoirs: An Integrated Machine Learning Assisted Workflow

Xupeng He, Dr. Hussain Hoteit, Marwah M. AlSinan and Dr. Hyung T. Kwak

Abstract / Gas injection in subsurface reservoirs is of significant interest to the petroleum industry for the enhanced oil recovery (EOR) process. There exists geological uncertainty in the subsurface due to the limited measurements. Optimization under such uncertainty is, therefore, required to make more robust operational decisions to achieve maximum EOR with a minimum risk of early breakthrough.

This work introduces an integrated machine learning assisted workflow for the optimization under uncertainty in subsurface reservoirs. The proposed workflow includes three steps: (1) Training sample generation. We first identify the uncertain parameters, which affect the objective of interests. We then generate the input designs using Latin Hypercube Sampling (LHS) based on the identified uncertain parameters. High fidelity simulations based on the MATLAB Reservoir Simulation Toolbox (MRST) are run for each of the input designs to obtain the objective of interests as outputs. (2) Surrogate model development. A data-driven surrogate model is then built to model the nonlinear mapping between the input and output results from Step 1. Herein, the Bayesian optimization technique is implemented to obtain the surrogate model. (3) Optimization under uncertainty. We first conduct a blind test on the proposed surrogate model with high fidelity simulations. Followed by Monte Carlo to perform the uncertainty quantifications and a genetic algorithm (GA) to conduct the optimization.

Graphene Modified with Linear Alkylamines for Oil Pollutants Removal from Water

Norah W. Aljuryyed and Fahd I. Alghunaimi

Abstract / Three stable and robust types of graphene, modified with linear alkylamines, including n-propylamine, n-hexylamine, and n-dodecylamine, were synthesized. The prepared materials, graphene modified with n-propylamine (GPA), graphene modified with n-hexylamine (GHA), and graphene modified with n-dodecylamine (GDA) were characterized and evaluated for their performance in removing oil component models.

Oil and organic pollutants were used as models to determine the absorption capacity of the synthesized materials. The functionalized graphene materials have efficiently absorbed oils. The separation efficiency of the oil from the water was high. The functionalized graphene, due to its branched chains, can be proven as an efficient porous material for the oil-water separation.

Improved Sand Fill Cleanout Utilizing an Integrated Vacuuming System and Real-Time Monitoring in Horizontal Extended Reach Wells

Hussain A. Almajid, Alaa S. Shawly and Usman Ahmed

Abstract / A variety of clean out methods have been developed in the past to remove scale and sand fill accumulation from the wellbore section to restore the well's potential. The success rate for such an operation is impacted by multiple factors, such as fluid properties, limited annular velocities, particle size, reservoir pressure, and wellbore diameter. In addition, this process commonly involves applying excess hydrostatic pressure on the formation to circulate wellbore fluids, which can result in lost circulation and formation damage.

This article will share the technical details along with the field results for a novel vacuuming system with integrated real-time data, which can be operated in three different modes, to remove both undesirable liquids and solids. The process involves pumping a low-cost clean out fluid down the internal string through a jet pump and venturi nozzle assembly. A localized pressure drawdown is created at the bottom-hole assembly (BHA), drawing wellbore liquids and solids into the return flow, and the entrained flow is returned up the outer coiled tubing (CT) string to the surface.

أرامكو السعودية
saudi aramco

Aramco
Journal
of Technology

Liked this issue? Sign up. It's free.

To begin receiving the *Aramco Journal of Technology* please complete this form, scan and send by email to ***william.bradshaw.1@aramco.com.***

Got questions?

Just give us a call at +966-013-876-0498 and we'll be happy to help!

Scan the QR code to go straight to your email and attach the form!

Subscription Form

Name

Title

Organization

Address

City

State/Province

Postal code

Country

Email address

Phone number

Number of copies